ABSTRACT

Title of Thesis: EXAMINATION OF THE THERMAL DECOMPOSITION OF CHRYSOTILE.

Courtney D. Crummett, Master of Science, 2005

Thesis Directed By: Professor Philip A. Candela and Professor Ann G. Wylie, Geology Department

The decomposition of pure chrysotile from Thetford, Quebec heated at constant temperature in air from 200-1000°C for 4 to 720 hours was studied by using X-ray diffraction and optical microscopy techniques. No morphological changes were observed optically below 450ºC and 24 hours, although X-ray diffraction data suggest that chrysotile degrades then recrystallizes below 450˚C. Throughout the temperature range of 500-1000ºC, changes in the refractive indices observed included several cycles of increasing and decreasing magnitudes and ranges. Chrysotile was no longer present above 575˚C and 24 hours. The lowest temperature of forsterite appearance was at 500˚C and 720 hours and the lowest temperature of enstatite appearance was at 800˚C for 8 hours. Broad reflections were observed within 500-750˚C at 16-8Å, 4Å, and 3Å spacings. These reflections suggested the possible presence of talc and tridymite-like mineral phases. X-ray diffraction and optical microscopy results of this study show that the decomposition of chrysotile is more complex than previously understood.

EXAMINATION OF THE THERMAL DECOMPOSITION OF CHRYSOTILE

By

Courtney Doyle Crummett

Thesis submitted to the Faculty of the Graduate School of the
University of Maryland, College Park, in partial fulfillment
of the requirements for the degree of
Master of Science
2005

Advisory Committee:
Professor Philip A. Candela, Co-Advisor
Professor Ann G. Wylie, Co-Advisor
Associate Research Scientist, Philip M. Piccoli

Dedication

I dedicate this thesis to my friends and family who have supported me throughout my graduate education. My immediate family has provided me with encouragement and support through, what seems at times, a never ending educational journey. Mom, I promise I am almost done with my education; thank you for all of your emotional and financial support. Throughout my life, my father's clever wit and intelligence have inspired me to continue learning. My Aunt Marg and Uncle Bill have provided me with a home away from home during my time in Maryland, offering welcoming hugs, a warm bed and unconditional love. Ray and Kathy Arsenault have been great mentors and second parents through the years. They have inspired me to challenge myself and I am grateful for their advice on education, career paths, and personal decisions. I only hope that in the end, I can be half the people they are.

Over the years, my friends across the country have also supported me during times of self doubt and discouragement. I am thankful for every time they have picked up the phone or answered an email. Without the enormous amount of encouragement supplied by Karyn Murphy, Rachel Maddux, Amelia Arsenault, and Amy Schulthess, I believe I would not have been able to get through grad school. I owe a great debt to each of them for all the time they spent building my spirit back up after a hard day of science. They have seen the best and worst of me, and have always remained by my side. I would like to thank Jared Samon for the long road trip, for always taking care of me, and providing me with endless excitement and great stories. Lastly, Jay Alday has been a source of insight and positive thinking during the last stages of this thesis. Thank you for all the reassuring conversations and for giving me something to look forward to.

Acknowledgements

The achievements and completion of this thesis would not have been possible without the support of many people. First and foremost, I would like to acknowledge Ford Motor Company, General Motors Corporation, and the DaimlerChrysler Corporation for their financial assistance. I would also like to acknowledge my two advisors, Dr. Philip A. Candela and Dr. Ann G. Wylie for their grand commitment to this research project. Phil has been a mentor and great teacher. His patience was never ending, and he taught me lessons in both science and life. Through his own confidence in science and academics, he taught me how to have faith in myself. I believe that through Phil's guidance, I have become a scientist. It has also been a privilege to have Ann as my advisor. She is an inspiring role model and I will admire her for the rest of my days. She showed me the awesome "re" of research with persistence; she is a patient and clear teacher. I would also like to thank Dr. Philip M. Piccoli, the third member of my thesis committee, for the arduous task of answering my off-the-wall questions about science, uncertainty, and Maryland tourism. In addition, the scientific advisement and friendship provided by Dr. Mark Frank, Dr. Adam Simon, and Dan Earnest throughout the course of this research project has been greatly appreciated.

I would like to thank the staff of the geology department for their never-ending assistance. The presence of Dorothy Brown, Ginette Villeneuve, and Jeanne Martin has made this department feel like a home for me and I will miss them greatly.

This thesis would not have come to completion if not for the endless help of Todd Karwoski, the department's computing assistant. He went above and beyond the call of duty and I am sincerely appreciative.

Lastly, I would also like to thank my fellow graduate students of the geology department for their support and camaraderie. Callan Bentley became a great friend and sympathizer of hardships experienced during the scientific process. He helped to

make my transition from student to teacher smooth and painless. I would like to thank Dave Johnston and Leah Englander for pulling me through this experience, for listening to my complaints, and for riding this roller coaster with me. Your friendships have made me a better person. Who knew an arbitrary office assignment would result in such friendships? We are we!

Table of Contents

List of Tables

List of Figures

Chapter 1: Introduction and Background

Introduction

Chrysotile is an asbestiform mineral that has numerous industrial applications including its use as a refractory component and in friction products, such as brake linings. It has been the subject of major health concerns associated with occupational and environmental exposure. Unfortunately, there is limited understanding of the composition and physical characteristics of mineral particles released to the environment during mechanical processes such as automotive braking. These characteristics determine the biological impact on exposed humans and depend upon the rate of chrysotile decomposition as a function of temperature, pressure, time, and chemical environment. This study examined the decomposition of chrysotile as a function of time and temperature. Chrysotile was heated at constant temperature in air from 200-1000°C for 4 to 720 hours. After heating, the refractive indices of the fibers were measured by oil immersion with the petrographic microscope. The decomposition of chrysotile and growth of mineral phases were investigated by using a Phillips analytical X-ray diffractometer. This study aimed to provide information that would help to understand the mineralogy of particulates released during processes such as automotive braking as well as information about the temporal and thermal boundaries of chrysotile decomposition and the formation of new mineral phases. No actual brake material was used in this study.

Background

Asbestos is a term given to the asbestiform varieties of amphibole and chrysotile minerals. The asbestiform habit consists of fiber bundles of extremely long and thin fibers that are easily separated from one another by hand pressure. Asbestiform amphiboles and chrysotile have industrial importance because they possess high tensile strength, flexibility, resistance to chemical and thermal degradation, electrical resistance, as well as the ability to be woven (Virta, 2001).

Chrysotile is the sole asbestiform species in the serpentine group and the most common type of asbestos used in the United States (Virta, 2001). Crocidolite (asbestiform riebeckite), amosite (asbestiform grunerite), anthophyllite asbestos, tremolite asbestos, and actinolite asbestos are all regulated as asbestos. Table 1 shows the classification of the asbestiform minerals within the amphibole and serpentine groups.

Table 1: Amphibole and serpentine minerals regulated as asbestos. Information provided includes the mineral group, variety within the group, and the chemical formula.

Group	Mineral	Formula
Amphibole	Anthophyllite-asbestos	$Mg_7Si_8O_{22}(OH)_2$
	Amosite	$(Fe^{2+},Mg)_7Si_8O_{22}(OH)_2$
	Crocidolite (Blue Asbestos)	$Na_2Fe^{3+}{}_2(Fe^{2+},Mg)_3Si_8O_{22}(OH)_2$
	Tremolite-asbestos	$Ca_2Mg_5Si_8O_{22}(OH)_2$
	Actinolite-asbestos	$Ca_2(Mg,Fe^{2+})_5Si_8O_{22}(OH)_2$
Serpentine	Chrysotile (White asbestos)	$Mg_3Si_2O_5(OH)_4$

There are many applications for asbestos, most being practical solutions to difficult problems. In general, the applications include: insulation, fireproofing, floor tiles, asphalt, automobile brakes-friction products, roofing shingles, gaskets, packing materials, textiles, and plastics. Asbestos has been used in thermal insulation and fire proofing for the construction industry, filler for plastics and cement, and in brake and clutch linings for the automotive industry. Asbestos is not normally used alone in its raw, fibrous state. It is added to materials such as cement, vinyl, plastic, asphalt, and cotton. Incorporating asbestos into industrial products helps to improve the reliability of the product and decreases the cost (Virta, 2001).

In particular, chrysotile has been vital to the automotive industry. Brake lining, clutch facings, and other heavy-duty friction materials have contained up to 60% chrysotile asbestos. Of the total amount of asbestos produced, more than half has been used in asbestos-cement products, the main function of which is to act as a

fibrous reinforcement in the cement. Uses include flat sheets, siding, tiles, roofing sheets, and water pipes. The bulk of the asbestos used in these building products is chrysotile (Hodgson, 1979). Most of these products are installed on a commercial basis under conditions regulated by OSHA (Virta, 2001).

Society's knowledge of the ill effects of asbestos arises directly from exposed workers. Adverse effects have been primarily associated with workers heavily exposed to asbestos in occupational settings, particularly those who applied asbestos to ships during World War II. Public concern for the potentially severe health effects of asbestos escalated in the 1970's when the United States Environmental Protection Agency (EPA) declared a ban on asbestos use for building materials (Benarde, 1990).

Asbestos production started to decline in the 1970's due to these concerns, especially the concerns over health risks caused by high exposures to airborne asbestos and the EPA ban on asbestos in building materials. Public pressure resulted in the reduction of exposure limits and the exploration for an asbestos alternative. Commercial products containing asbestos were slowly pulled back due to the fear of impending liability (Virta, 2001). On July 12, 1989, EPA issued a rule banning most asbestos-containing products. In 1991, this regulation was modified which resulted in the ban of the following specific asbestos-containing products: flooring felt, rollboard, and corrugated, commercial, or specialty paper. In addition, the regulation continues to ban the use of asbestos in products that have not previously contained asbestos, otherwise referred to as "new uses" of asbestos (Fisher, 1992).

However, today chrysotile is classified as a carcinogen and exposure is regulated. Research, followed by the 1970's asbestos concern, led to the consensus that asbestiform amphibole minerals are mainly responsible for mesothelioma, whereas chrysotile alone has little or no mesothelioma-producing potential (Dunnington, 1988). Ross (1984) reported that chrysotile has had only a small carcinogenic effect on humans who have been occupationally exposed, and there is little evidence that nonoccupational exposure has caused any harm. Lung cancer has

been reported to have been caused by chrysotile, anthophyllite asbestos, amosite, and crocidolite, particularly in asbestos workers who smoke cigarettes. Studies have shown that asbestos and cigarette smoke combine to produce a significant risk of lung cancer to those who have been heavily exposed. It is very difficult to predict accurately the health effects of occupational exposure to carcinogens such as asbestos because health effects are modified by the individual's life-style, although it is clear that risk of lung cancer due to asbestos exposure is lower in nonsmokers than smokers (Ross, 1984). To avoid exposure to humans, industries now market dense and non-friable materials in which the chrysotile fiber is encapsulated in a matrix of either cement or resin. These modern products include chrysotile-cement building materials, friction materials, gaskets and certain plastics (Virta, 2001). Although legislation has been introduced in the U.S. Senate to ban all uses of asbestos, health concern is prevalent and the release of chrysotile into the air of garages where brake maintenance and repair is undertaken is currently studied worldwide (Langer, 2003).

Both chrysotile and asbestiform amphibole minerals originate from metamorphic processes. In the United States, they occur predominately along the eastern seaboard from Alabama to Vermont, the western seaboard from California to Washington, and in the upper Midwest from Minnesota to Michigan. These altered rock occurrences commonly yield commercial asbestos deposits containing less than 6% asbestos by volume. Currently, no asbestos is mined in the US (Virta, 2001, 2002). Major chrysotile deposits located outside the United States are found in the southern Ural Mountains of the Soviet Union, southeastern Quebec, the Italian Alps, Australia, and Africa (Myer, 1990). Nearly all of the asbestos produced worldwide is chrysotile, and it is the only type of asbestos used in the US today. US consumption of asbestos was estimated to be 6,850 metric tons in 2002, a decrease from 13,100 metric tons in 2001, most being imported from Canada. Peak US consumption of asbestos was 719,000 metric tons in 1973, whereas the peak world production was 5.09 million metric tons in 1975. Worldwide, the use of asbestos has also declined (Virta, 2002).

Although the common link of asbestiform minerals is their fine fibrous habit, chrysotile and amphibole are different from one another in both structure and composition. Chrysotile asbestos is the only asbestiform mineral of the serpentine mineral group; it is a hydrated magnesium silicate with the general formula of $Mg_3Si_2O_5(OH)_4$. It has a layered structure with one layer consisting of linked silicate tetrahedra joined to a brucite octahedral layer. The dimensions of the tetrahedral layer are about 9% smaller than the corresponding brucite layers resulting in a mismatching of the two units. The curvilinear scroll or coil structure of chrysotile is attributed to this mismatch. The central axis of this coiling forms the long axis of the fiber. The brucite layer forms the external surface of chrysotile resulting in the fiber having characteristically alkaline surface chemistry, high surface potential, and hydrophilic tendencies (Deer et al., 1966; Hodgson, 1979; Myer, 1990). A structural depiction of chrysotile asbestos is shown in Figure 1.

Figure 1: Diagram of the structure of a chrysotile fiber formed of several scrolls of individual crystallites. Each scroll consists of a connected double layer consisting of brucite-like units on the outer surface and silicate tetrahedra units in the inner surface. Adapted from Hodgson (1979) and O'Hanley (1996).

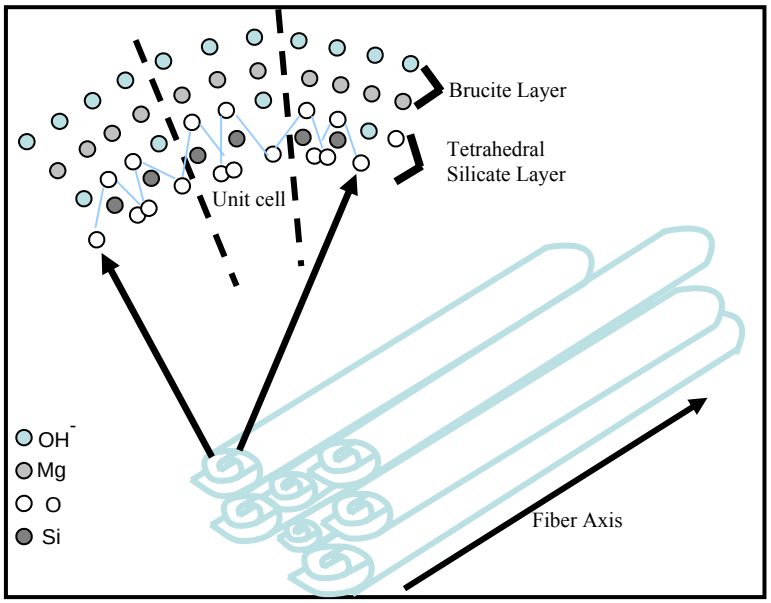

The foundation of serpentine crystal structure was established by Whittaker and Zussman (1956) by the analysis of X-ray power-diffraction patterns. They clarified that serpentine could form three different crystal structures: (1) the rolled-cylindrical structure of chrysotile, (2) the planar structure of lizardite, and (3) the modulated wave structure of antigorite. Further study of chrysotile's complex structure led Wicks and Whittaker (1975) to suggest that the layers of chrysotile could be stacked in three different ways producing three different polytypes. All three have the same structural design and composition, but differ in the way the successive layers are stacked. Clinochrysotile (chrysotile-$2M_{c1}$) is the most abundant and occurs alone or mixed with small amounts of orthochrysotile (chrysotile-$2O_{cl}$) or with lesser amounts of parachrysotile (where 2=the number of layers in the cell, M=monoclinic c=cylindrical, and 1= the polytype number). Clinochrysotile and orthochrysotile have the *a* axis parallel to the fiber and parachrysotile has the *b* axis parallel to the fiber. As a result of the work performed by Whittaker and Zussman (1956) and later publications, the X-ray diffraction criteria necessary for the identification of serpentine minerals is well established, and high quality X-ray patterns have been published and refined (Wicks, 2000).

The composition of chrysotile rarely deviates from the ideal composition of $Mg_3Si_2O_5(OH)_4$. Substitutions that occur include coupled substitution of aluminum or ferric iron for magnesium and silicon and the substitution of ferrous iron for magnesium (Deer et al, 1966). Trace amounts of Ni, Co, Cr, and Mn are found in all chrysotile asbestos products; this presence is believed to be partially due to the accessory minerals and partially due to free metallic impurities derived from milling machinery (Hodgson, 1979).

Chrysotile fibers are flexible, parallel in columnar growth, strong and easily separable by hand pressure. Fibers have a silky luster, are rarely brittle, and vary in color from green to brown (Myer, 1990). In thin section, chrysotile has a low to moderately low relief and is colorless to pale green with weak pleochroism. The optic orientation requires the slow ray vibration direction to be parallel to the length

of the fibers, which results in parallel extinction. Indices of refraction correspond to changes in cation composition and as a general rule can be related directly to Fe:Mg ratios. Indices of refraction increase rapidly with substitution of Fe for Mg, and less rapidly with substitution of Al. Determining indices of refraction is difficult and only those parallel and perpendicular to elongation can be measured in grain mount. Reported indices of refraction for serpentine minerals include: n_α=1.529-1.595, n_β=1.530-1.603, and n_γ=1.537-1.604. Birefringence is 0.001-0.010 (Deer et al., 1966; Hodgson, 1979; Nesse, 1991).

Serpentinites are rocks composed predominately of the serpentine minerals lizardite, chrysotile, or antigorite with accessory magnetite, brucite, and Mg and Ca-Al silicates. Serpentinites are of fairly widespread occurrence, being found in Alpine–type setting and on the ocean floor. In most occurrences serpentinites were originally ultramafic igneous rocks, such as periodite and dunite. Serpentinites are formed from these rocks by hydrothermal metamorphic processes, that result in fine-grained serpentine minerals. The formation of serpentinites involves the hydration of anhydrous (olivine and pyroxene) or less-hydrated (anthophyllite and talc) Mg-rich silicates and carbonates by the hydration of forsterite to serpentine + brucite:

$$2Mg_2SiO_4 + 3H_20 \rightarrow Mg_3Si_2O_5(OH)_4 + Mg(OH)_2.$$

Serpentine minerals can form by the recrystallization other existing serpentine minerals to other serpentine minerals. One or more of the minerals lizardite, chrysotile, and antigorite dominate mineral modes in serpentinites.

Chrysotile is probably produced in an episode of transformation from other serpentine minerals under conditions of relatively low but increasing temperature. Chrysotile can alternatively be derived from impure siliceous dolomite. Chrysotile is usually found in veins within serpentinites or in the form of disseminated short fibers (Zussman, 1979). O'Hanley (1987) performed a detailed geologic study of chrysotile ore from the Jeffery Mine located in Thetford, Quebec and found that the chrysotile was localized in veins that developed in large blocks of partially serpentinized

peridotite bound by zones containing schistose serpentine. In general, chrysotile deposits usually have cross-fiber veins filling extension fractures in large blocks bound by shear zones.

The equilibrium relationships involving serpentine minerals in the system are MgO-SiO_2-H_2O discussed by O'Hanley (1996). He states that serpentine minerals are dehydrated to form less-hydrous mineral assemblages such as olivine + talc (± chlorite). Within this process, starting minerals such as antigorite, lizardite, or chrysotile are replaced by olivine plus other phases as temperature increases. These reactions are endothermic and produce water. Pressure-temperature relations among the phases chrysotile, antigorite, brucite, forsterite, talc, enstatite, anthophyllite, quartz, and water illustrated by Berman et al. (1986) show that chrysotile → antigorite + brucite at temperatures above ~250˚C and antigorite + brucite → forsterite + water at temperatures above ~400˚C (Figure 2). Also, as pressure increases the temperature at which chrysotile → antigorite + brucite decreases. A better understanding of the mineral reactions at equilibrium will serve as a basis for the experimental study of the thermal transformation of chrysotile.

Figure 2: Diagram adapted from Berman et al. (1986) depicting the pressure-temperature relations in equilibrium among the phases of chrysotile (Ctl), antigorite (Atg), brucite (Brc), forsterite (Fo), talc (Tlc) enstatite (En), anthophyllite (An), quartz (Qtz) and H_2O, in the system of MgO-SiO_2- H_2O. This diagram does not accurately portray the phase relations at P< 1 kbar.

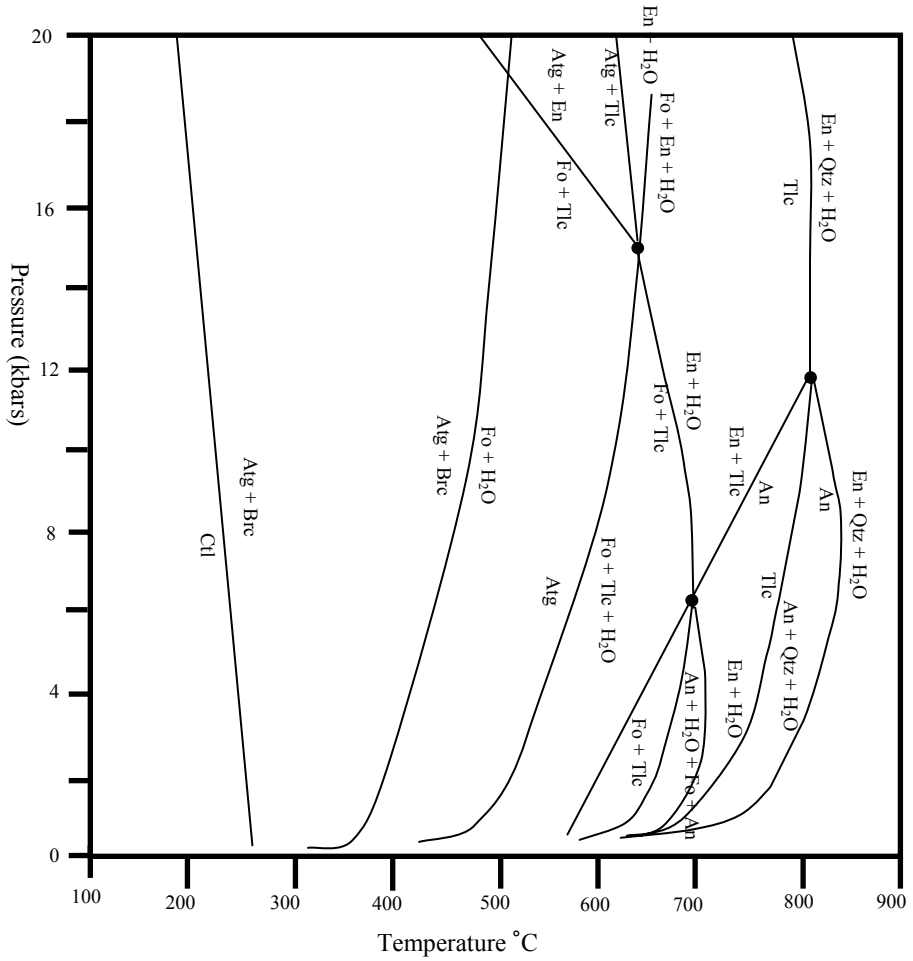

Chapter 2: Previous Work

Thermal Decomposition of Chrysotile

Faust and Fahey (1962) reported that since the early work of Rammelsberg in 1869 and Caillere in 1933, the nonequilibrium thermal decomposition of chrysotile has been studied in depth by differential thermal analysis (DTA), thermogravimetric analysis (TGA), and X-ray diffraction. DTA involves heating and cooling a test sample and inert reference under identical conditions while recording any temperature difference between the sample and reference. TGA measures the amount and rate of change in the weight of a material as a function of temperature or time in a controlled environment. Variation and contradiction in the temperature ranges for the step processes in the decomposition sequence are prevalent in the literature.

Typical thermal analysis curves (DTA) (Figure 3) show a dehydration endotherm occurring at ~650˚C, whereas on TGA, initial dehydration is shown as a gradual weight loss between 100-600˚C. Weight loss results from the exit of any volatile component; for chrysotile the volatile component is water. Most commonly, the literature reports that the dehydration of chrysotile is complete within the range of 600-780˚C (Hodgson, 1979). Faust and Fahey (1962) performed DTA and reported an endothermic peak, representative of chrysotile dehydration, between 525-665˚C. Cattaneo et al. (2003) performed DTA and reported a broad endothermic peak between 600-800˚C, also representative of chrysotile dehydration. Ross and Vishwanathan (1981) studied the dehydration reactions of chrysotile asbestos below 500˚C by using TGA and IR spectroscopy, and found water as the main product due to the presence of two stages of endothermic reactions; one between 200-300˚C and the other between 300-500˚C. Most recently, Langer (2003) reported complete water loss for chrysotile heated at 650±20˚C.

Typical thermal analysis curves (DTA) represent the recrystallization as an exotherm occurring at 800˚C whereas this is represented as a sharp weight loss above

600˚C on TGA (Figure 3). This weight loss may be a step function, with peaks at ~260˚C and ~320˚C. Literature reports that the transformation to forsterite takes place in the range of 800-850˚C via X-ray diffraction techniques (Hodgson, 1979). Using single crystal and powder X-ray diffraction, Brindley and Zussman (1957) found the presence of a forsterite pattern within the temperature range of 575-600˚C and absence of the serpentine pattern at 625˚C. Cattaneo et al. (2003) reported a decrease in the intensity of the chrysotile pattern starting at 600˚C via synchrotron powder diffraction techniques. Examining results of past DTA experiments, Martinez (1966) reported forsterite above 750˚C and enstatite present above 850˚C. Faust and Fahey (1962) performed DTA and reported an exothermic reaction between 785-803˚C, which they attributed to recrystallization. de Souza Santos and Yada (1979) used high resolution electron microscopy and selected area electron diffraction and reported forsterite nucleation when chrysotile was heated at 650˚C.

Figure 3: Typical thermal analysis diagram for the decomposition of chrysotile adapted from Hodgson (1979). For the DTA, the endotherm represents the dehydration and the exotherm represents forsterite crystallization. For the TGA, the gradual weight loss between 100-600˚C corresponds to the dehydration reaction of chrysotile.

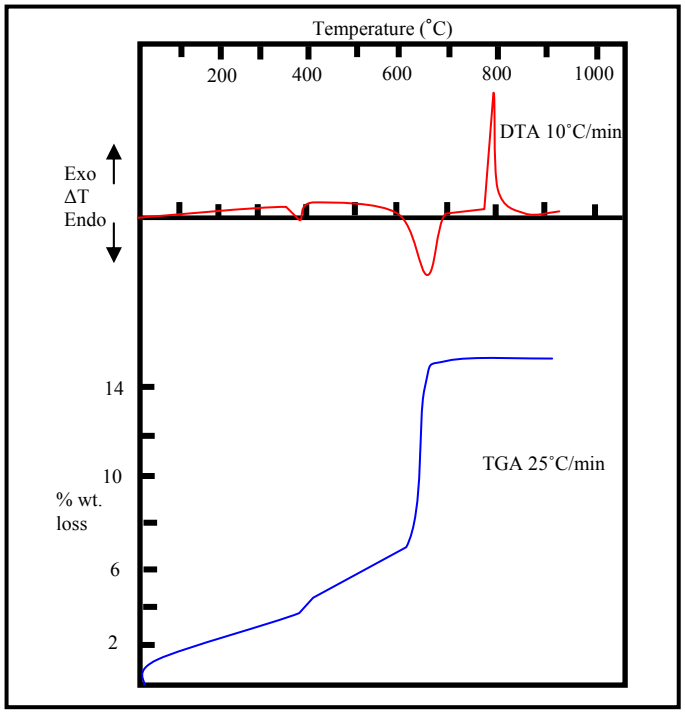

Mechanisms of Dehydration and Recrystallization

An investigation of the decomposition of chrysotile performed by Ball and Taylor (1963) via X-ray rotation photography suggested that the sequence of reactions can be detailed by using four stages as follows:

(1) Dehydration: Protons migrate to reaction zones where water molecules are condensed and liberated. Simultaneously, Mg and Si ions counter-migrate and the oxygen packing remains essentially intact. The product is partially disordered.

(2) Cation Reorganization: Mg and Si ions begin to diffuse in opposite directions, forming Mg-rich and Si-rich regions.

(3) Forsterite Crystallization: Ordering of the Mg-rich region and a change in the packing of oxygen ions results in the formation of forsterite.

(4) Enstatite Formation: The Si-rich regions change to enstatite. This stage resembles stage (3) yet occurs less readily and is easily halted.

Brindley and Hayami (1965) confirmed the first stage of dehydration and the formation of an X-ray amorphous phase, and simplified the mechanism proposed by Ball and Taylor (1963) stating that below 1000˚C, the reactions can be broken down into two stages of (1) dehydration and (2) recrystallization.

MacKenzie and Meinhold (1994) investigated the decomposition of chrysotile via solid state nuclear magnetic resonance and reported that the thermal behavior of chrysotile is more complex than reported by previous studies based on X-ray diffraction and electron microscopy, in that two different dehydroxylates are formed. Dehydroxylate I forms first and contains Si environments with interatomic distances and Mg coordination numbers not different from the original chrysotile. Dehydroxylate II appears concomitant with the forsterite formation and is Si-rich when compared to Dehydroxylate I. Dehydroxylate II is X-ray amorphous although it has well defined Si sites and has a greater thermal stability than dehydroxylate I. Dehydroxylate II disappears above temperatures where free silica is found and forsterite continues to form.

Mechanisms of two kinds have been suggested to explain the ordered nature of the reaction which occurs when hydrated silicates are heated in air and water molecules exit the crystal structure:

(1) OH-pair interaction: $OH + OH \rightarrow H_2O\uparrow + O$ and

(2) Proton migration: $H + OH \rightarrow H_2O$.

Although these mechanism focus on the formation of water molecules and their departure from the crystal structure which represents the dehydration, the counter-migration of Mg and Si ions is also included which represents the recrystallization.

OH-pair interaction is called the homogeneous mechanism and appears to offer a reasonable explanation for the maintenance of the crystallographic order, yet has serious difficulty explaining the departure of the water molecules without disordering the structure and the migration of SiO_2.

Protons migration, called the heterogeneous mechanism, emphasizes the maintenance of an oxygen arrangement and accounts for the topotactic character of the reaction as well as providing plausible mechanisms for the loss of water. This mechanism also provides an explanation for the formation of intermediate and transitional states mentioned throughout the literature. Within this mechanism, protons migrate to reaction zones such as external surfaces or grain boundaries. It is suggested that as the counter-migration of cations occurs away from these reactions zones pores form within the crystal structure providing a pathway for the loss of water. These pores were later confirmed by Martin (1997) by using transmitted electron microscopy. He found that long cavities opened within the (00*l*) planes in the fiber wall and extended along the fibers. Cattaneo et al. (2003) suggested that the preferred diffusion pathway of water molecules occurs along the fibril axis.

Whichever mechanism of dehydration and recrystallization occurs, it is reported that the anhydride phase tends to be disordered and could be the origination of the broad, low angle X-ray reflections reported in the literature. It has also been

suggested that the rate of dehydration determines which mechanism is used. It is possible that as the rate of dehydration increases, the reaction mechanism passes from proton migration towards an interaction of paired hydroxyl ions; the latter is likely to create disorder while proton migration would facilitate a topotactic reaction (Brindley and Zussman, 1957).

Further, Hodgson (1979) also relates that the water loss discussed in the literature has the possibility to originate from two different environments within the structure of chrysotile. Based on the ideal formula, the tetrahedral layer contains 3.25% water while the brucite layer contains 9.75% water. The main dehydration loss of chrysotile comes from the hydroxyls of the external brucite layer while the remaining dehydration observed by thermal analysis curves comes from the remaining internal hydroxyl groups. It is concluded from the literature that once heated, protons migrate within the tetrahedral layer to a donor site within the tetrahedral layer resulting in the formation of water. This initial proton migration takes place beginning at 100˚C and extends until 600˚C. This process does not begin in the brucite layer until chrysotile is heated at 600˚C. This two step dehydration occurring from two locations within the structure has been observed on some thermal analysis curves (TGA) (Figure 3).

Selected Observations from the Literature

Despite the variations and inconsistencies discussed above, many interesting observations can be taken from the literature. Hodgson (1979) reported past studies that found a slight increase in tensile strength followed by a rapid decrease in tensile strength when asbestos fibers were heated up to 800˚C (Figure 4). He suggests that the slight increase in tensile strength seen in chrysotile is due to increases in shear modulus arising from modifications to the interfibrillar component in the fiber. The decrease in tensile strength is thought to be due to the structural and decompositional changes associated with the loss of structural water.

Figure 4: Tensile strength of heated chrysotile asbestos adapted from Hodgson (1979). The tensile strength changes when chrysotile is heated up to temperature of 800˚C; it increase slightly before diminishing rapidly.

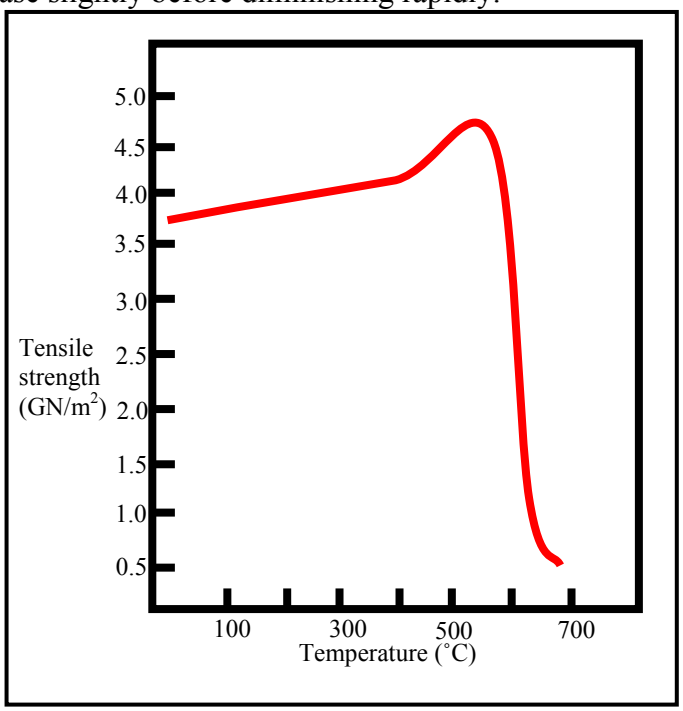

Brindley and Hayami (1963) reported that particle size has a relationship to the decomposition of chrysotile and formation of forsterite. For any given temperature studied, forsterite developed more rapidly from coarse powdered massive serpentine than the fine powdered serpentine. This was the reverse of dehydration behavior in which smaller particles reacted more quickly than larger particles. They observed that the dehydration and forsterite formation show an inverse relationship wherein the faster the dehydration, the slower the forsterite formation and vice versa. They also observed that with slow rates of dehydration, the amount of forsterite developed was greater than with more rapid dehydration. Martinez (1961) confirmed the observation of Brindly and Hayami (1963). He examined the effect of particle size by using DTA and TGA and found that the dehydration of chrysotile occurred at lower temperatures when ground. He concluded that this occurred due to the increase in surface area which allowed the OH^- to leave the crystal structure more readily.

Low angle background scattering present in X-ray photographs of heated chrysotile was first reported by Hey and Bannister (1948). This was later expounded on by the reported presence of broad X-ray reflections corresponding to approximately 10-15Å spacing range found by Brindley and Zussman (1957) when chrysotile fibers were heated above 550˚C. These findings were confirmed repeatedly within the literature that followed. Brindley and Zussman (1957) suggest that these broad low angle reflections represent an intermediate phase in the decomposition, specifically after the dehydration of chrysotile in air. They also suggest that the broad reflection signifies a disordered phase, the formation of a new phase with a very fine-grained texture or small crystallites, but not a representation of a structure of any reaction product. Martin (1977) also reported strong broad low angle X-ray reflections in the 10-13Å spacing region when chrysotile was heated at 580˚C. The NMR data of McKenzie and Meinhold (1994) showed the presence of a broad X-ray reflection possibly associated with the first of the two weight loss processes that produced an amorphous anhydrous phase classified as dehydroxylate I. They suggest that the broad, low angle X-ray reflections represents diffraction from long cavities observed by electron microscopy which open up on the fiber walls when chrysotile is heated at certain temperatures.

de Souza Santos and Yada (1979) studied the thermal transformation of chrysotile in air by using high resolution electron microscopy and selected area electron diffraction. No morphological changes were observed when chrysotile was heated up to 600˚C, although further confirmation of the X-ray reflection within the 10-15Å d-spacing was made. They suggest this reflection is parallel to the 7.3Å d-spacing present in chrysotile and a favorable site for the nucleation of forsterite. When heated at temperature above 650˚C the chrysotile pattern degraded and the forsterite pattern appeared; at 1000˚C enstatite formed intergrown with grains of forsterite. From the lattice images, a topotactic relationship between chrysotile and forsterite as well as between forsterite and enstatite was observed.

The only optical analysis related to the decomposition of chrysotile reported in the literature was performed by Hey and Bannister (1948). The refractive indices and the sign of elongation were measured for three heated treated samples from Thetford, Canada. The experimental conditions include 900˚C for 5 hours, and 1000˚C for 5 and 12 hours. The indices of refraction were reported to be 1.56-1.57, 1.59, and 1.61-1.62 respectively while the signs of elongation were reported to be positive, positive, and negative respectively.

Project Scope

Inconsistencies found in the previous DTA and TGA studies concerning the nonequilibrium thermal decomposition of chrysotile can be attributed to numerous factors such as sample source, sample preparation, sample mineralogy, experimental methodology, and analysis technique. Temperature calibration or methodology could have also contributed to variation in the data collected. Both DTA and TGA are rate-specific and cannot conclusively identify any products. Information from TGA and DTA is only pertinent to the heating rates of the particular experiment in question. Mineralogical compositions and transitions in relation to temperature cannot be evaluated from the experiments by using DTA or TGA because the temperature is always changing. Further, conditions such as sample source, treatment, method of heating and rate, and method of product identification were not always communicated in the literature discussed above. This study aims to clarify the temperature and time decompositional boundaries of dehydration and recrystallization as well as reaction products and intermediate phases.

In this study, the extent of reaction will be determined after specified periods of time at selected temperatures. The extent of any reaction is a function of the rate of the reaction and the time scale of the experiment. The rate of reaction can be related to temperature as well as other variables by the equation presented by Lasaga (1998):

$$\text{(Equation 1)} \quad r = A * e^{-E/RT} * f(\Delta\mu_r)$$

where A=the surface area, and therefore related to the particle size, E=the activation energy, R=the gas constant, T=the absolute temperature, and $\Delta\mu$=the chemical potential of the reaction. The first term in equation 1, the reactive surface area (A), is clearly important in reactions of the form

$$A + B \rightarrow \text{Products}$$

because such reactions occur at interfaces. In chrysotile, particle size or surface area may still be important because water must diffuse out of the chrysotile fiber.

In general, the rate of the chemical reaction is usually limited by the slowest or rate-determining step. In this study, we are concerned primarily with the rate of reaction, as well as the specifics products formed as a function of time and temperature. Whatever the rate determining step is, it will have a characteristic activation energy (E). For example, if Mg-O bond breaking is a rate determining step then the activation energy will be related to the Mg-O bond energy. Alternatively, the activation energy may be more characteristic of a diffusive mechanism.

The second term in equation 1 shows that the rate of the reaction decreases as the activation energy increases. Further, this term shows that the effect of the magnitude of the activation energy lessens with increasing temperature.

The third term in equation 1 is a function of the chemical potential of the reaction; that is, this term indicates the irreversibility of the reaction as measured by the change in the chemical potential of the reaction ($\Delta\mu_r$) where:

$$\Delta\mu_r = \mu^o_{\text{forsterite}} + \mu^o_{\text{enstatite}} + 2\mu^o_{\text{water}} - \mu^o_{\text{chrysotile.}}$$

The individual μ^o values represent the chemical potentials of the end-member minerals at the pressure and temperature of interest. At equilibrium, the change in chemical potential of the reaction equals zero ($\Delta\mu_r = 0$), with the change in chemical

potential becoming increasingly negative with increasing departure of the reaction from equilibrium.

Nagy and Lasaga (1992) expressed the general equation

$$\text{(Equation 2)} \quad f(\Delta\mu_r) = 1\text{-exp}\ (m * (\Delta\mu_r/RT)^n)$$

where m and n are adjustable constants. As $\Delta\mu_r$ becomes increasingly negative, the exponential term becomes smaller and $f(\Delta\mu_r)$ therefore increases. When $\Delta\mu_r = 0$ at equilibrium, $f(\Delta\mu_r) = 0$ and therefore according to equation 1 the rate of the overall reaction equals zero.

In this study, surface area and particle size are not varied. Increased temperature affects both the second and the third term of equation 1. In particular, the rate of the reaction is promoted by the irreversibility of the reaction with increasing temperature as seen by the third term of equation 1, and by the intrinsic effect of temperature on the rate of the reaction for a given degree of irreversibility as seen by the second term in Equation 1.

This study provides information concerning a time-temperature relationship in the thermal decomposition of chrysotile that has yet to be considered in any of the literature relevant to the topic. This is possibly due to the fact that published research concerning the thermal decomposition of chrysotile has only been performed on a short time scale; there are no studies that extend beyond a few days while most studies are no longer than eight hours.

It has been suggested that the decomposition of chrysotile to forsterite, and later enstatite, may involve the formation of intermediate phases represented by broad X-ray reflections observed by using X-ray diffraction. There is much speculation concerning the degree of structure in these intermediate phases and the origination of

the broad X-ray reflections. This study provides further information concerning the nature of these phases.

Lastly, the use of optical mineralogy as a systematic and extensive analytical technique to investigate the thermal decomposition of chrysotile has not been found in the literature. The refractive index of a mineral is an indicator of chemical and/or structural change. This study aims to provide additional information about the thermal decomposition of chrysotile by measuring the changes in RI after heating.

Chapter 3: Experimental Design and Analytical Procedures

Sample Preparation

Sample Source

Chrysotile from Thetford Mines District in Quebec, Canada from the USGS given to Dr. Wylie was used as the starting material for all experiments. The sample used in this study is pure clinochrysotile (chrysotile-$2M_{cl}$). Thetford is located in one the world's largest asbestos producing regions. It is 50 miles south of Quebec in the Notre Dame Mountains and located on the River Becancour. Asbestos was first discovered in the region in 1876 (www.tiscali.co.uk). Clinochrysotile was selected because it is representative of the asbestos raw materials used within the past fifty years for a variety of industrial applications (Cattaneo et al., 2003)

Experimental Procedure

Samples were heated at constant temperature in air from 200 to 1000°C for run times between 4 to 720 hours. All experiments were conducted by using calibrated Lindberg one atmosphere furnaces. The thermal gradient for each furnace at different temperatures was determined by using a Type-K thermocouple made of Chromel-Alumel. The average lateral gradient, within the area of the oven utilized, was determined to be 1˚C/ 3.0 cm. Each furnace was heated at specified experimental temperatures; the temperature was maintained and recorded with an internal thermocouple. For each experimental temperature, the tip of the thermal couple was within 1.0-5.0 cm of the sample. This analysis suggests that the experimental temperature for each experiment was within 2˚C of the measured temperature.

For experiments performed at 450˚C and below, fibers were placed onto Corning Glass No. $1^1/_2$ glass slides and stored within Petri dishes. The Petri dishes were placed inside the temperature controlled furnace at the desired experimental temperature and time. For this encapsulation method, all analytical techniques were

performed directly on the glass slide to observe the transformation of chrysotile. Glass slides were stored indefinitely and not reused. For experiments performed above 450˚C, fibers were placed into gold capsules 3 inches long. The tubing had an outer diameter of 0.276 inches and a 0.005 inch wall. A mechanical seal was placed on both open ends of the gold tubing to make a capsule which was then placed inside the furnace at the desired temperature and time. Gold capsules were washed with ethyl alcohol and distilled water and dried between experiments. Heated samples were stored in glass screw top vials. Experiments performed above 450˚C did not utilize the glass slide encapsulation method because the glass slides are unstable at temperatures greater than 450˚C. The approximate weight of each sample used prior to heating was 0.10 grams.

Optical Analysis

The starting material and run products (after heating) were optically characterized by measuring the refractive indices of single fibers. The refractive index is a primary optical property used to characterize transparent minerals, including those that are asbestiform, during microscopic analysis. Index of refraction (IR) is defined as the ratio of the speed of light in a vacuum to the speed of light in a crystal (Nesse, 1991) and for all the data in this study, IR is for radiation with a wavelength of 589 nm or n_D. Optical analysis was preformed with a Lietz Binocular Petrographic Microscope. Fibers were observed at 125x-250x magnification depending on the dimensions of the fiber of interest. Immersion techniques for microscopic measurement of refractive indices used were dispersion staining and the Becke Line method. Cargille refractive index oils, held between a reservoir with a glass bottom and a glass cover slip, calibrated at 25˚C (dn_D/dT = ~0.0004/˚C) were used as the immersion medium. Both optical analysis methods required a correction for temperature. Temperature was monitored by using a calibrated micro Type-E thermocouple, made of Chromega-Constantan and Teflon, attached to the microscope stage.

The fiber (in situ from heating) was immersed in a liquid of known refractive index. For the dispersion staining method the wavelength at which the refractive index of the liquid matched that of the fiber of interest was obtained from the dispersion staining "color" as detailed in McCrone (1972) (Table 2). The maximum and minimum wavelength of match was determined from the dispersion staining color seen by using the dispersion staining objective. This procedure was repeated on hundreds of separate fibers for each experimental condition. Multiple immersion liquids of known refractive index and dispersion staining plotting paper were used to determine and record the IR ± 0.002 for each experimental condition.

Table 2: Dispersion staining colors observed with the dispersion staining objective with the equivalent wavelength value (nm). Information provided includes the color name observed and corresponding wavelength at which $n_{mineral}$-n_{oil} (McCrone, 1974).

Matching λ_0 (nm)	Dispersion Staining color
<420	light yellow
430	yellow
455	golden yellow
485	golden-magenta
520	red-magenta
560	magenta
595	blue-magenta
625	blue
660	blue-green
>680	pale blue

For experiments heated at temperatures greater than 600˚C, the Becke Line method was used because the dispersion staining "color" was difficult to see. The fiber (in situ from heating) was immersed in a liquid of known refractive index and matches were determined from Becke line colors. This procedure was also repeated on hundreds of separate fibers for each experimental condition. Multiple immersion liquids of known refractive index were used to determine and record the IR ± 0.002 for each experimental condition.

The refractive indices, and the mean refractive index, of minerals observed or referred to in this study are listed in Table 3. All refractive indices are for 589 nm and represent magnesium end-members of mineral where applicable. For identification and comparison purposes, the mean refractive index will be used throughout this study.

Table 3: Refractive Indices and the mean refractive index of minerals observed or referred to in this study. Chrysotile values were taken from this study. The mineral taken from Nesse (1991) are γ-α and the means are γ-α/2.

Mineral	Refractive Index	Mean Refractive Index
Chrysotile	1.554-1.544	1.549
Enstatite	1.657-1.649	1.653
Forsterite	1.669-1.636	1.653
Talc	1.575-1.538	1.557
Tridymite	1.474-1.468	1.471

X-ray Diffraction Analysis

The starting material and run products (after heating) were characterized by using X-ray diffraction analytical techniques. When constructive interference is achieved, Bragg's Law states that if the spacing between the reflecting planes of the atom is d and the half angle of deviation between the beam's incidence and reflection by the plane is θ, the path difference for the waves reflected by successive planes is $2 d \sin \theta$. Constructive interference between radiations reflected from the successive planes occurs when the path difference is an integral number, n, of wavelength λ, resulting in $n\lambda = 2 d \sin \theta$ where n = an integral number, λ = wavelength of the X-ray, d = spacing between the reflecting planes of an atom, and θ = the half angle of deviation between the beam's incidence and reflection by the plane (Klugg and Alexander, 1974). Destructive interference destroys the possibility of reflections that exist at angles other than θ.

All samples were analyzed by using a Philips analytical X-ray diffractometer, model XRG 3100 with a copper target and an excitation potential of 8.86 kV. The samples were placed in aluminum specimen holders. No special methods were used for the sample preparation; sample material was packed into the specimen holder. Due to the fibrous nature, preferred orientation probably occurred and it was a challenge to produce a sample surface that was parallel to the sample holder. The accelerating voltage of the tube was 40kV and the beam current was 25mA with a copper anode with $\lambda(K\alpha 1) = 1.540598$. Samples were run between 2θ angles of 5.5-73.0˚, with a step size of 0.02˚ per second at 0.8 seconds per step. The diffraction patterns were processed and analyzed with the Materials Data Jade software, "Jade 5 XRD Pattern Processing." The Jade software removed data spikes, smoothed the pattern, stripped $K\alpha 2$ peaks, removed background, corrected for an external silicon standard calibration, and identified the likely phases present. For samples that contained forsterite, the Jade software corrected for an internal forsterite calibration (JCPDS file # 34-189) and displaced the pattern to a best fit in addition to the procedures listed above. The phases present in all samples were identified manually. Peaks were manually determined based on the following criteria: symmetrical shape, belonging to set of known peaks within a reference pattern, a width equal to or greater than 0.5˚ theta, and a height equal to or above 1.5 times the noise observed in the diffraction pattern. Phases were identified by matching relative intensity of peaks within the pattern and observed d-spacing to reference patterns found in the International Center for Diffraction Data powder diffraction file (1994). The patterns used are listed in Table 4. The choice of reference pattern used for the starting material of chrysotile was based on the referral by Wicks (2000).

Table 4: Reference patterns used for X-ray Diffraction analytical techniques. Information provided includes the mineral name, the Powder Diffraction File number (PDF#) published by the International Centre for Diffraction Data, formerly the Joint Committee for Powder Diffraction Standards (JCPDS), the chemical formula, and the crystal system.

Mineral	**PDF #**	**Chemical Formula**	**Crystal System**
Anthopholite	9-455	$Mg_7Si_8O_{22}(OH)_2$	Orthorhombic
Brucite	7-239	$Mg(OH)_2$	Hexagonal
Calcite	5-586	$CaCO_3$	Hexagonal
Chrysotile	10-381	$Mg_3Si_20_5(OH)_4$	Monoclinic
Cristobalite	11-695	SiO_2	Tetragonal
Enstatite	22-714	$MgSiO_3$	Orthorhombic
Forsterite	34-189	Mg_2SiO_4	Orthorhombic
Periclase	4-829	MgO	Cubic
Quartz	33-1161	SiO_2	Hexagonal
Talc	13-558	$Mg_3Si_4O_{10}(OH)_2$	Monoclinic
Tremolite	13-437	$Ca_2Mg_5Si_8O_{22}(OH)_2$	Monoclinic
Tridymite	18-1170	SiO_2	Monoclinic

Chapter 4: Results and Discussion

Overview of Results

A total of eighty-two experiments heated at constant temperatures between 200-1000ºC for 4-720 hours were conducted to explore the time-temperature relation of the thermal decomposition of chrysotile. All results are listed in Appendix I. Information provided in Appendix I includes the experimental temperature and run duration, the encapsulation method, the color observed in standard, commercial fluorescent illumination after heating, the morphology observed after heating (1 and 2 discussed below), the refractive index, measured parallel and perpendicular to the length of the fiber, after heating, and the summation of the area under the chosen diffraction peaks of chrysotile, forsterite, and enstatite after heating.

Samples heated at 950˚C for 20 hours and 1000˚C for 24 hours were duplicated to explore the reproducibility of the experimental design. Optical microscopy and X-ray diffraction results of the original and the duplicate for each of the experimental conditions were identical. The results are listed in Appendix I as 950:20-1, 950:20-2, 1000:24-1, and 1000:24-3.

Morphology

The changes in color of the sample, relative to the starting material, was observed and recorded as a function of heating temperature and time. The color transitioned in the following order as temperature and time of heating increased: white, grey white, yellow white, light yellow orange, light orange, orange, and red orange (Figure 5). The color transition suggests that oxidation of the iron end-member component of chrysotile took place and occurred more readily at higher temperatures.

Figure 5: Color transition of samples observed in standard, commercial fluorescent illumination. Pictured from left to right: sample of the starting material from Thetford, Canada, sample heated at 550°C for 24 hours, and sample heated at 1000°C for 24 hours. Throughout heating to 1000°C, the sample retains a fibrous morphology, but the fibrillar structure that is characteristic of asbestos disappears at approximately 600°C.

The starting material, and samples heated at temperature below 600˚C, consisted of wavy fibers and straight bundles within composite clumps (morphology type 1 in Appendix I). Samples heated at temperatures above 600˚C consisted of small fibers and straight bundles within smaller composite clumps which turned to dust when a shearing stress was applied by hand (morphology type 2 in Appendix I). Prior to heating temperatures of 600˚C, the width of individual fibers ranged from approximately 70-130 microns. After heating at temperatures above 600˚C, widths ranged from approximately 10-130 microns. Throughout heating to 1000˚C, the sample retained a fibrous, but not fibrillar, morphology even when chrysotile was no longer detectable.

The optical microscopy portion of this study clearly shows that there is a relationship between particle size of the fiber and the variability observed in the refractive indices. For any given temperature and heating time and within the range of refractive indices measured, larger fibers displayed the lowest refractive index while the smaller fibers displayed the highest refractive index. The observations made from this study concerning particle size are in accordance with the observations of Brindley and Hayami (1963) discussed previously. They found that smaller particles dehydrated more quickly than larger particles. It is possible that the smaller

particles observed are more crystalline and less hydrous, resulting in a higher refractive index when compared to the larger particles which have a lower refractive index; in other word the smaller particles lose water faster than the larger particles. The largest variability in particle width was observed at temperatures between 650-900˚C.

Optical microscopy

In general, index of refraction is determined by chemical composition, atomic structure, and density of a solid or mixture of solids. Often these factors are interrelated. Chemical composition changes when components are added or removed from a system. This would also change the atomic structure due to crystal structure rearrangement which could further lead to a change in density. In this study, changes in chemical composition on the scale of the fibers must only be due to the loss of water or oxidation with atmospheric oxygen because all samples have the same chemical composition, other than volatile contents. The loss of structural water, in general, increases the density of a mineral, therefore increasing the refractive index. In general, crystalline minerals are denser than amorphous minerals due to their atomic structure and therefore have higher refractive indices (Bloss, 1994). In terms of chrysotile decomposition, optical properties could be affected by the formation of nanoporosity as water leaves the structure, the formation of low density minerals or high density minerals, as well as submicroscopic mineral mixtures.

After heating, the refractive indices (IR) of all samples were measured, parallel and perpendicular to the length of the fiber. The IR measured for each experimental condition are listed in Appendix I. These IR ranges represent the indices of refraction observed after the examination of hundreds of individual fibers.

Heating Times of 4-24 hours

Measurements of the IR, measured in polarized light both parallel and perpendicular to the length of the fiber, of samples heated at temperatures of 200-1000ºC for 24 hours are shown in Figure 6. Optical data from this study display a sinusoidal pattern of decreasing and increasing IR as temperature increases. This pattern is also present in shorter heating times, as shown in Figure 7.

Figure 6: IR, measured in polarized light both parallel and perpendicular to the length of the fiber, of samples heated at temperatures of 200-1000ºC for 24 hours. IR is plotted versus temperature (˚C). The length of each bar shows the range from the maximum to the minimum IR observed for each sample from the measurement of hundreds of fibers.

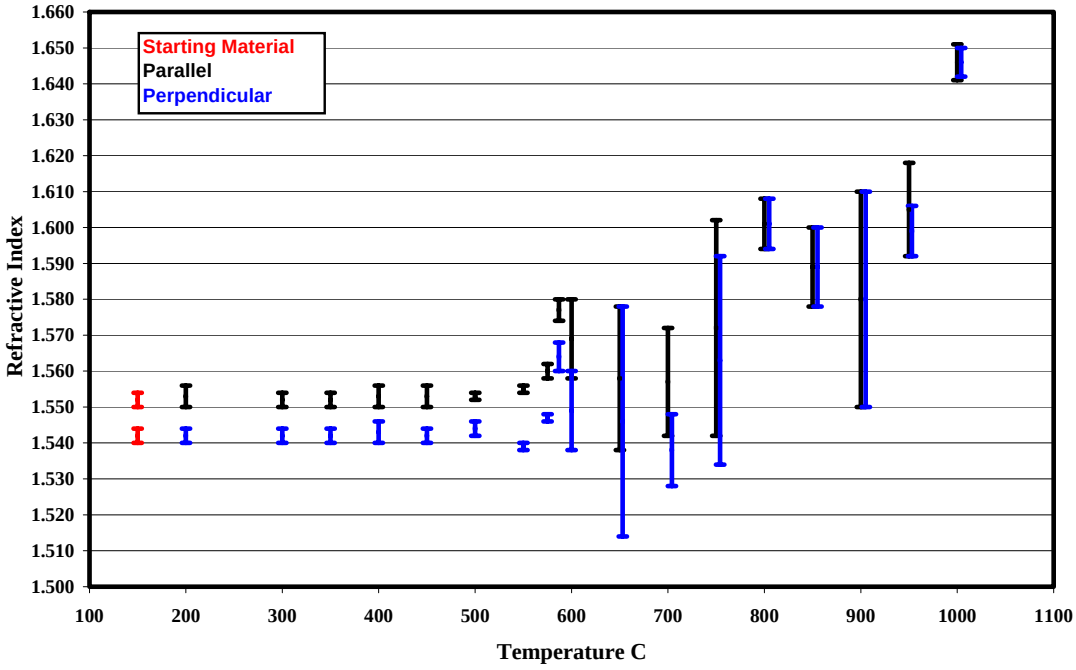

IR measurements of fibers, parallel and perpendicular to the length of the fiber, heated up to 450ºC for 24 hours exhibit no change from those of the starting material. Variability in the IR of the starting material was observed in this study. This variability is due to the inhomogeneity of the starting fibrous material and not considered a cause or directly related to the greater variability seen in IR measurements of samples heated at temperatures above 500˚C.

As temperature increases above 500-1000ºC, an overall trend of increasing IR is observed. This increase is possibly due to the transformation of the amorphous material to crystalline materials with higher IR values than the starting material, such as forsterite ± enstatite. Enstatite and forsterite both have a mean IR of 1.653 while the starting material has a mean IR, measured parallel to the fiber, of 1.552. Also, an increase in IR due to loss of water could result in an increase in the density and therefore an increase in the IR of the fibers. The first change in IR observed occurred at 500ºC where the range of the IR decreased when compared to the IR range of the starting material. This decrease could be reflection of a difference in atomic structure and/or density as chrysotile is dehydrated.

Figure 7: IR, measure in polarized light parallel and perpendicular to the length of the fiber, of samples heated at 200-1000ºC for 4 hours. IR is plotted versus temperature (˚C). The length of each bar shows the range from the maximum to the minimum IR observed for each sample from the measurement of hundreds of fibers. The sinusoidal pattern of increasing and decreasing IR is present in all heating times. Experimental conditions did not include 575ºC for 4 hours.

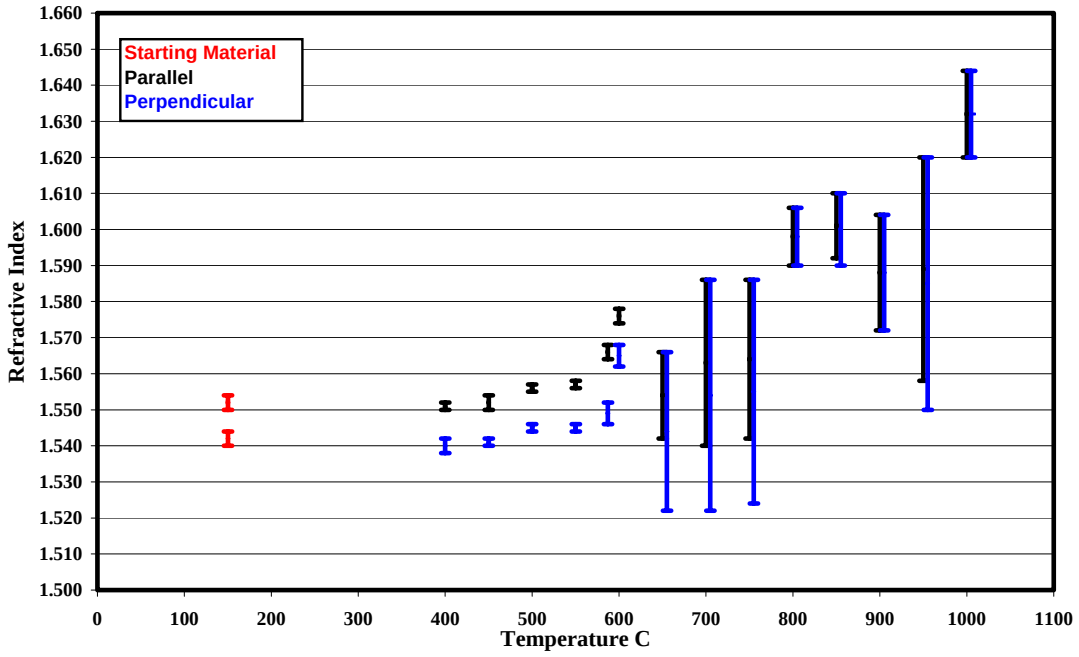

Within the temperature range of 500-1000ºC where an overall trend of increasing IR is observed there are three temporal regions where a decrease, either in the maximum IR or the minimum IR, is observed. These were unexpected results, considering that as a mineral dehydrates, the loss of water should result in the density and a concomitant increase in IR. These regions of decreasing IR within the overall trend of increasing IR are shown in Figure 8. First, at 550˚C, the IR measured perpendicular to the fiber decreased while the IR measured parallel to the fiber increased slightly (the decrease in IR measured perpendicular to the fiber was not observed in shorter time periods). Secondly, a decrease in the maximum IR and the minimum IR was observed between 587-700˚C and thirdly, a decrease in the maximum IR was observed between 800-850˚C and a decrease in the minimum IR was observed between 800-900˚C (the second and third regions of decreasing IR were also observed for all run times <24 hours). The decrease in IR could be due to the formation of nanoporosity within the structure as water is removed, the formation of amorphous material, and/or the formation of low density phases; fibers within the sample are transitioning into amorphous phase(s) and becoming less dense. However, is it possible that the decreases in IR observed at higher temperatures, 800-850˚C or 800-900˚C, may be indicative of the dehydration of amorphous material as opposed to chrysotile.

Figure 8: Areas of decreasing IR, parallel and perpendicular to the length of the fiber, of samples heated at temperatures of 200-1000ºC for 24 hours. IR is plotted versus temperature (˚C). The length of each bar shows the range from the maximum to the minimum IR observed for each sample from the measurement of hundreds of fibers. Regions of decrease IR are shaded with a grey box.

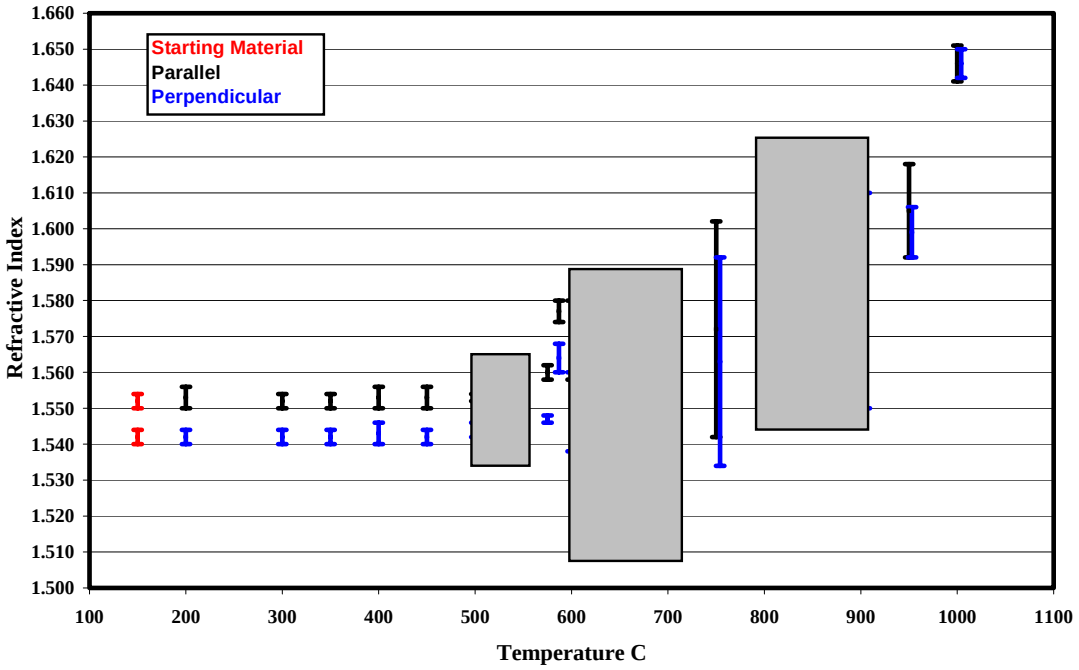

Figure 6 shows that as temperature increases above 650ºC, the fibers exhibit birefringence, lower than the starting material and behave more isotropically, displayed by the indistinguishable measurements of the IR parallel and perpendicular to the length of the fiber. This isotropic behavior begins at 750ºC and continues through 1000ºC and is characteristic of all heating times (compare Figures 7 and 8). Whereas the fiber axis controls the nucleation of new phases at lower temperatures, the crystallographic orientation of new mineral phase nucleation is independent of the fiber axis at higher temperatures, resulting in isotropic fibers.

Variability in the IR of samples heated above 500˚C was observed by the vertical length of the data bar representative of the range in IR. This range is composed of a maximum IR and minimum IR resulting from the measurement of hundreds of fibers within each run product. The progress of water loss, the proportion of amorphous phase present, and the physical state of the mixtures of

fibers and amorphous or new mineral phases occurs at length scales smaller than the wavelength of the incident light and the resolution limit of polarizing light microscopy. At temperatures above 500ºC, mixtures of chrysotile, amorphous material, poorly crystallized material including talc or tridymite, and forsterite and/or enstatite, in any combination could be possible, and the observed range in IR shows the mineralogy of the fibers is quite variable.

The smallest range in IR measured parallel to the length of the fiber, 0.002, occurred when the sample was heated at temperatures between 400-575ºC for numerous heating times. The largest range in IR measured parallel to the length of the fiber, 0.062, occurred when the sample was heated at 950ºC for 4 hours. The smallest range in IR measured perpendicular to the length of the fiber, 0.002, occurred when the sample was heated at temperatures between 200-575ºC for numerous heating times. The largest range in IR measured perpendicular to the length of the fiber, 0.072, occurred when the sample was heated at 950ºC for 4 hours.

The largest decrease in IR, measured both parallel and perpendicular to the length of the fiber, occurred between 600˚C and at 750ºC for all heating times; the decrease was greater when measured perpendicular to the length of the fiber. The largest increase in IR, measured both parallel and perpendicular to the length of the fiber, occurred between 950-1000ºC for all heating times.

The lowest IR measured parallel to the length of the fiber, 1.540, occurred when the sample was heated at 700ºC for 4 hours and 750ºC for 20 hours. The highest IR measured parallel to the length of the fiber, 1.650, occurred when the sample was heated at 1000ºC for 16, 20, and 24 hours. The lowest IR measured perpendicular to the length of the fiber, 1.514, occurred when the sample was heated at 650ºC for 24 hours. The highest IR measured perpendicular to the length of the fiber, 1.650, occurred when the sample was heated at 1000ºC for 16, 20, and 24 hours. The lowest IR measurements both parallel and perpendicular were lower than those of the starting material.

Extended Heating Times

Extended heating times where performed for 2 days, 10 days, and 30 days at specific temperatures of 200, 400, 450, and 500˚C. Among the extended heating times, the largest decrease in IR, measured perpendicular to the fiber, when compared to the starting material, was observed when the sample was heated at 500˚C for 30 days. The IR of the sample heated at 500˚C for heating times up to 30 days is shown in Figure 9. Heating times of 10 days and 2 days did not change the IR significantly as shown is Figure 10.

Figure 9: IR, measure in polarized light parallel and perpendicular to the length of the fiber, of the sample heated at 500˚C for 4-720 hours. IR is plotted versus log time. The length of each bar shows the range from the maximum to the minimum IR observed for each sample from the measurement of hundreds of fibers. The IR, perpendicular to the fiber, changed significantly when compared to the starting material when heated at 500˚C for 30 days (720 hours).

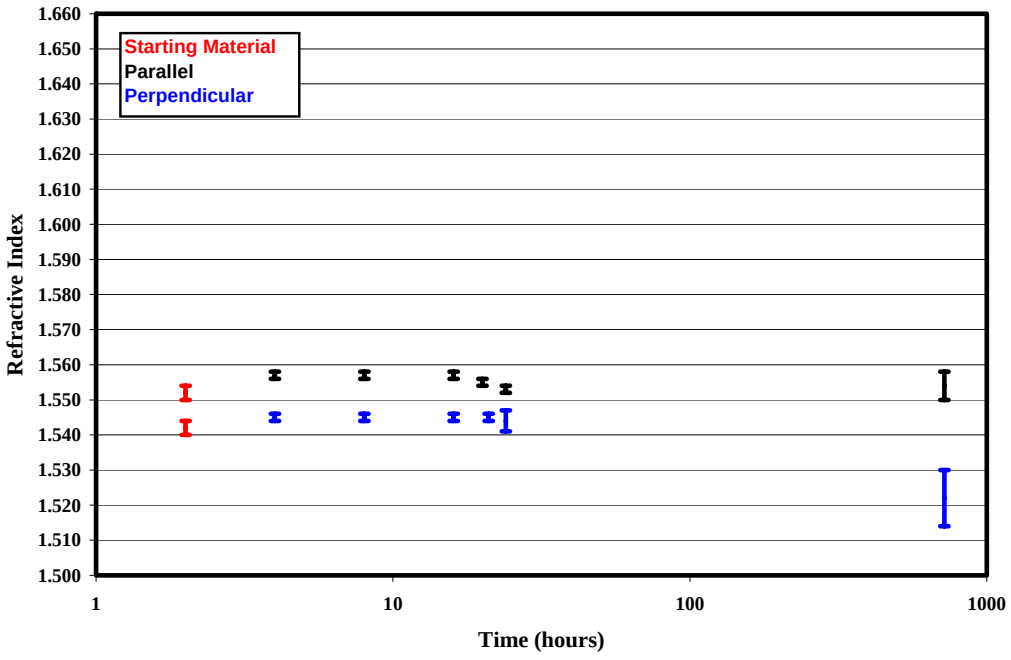

Figure 10: IR, measure in polarized light parallel and perpendicular to the length of the fiber, of the sample heated at 450˚C for 4-240 hours. IR is plotted versus log time. The length of each bar shows the range from the maximum to the minimum IR observed for each sample from the measurement of hundreds of fibers. The IR, perpendicular and parallel, did not change significantly as compared to the starting material when heated for extended times of 2 days (48 hours) or 10 days (240 hours).

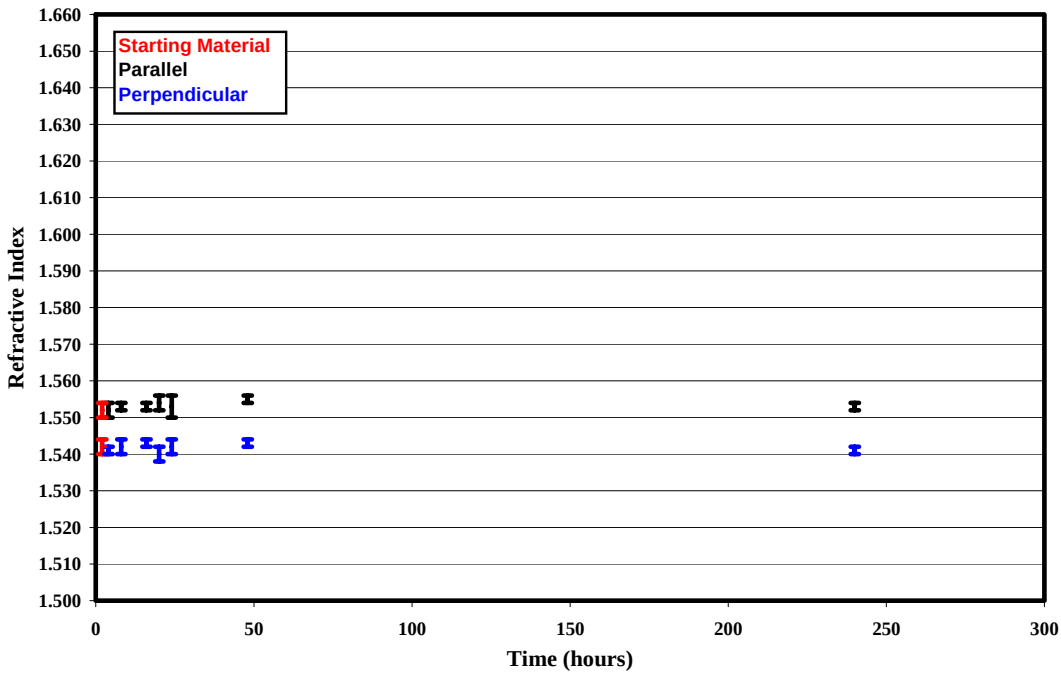

Variability in the IR measurement on the scale of single fibers was also observed as seen in Figure 11. This is possibly a result of the original variability of the starting material and local changes in IR within the fiber after heating. For some fibers heated at various temperatures for various times, different regions along the length of the fiber exhibited different IR measurements.

Figure 11: Photograph of fiber in plane polarized light displaying variability in refractive index along the length of the fiber. This fiber was heated at 600˚C for 24 hours and is immersed in 1.558 Cargille refractive index oil. From left to right the IR increases along the length of the fiber. The field of view is approximately 70 microns by 30 microns.

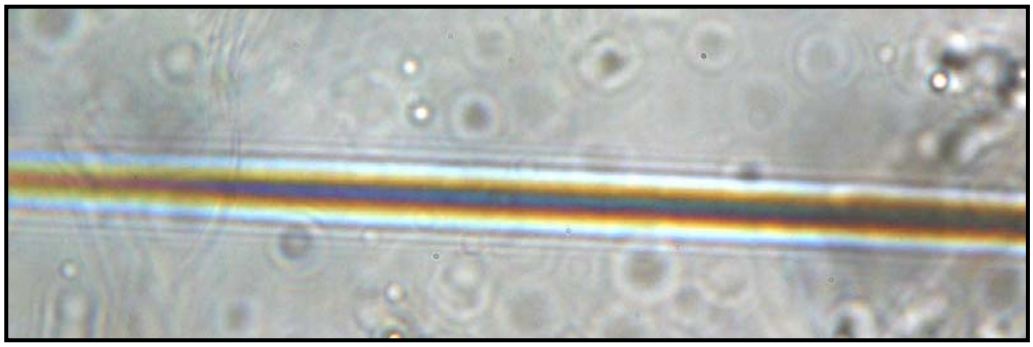

IR measurements reported in this study differ significantly from those reported by Hey and Bannister (1948). Hey and Bannister (1948) also reported a change in the sign of elongation of fibers of heated samples from positive (length slow) to negative (length fast). This was not observed in this study. Comparable results are listed below in Table 5.

Table 5: Comparison of heated chrysotile optical data reported by Hey and Bannister (1948) and current data. Hey and Bannister (1948) only investigated the optical properties of three experimental conditions.

Experimental Conditions (˚C, hours)	Refractive indices	Sign of Elongation
Hey and Bannister (1948)		
900, 5	1.56-1.57	positive
1000, 5	1.59	positive
1000, 12	1.61-1.62	negative
This Study		
900, 4	1.604-1.572	positive
1000, 4	1.644-1.620	positive
1000, 16	1.650-1.638	positive

X-ray Diffraction

The minerals chrysotile, forsterite, and enstatite were identified by using X-ray diffraction and characterized by using the area summation of specific peaks (counts). X-ray diffraction patterns gathered on all samples are located in Appendix II. A geometrical error in peak position was produced due to the fibrous morphology of the sample and the resulting inability to pack the material in the sample holder such that the upper surface of the sample is parallel to the sample holder surface. Therefore, small variations in peak positions were not considered. For chrysotile the peak areas of the (002), (004), and (008) reflections were summed; for forsterite the peaks areas of the (020), (120) and (031) reflections were summed; and for enstatite the peak areas of the (420) and (610) reflections were summed. The Jade software calculated area by summing the intensity (counts) per step size designated by the X-ray diffractometer. The background was subtracted from this summation. Appendix III provides the peaks of the most well developed X-ray diffraction reflections from which the minerals phases were identified and corresponding reference patterns used in this study. These peaks were chosen based on the least interference from the other mineral phases identified. Peak area summations of chrysotile, forsterite, and enstatite are listed in Appendix I. From trials involving multiple analyses, the 1 sigma uncertainty (standard deviation of the mean) of the peak area sum is on the order of 11%. Calculations of the uncertainty are located in Appendix IV. Uncertainty of the 2-theta and d-spacing values is also discussed in Appendix IV.

Heating times of 4-24 hours: chrysotile, forsterite, and enstatite

Peak area summations of chrysotile, forsterite, and enstatite as a function of temperature, for 4-24 hours, are shown in Figure 12.

Figure 12: Peak Area Sums for chrysotile (Chr), forsterite (Fo), and enstatite (En) as a function temperature for 4-24 hours. Peak area sum is plotted versus temperature (ºC). Peak Area Sum is the sum of the area under the (002), (004), and (008) peaks of chrysotile, the (020), (120), and (031) peaks of forsterite, and the (420) and (610) peaks of enstatite. The peak area sum of the starting material is depicted by a red box and labeled "starting material." The 1 sigma uncertainty of the peak area sum is on the order of 11% and shown on the starting material. Heating times are from 4 to 24 hours.

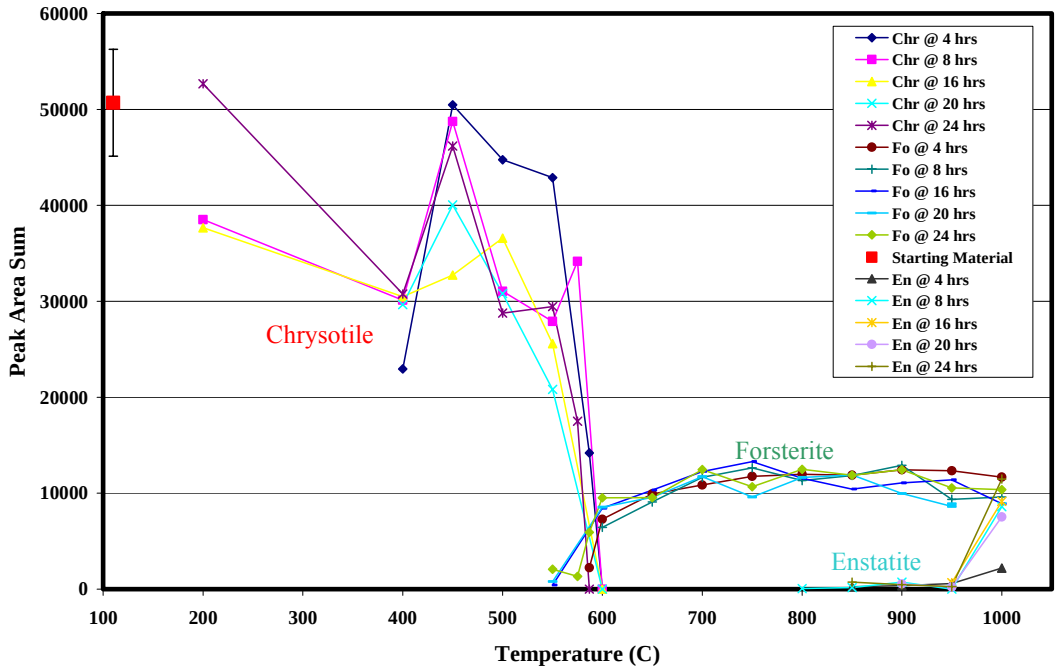

Figure 12 shows the decomposition of chrysotile and the growth of two new minerals; forsterite and enstatite. The decomposition of chrysotile is observed by the decrease of the chrysotile peak area sums, the growth of forsterite is observed by the first appearance and increase of the forsterite peak area sums, and the growth of enstatite is observed by the first appearance and increase of the enstatite peak area sums.

Loss of X-ray intensity of chrysotile first occurred between temperatures of 200-400˚C and times of 4-24 hours. Peak area sums for chrysotile ranged from 52,700 at 200˚C for 24 hours to 30,800 at 400˚C for 24 hours. This loss of X-ray intensity is shown in Figure 12 as the initial decrease in the chrysotile peak area sums, as compared to the starting material, for samples heated at those temperatures and

time conditions. Directly following the decrease, an abrupt increase was observed in the chrysotile peak area sums of samples heated to 450˚C for 4-24 hours. This increase suggests recrystallization and annealing of the mineral. Upon heating above 450˚C, the peak area sums for chrysotile decreased drastically signifying the destruction of the chrysotile structure. The highest temperature at which chrysotile persisted was 587˚C for 4 hours; it was not present at higher temperatures. The highest peak area sum (52,700) for chrysotile was observed in the sample heated at 200˚C for 24 hours. The lowest peak area sum (14,200) for chrysotile was observed in the sample heated at 587˚C for 4 hours.

Within the time range of 4-24 hours, the first appearance of forsterite was observed via the (031) reflection corresponding to the 2.76Å peak when the sample was heated at 550˚C for 16 hours. Although this first detection of forsterite was made with the presence of one reflection, successive data show the (031) reflection increasing in area as well as the appearance of the (020) and (031) reflections. All specific peaks ((020), (120) and (031)) used to monitor the growth of forsterite and the forsterite peak area sum were present in all patterns generated from samples heated at temperatures above 575˚C and for 4-720 hours. The maximum growth of forsterite represented by the highest forsterite peak area sum (13,300) occurred when the sample was heated at 750˚C for 16 hours. The presence of forsterite was observed at all higher temperatures in this study.

The first appearance of enstatite was observed via the (420) reflection corresponding to the 3.88Å peak when the sample was heated at 800˚C for 8 hours. Once again, although the first detection of enstatite was made with the presence of one reflection, successive data show the (420) reflection increasing in area as well as the appearance of the (610) reflection. Enstatite was sporadically present in patterns generated from samples heated at higher temperatures and longer times than 800˚C for 8 hours. All specific peaks ((420) and (610)) used to monitor the growth of enstatite and the enstatite peak area sums were present in all patterns generated from samples heated at 1000˚C. Peak area summations of forsterite and enstatite as a

function of time and temperature are shown in Figure 13 and peak area summations of enstatite as a function of time and temperature are shown in Figure 14.

Figure 13: Peak Area Sums for forsterite (Fo) and enstatite (En) as a function of time and temperature. Peak area sum is plotted versus temperature (ºC). Note the difference in scale on the x axis when compared to Figure 12. Peak Area Sum is the sum of the area under the (020), (120), and (031) peaks of forsterite and (420) and (610) peaks of enstatite. The 1 sigma uncertainty of the peak area sum is on the order of 11% represented by the black error bar on the left side of the graph. Heating times are form 4 to 24 hours.

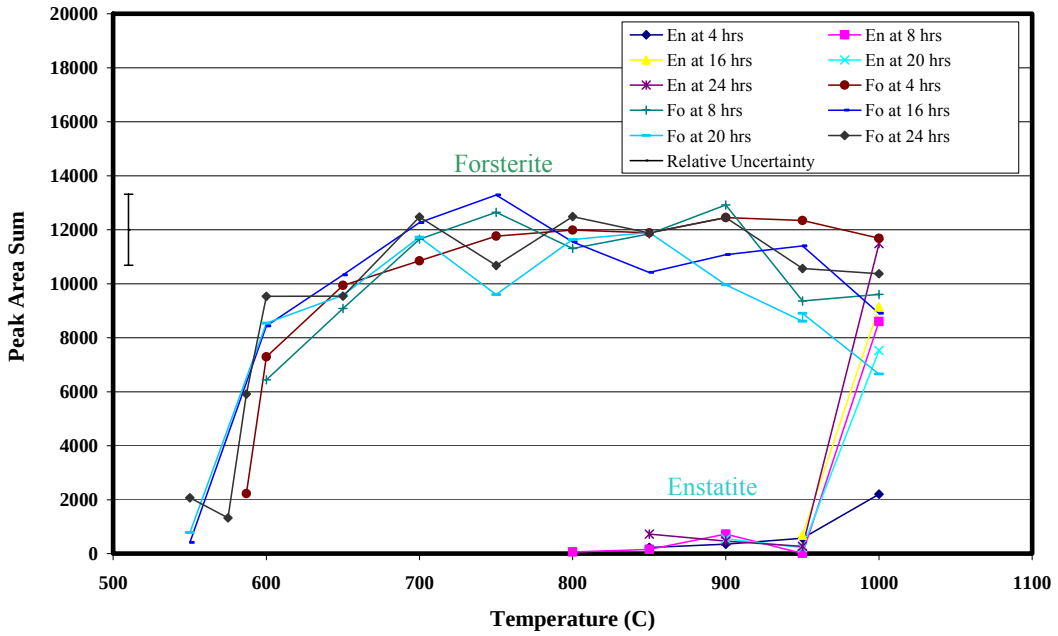

Figure 13 shows the peak area sums for forsterite coupled with the peak area sums for enstatite and more accurately displays the first occurrence and stability of forsterite as time and temperature increase. No increase in the peak area sums for forsterite was observed above 750ºC. A slight decrease in the peak area sums for forsterite is observed at 950˚C as the peak area sums of enstatite increases. This suggests that enstatite may grow at the expensive of forsterite.

Figure 14: Peak Area Sums for enstatite (En) as a function of time and temperature. Peak area sum is plotted versus temperature (ºC). Note the difference in scale on the x and y axis when compared to Figure 12 and Figure 13. Peak Area Sum is the sum of the area under the (420) and (610) peaks of enstatite. Heating times are from 4 to 24 hours. Error bars represent a 1 sigma uncertainty on the order of 11%.

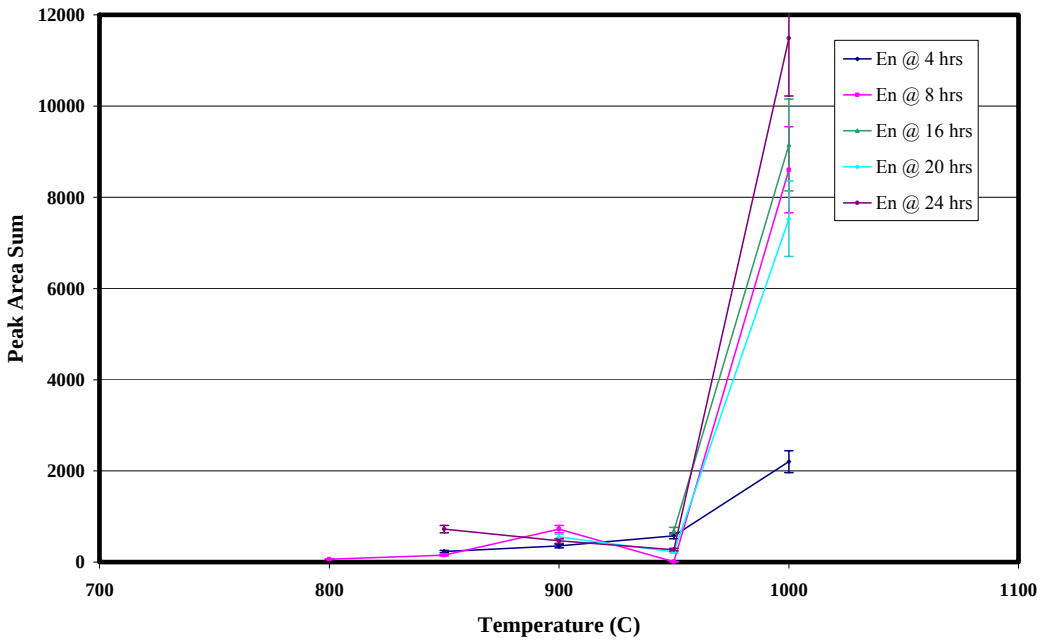

Figure 14 shows the peak area sums for enstatite. The sporadic appearance of enstatite between 800ºC and 950ºC is evident and suggests that enstatite has difficulty nucleating and growing. The maximum growth of enstatite represented by the highest enstatite peak area sum (11,500) occurred when the sample was heated at 1000˚C for 24 hours. The peak area sum for enstatite appears to be approaching a constant value, and may reach a plateau at somewhat longer reaction times. Figure 15 shows the peak area sums for enstatite heated at 1000ºC for 4 to 24 hours.

Figure 15: Peak Area Sums for enstatite (En) as a function of time and constant temperature, 1000ºC. Peak area sum is plotted versus time (hours). Peak area sum is the sum of the area under the (420) and (610) peaks of enstatite. Heating times are from 4 to 24 hours. Error bars represent a 1 sigma uncertainty on the order of 11%.

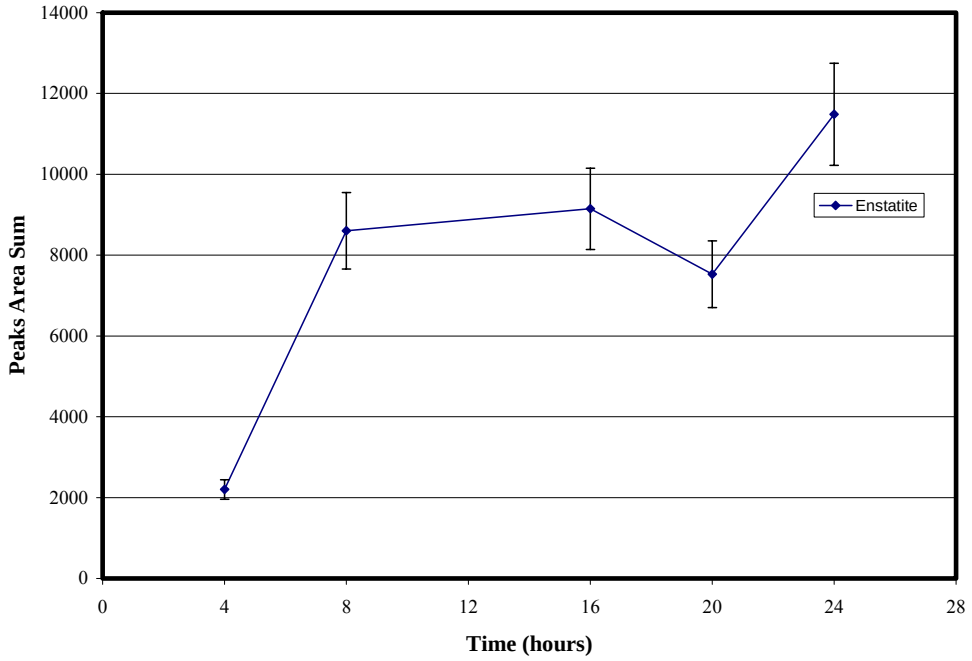

Extended Heating Times: chrysotile and forsterite

Extended heating times were performed for 2 days, 10 days, and 30 days at 200, 400, 450, and 500˚C. The first appearance of forsterite coupled with the complete absence of chrysotile occurred when the sample was heated at 500˚C for 30 days; this was the lowest temperature that forsterite was found in this study. All peaks used to monitor the growth of forsterite ((020), (120) and (031)) were present in the pattern generated from heating the sample to 500˚C for 30 days; no chrysotile peaks were present. Figure 16 shows the peak area sums for chrysotile and forsterite for the extended heating times discussed above.

Figure 16: Peak Area Sums for chrysotile (Chr) and forsterite (Fo) for extended heating times and specific temperatures. Heating times are from 4 to 720 hours. Peak area sum is plotted versus log time. Peak Area Sum is the sum of the area under the (002), (004), and (008) peaks of chrysotile and the (020), (120), and (031) peaks of forsterite. The peak area sum of the starting material is depicted by a red box and labeled "starting material." The 1 sigma uncertainty of the peak area sum is on the order of 11% and shown on the starting material.

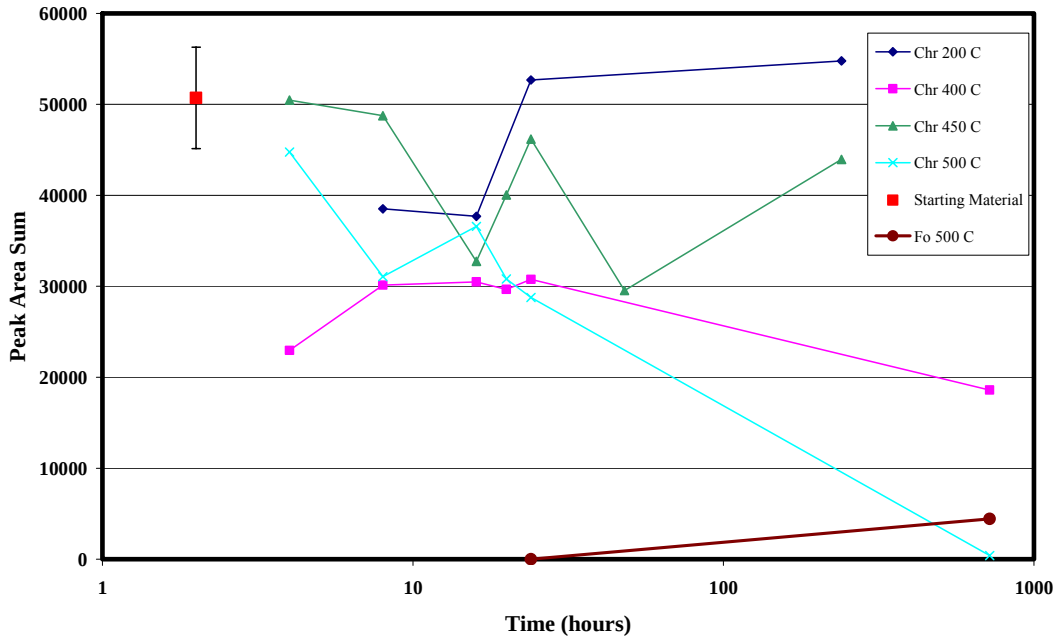

Time-Temperature-Transformation: chrysotile → forsterite

Forsterite data extracted from experiments performed for extended heating times as well as those performed for 4-24 hours resulted in the construction of a time-temperature-transformation curve, shown in Figure 17. Each data point on the curve represents the first appearance of forsterite as a function of time and temperature. Peak area sum of forsterite is not plotted. Figure 17 shows clearly that forsterite formation is a function of temperature and a function of temperature at time. The green line representing the time-temperature-transformation curve flattens out at 500˚C because no forsterite was observed below 500˚C

Figure 17: Time-Temperature-Transformation Curve illustrates the first appearance of forsterite as a function of time and temperature. Temperature is plotted versus log time. Each data point represents the temperature and time at which forsterite first appeared.

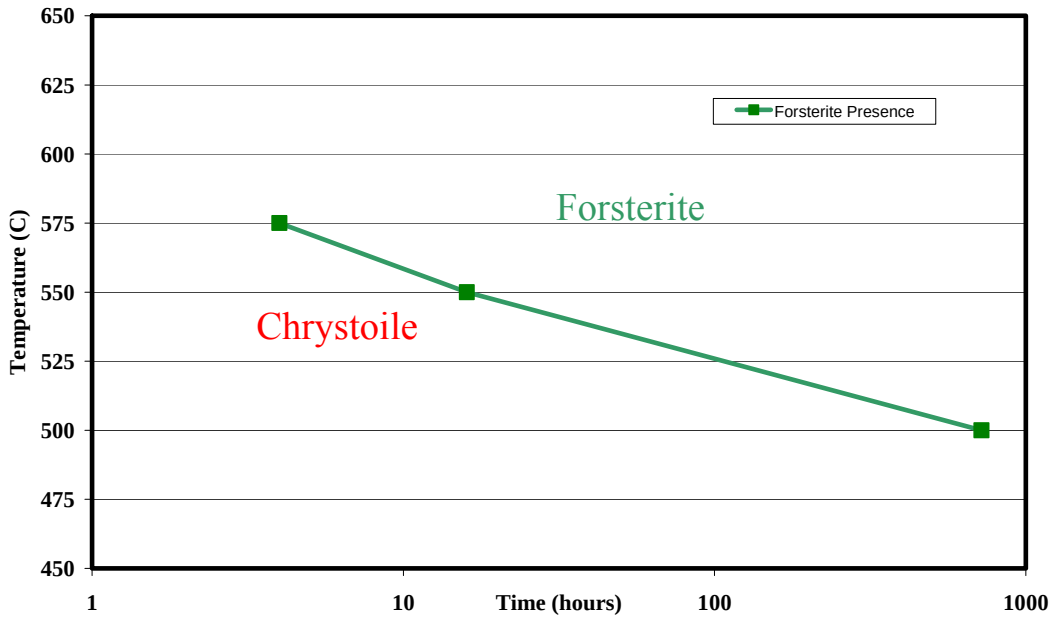

Other Phases

In addition to the peak area sum observations made by using X-ray diffraction techniques, the presence of broad reflections was observed throughout this study. These reflections arise from regions lacking well developed long range order. In general broad reflections are caused by limited order within the atomic structure or the presence of small crystallites (Klugg and Alexander, 1974). A table listing all the experiments where the broad reflections were observed, the dimensions (Å), shape, height, and possible mineral and structural associations of each is found Appendix V. Appendix VI contains images of diffraction patterns with broad X-ray reflections. Broad reflections observed in this study are consistent with those reported in the literature (Brindley and Zussman, 1957, Martin, 1977, de Souza Santos and Yada, 1979, and McKenzie and Meinhold, 1994). Although mineral identification can not

be made with the analytical techniques used in this study, mineral associations corresponding to these reflections can be implied.

Broad reflections were observed between 16-8Å (~0-10.5˚ 2θ) in experiments that included the presence of chrysotile as well as experiments with no chrysotile. In general, because only hydrous silicate minerals exhibit reflections in these higher d-spacing ranges, broad reflections in the 16-8Å spacing range are evidence of the persistence of water. In this study, reflections observed in the 16-8Å area were present between temperatures of 500-750˚C. Experiments that contained broad reflections in the 16-8Å spacing and chrysotile include: 550ºC for 20 hours, 575ºC for 24 hours, and 587ºC for 4 hours. These broad reflections were asymmetrical when chrysotile was present; an example is shown in Figure 18. The d-spacing of these reflections observed in patterns containing chrysotile can be possibly associated with a 14Å double layer of the 7.36Å chrysotile peak.

Figure 18: Diffraction pattern illustrating the broad X-ray reflection observed in the 16-8Å spacing range; this broad X-ray reflection is asymmetrical. This diffraction pattern was generated by heating the sample at 587˚C for 4 hours; this experiment contained chrysotile after heating. The 0-34˚ 2-theta scale on the x axis is equivalent to 17-2.5Å.

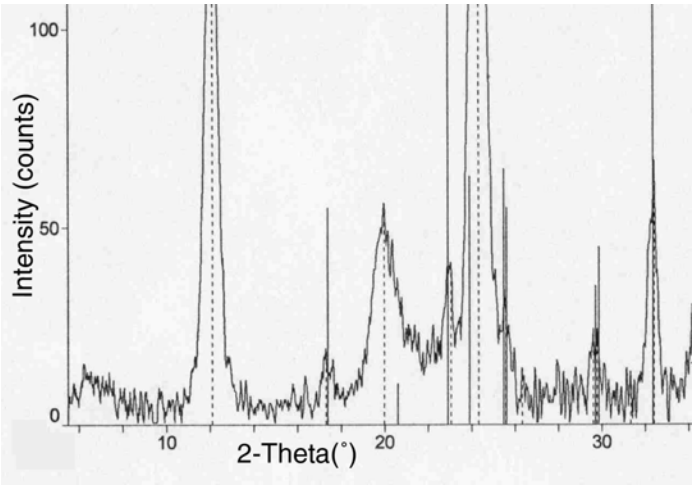

A broad reflection in the same d-spacing range was also observed in patterns generated from samples heated at temperatures and times beyond the presence of chrysotile. Experiments where this reflection was observed without the presence of

chrysotile include: 587ºC for 24 hours, 600ºC for 4, 8, 16, and 24 hours, 650ºC for 4, 8, 16, 20, and 24, 700ºC for 4, 8, 16, and 20, and 750ºC for 24 hours. However, these broad reflections in the 16-8Å spacing range are shifted slightly and centered at approximately 10Å when compared to the broad reflection in the 16-8Å spacing range with the presence of chrysotile (see Figure 19). Since no chrysotile was observed in this experiment, this broad reflection can no longer be associated with a 14Å double layer of the 7.36Å chrysotile peak. It is possible that this broad X-ray reflection may be associated with the 9.34Å talc peak. Complimentary research preformed by Earnest et al. (2004) confirms the presence of talc when chrysotile was heated at 800˚C.

Figure 19: Diffraction pattern illustrating the broad X-ray reflection observed in the 16-8Å, 4Å and 3Å spacing ranges; the broad X-ray reflection in the 16-8Å spacing range is symmetrical. This diffraction pattern was generated by heating the sample at 650˚C for 8 hours; this experiment did not contain chrysotile after heating. The 0-34˚ 2-theta scale on the x axis is equivalent to 17-2.5Å.

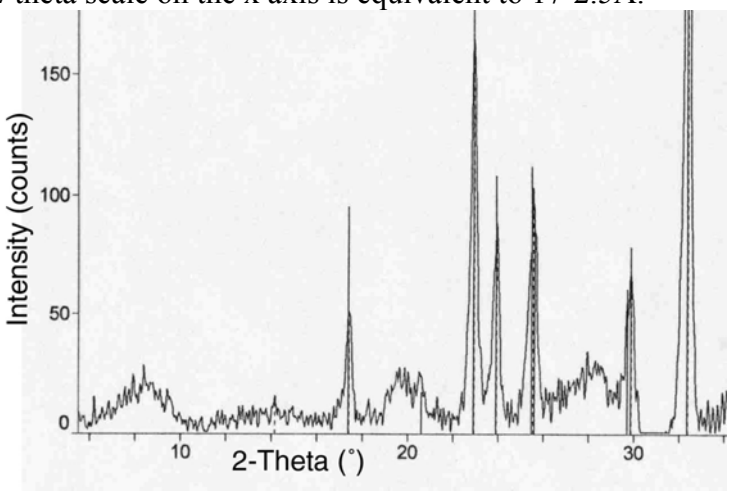

Broad reflections were observed between 4.8-4.1Å (~18-22˚ 2θ) and between 3.4-2.8Å (26-30˚ 2θ) in samples heated at varying temperature and times with and without the presence of chrysotile. These experiments include: 500ºC for 720 hours, 550ºC for 20 hours, 587ºC for 24 hours, 600ºC for 4,8, 16, 20, and 24 hours, 650ºC for 4, 8, 16, 20, and 24 hours, 700ºC for 4, 8, 16, 20, and 24 hours, and 750ºC for 20 and 24 hours. The midpoints of these reflections correspond to the 4.66Å and 3.116Å talc peaks. An example of these broad X-ray reflections can be seen in Figure 19.

The broad reflection located in the 4.8-4.1Å area in samples heated at varying temperature and times with and without the presence of chrysotile could also suggest the presence of tridymite due to its correspondence with the 4.107Å and/or 4.328Å tridymite peaks. These experiments include: 500ºC for 720 hours, 550ºC for 20 hours, 587ºC for 24 hours, 600ºC for 4,8, 16, 20, and 24 hours, 650ºC for 4, 8, 16, 20, and 24 hours, 700ºC for 4, 8, 16, 20, and 24 hours, and 750ºC for 20 and 24 hours. Complimentary research performed by Earnest et al. (2004) observed a limited ordering with a tridymite-like structure. An example of this broad X-ray reflection can be seen in Figure 19.

The X-ray diffraction pattern generated from the sample heated at 500ºC for 30 days displays three broad reflections, two of which differ from all other broad reflections observed (see Figure 20). Reflections were observed in the 16-8Å area (~0-10.5˚ 2θ), 7.9-6.6Å (~12-16˚ 2θ) area, and 4.66-4.17Å (~19-21˚ 2θ). The reflection observed in the 16-8Å area can be associated with a 14Å double layer of the chrysotile 7.36Å peak. The reflection observed in the 7.9-6.6Å area suggests a disordering of the 7.36Å chrysotile peak. The reflection observed within the 4.66-4.17Å is centered at 4.32Å which is equivalent to the major tridymite peaks at 4.328Å.

Figure 20: Diffraction pattern generated from heating the sample at 500˚C for 30 days containing 3 regions of broad X-ray reflections. This experiment contained both chrysotile and forsterite after heating. The 0-34˚ 2-theta scale on the x axis is equivalent to 17-2.5Å.

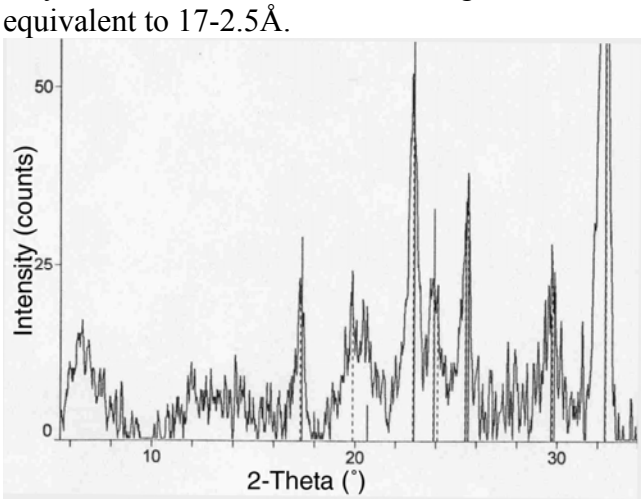

Figure 21 plots the occurrence of all broad X-ray reflections discussed above as a function of time and temperature. This figure clearly outlines the region of stability of these intermediate phases likely associated with disordered chrysotile, talc, and tridymite. No broad reflections were observed when the sample was heated above temperatures of 800˚C for all durations of the experiment. Figure 22 is a time-temperature-transformation curve of the first appearance of the 16-8, 4, and 3Å broad X-ray reflections in addition to the first appearance of forsterite. The time-temperature-transformation curve representing the first appearance of the broad X-ray reflections follows the same trend as the time-temperature-transformation curve representing the first appearance of forsterite. Figure 22 further illustrates the idea that the mineralogical transformations taking place during the dehydration of chrysotile are a function of temperature at time. Forsterite forms in concurrence with the formation of broad X-ray reflection in the 16-8Å and 4Å area when the sample is heated at 500˚C for 720, yet when heated for 20 or 24 hours, forsterite or the broad reflections are not detected until heated at 550˚C.

Figure 21: Occurrence of broad X-ray reflections. Temperature is plotted versus log time. Each data point represents the temperature and time at which 16-8Å (blue squares), 4Å (red dots), and/or 3Å (green X) was observed.

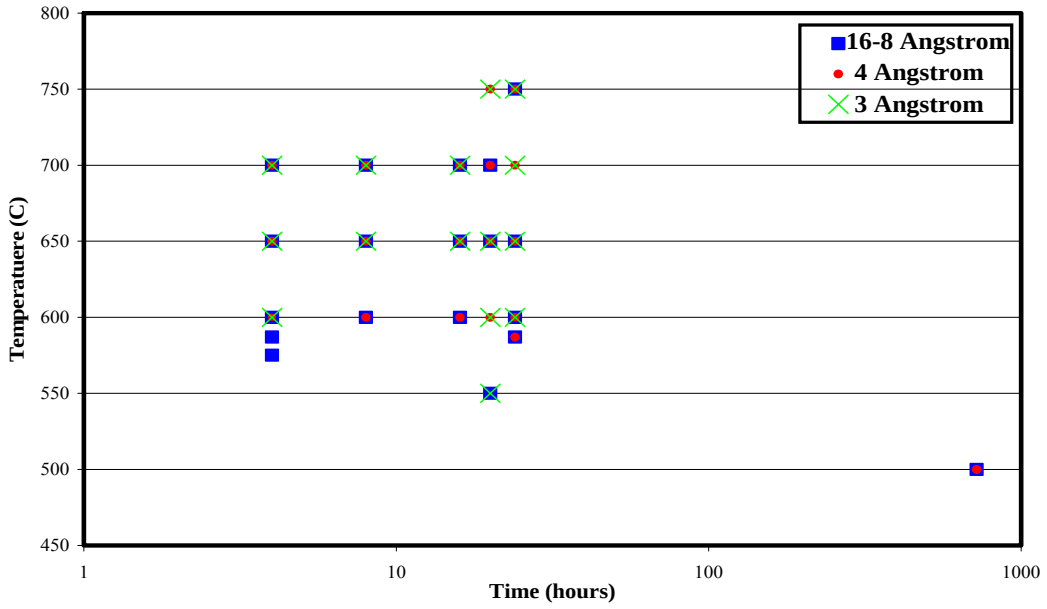

Figure 22: Time-Temperature-Transformation Curve of the first appearance of broad X-ray reflections in the 16-8, 4, 3Å area and the first appearance of forsterite as a function of time and temperature. Temperature is plotted versus log time. Each data point represents the temperature and time at which the broad X-ray reflections or forsterite first appeared.

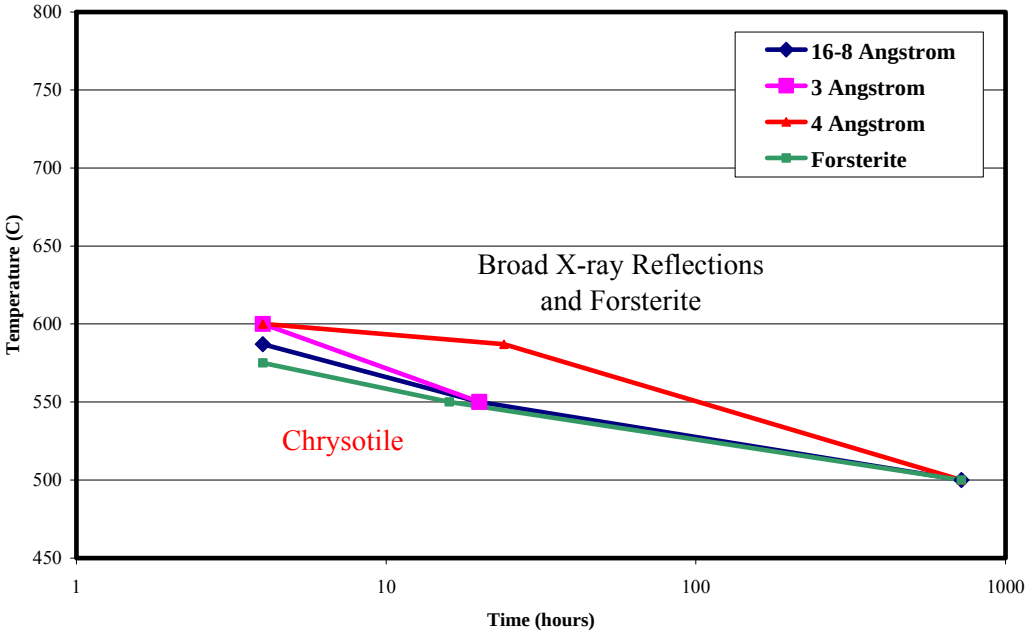

Chapter 5: Summary Discussion

Regions of Mineralogical Transformation within Heating Times of 4-24 hours

X-ray diffraction and optical mineralogy results from this study suggest that the decomposition of chrysotile is a much more complex process than previously described in the literature. For purposes of discussion, the temperature range of chrysotile decomposition observed between 4-24 hours can be divided into five separate regions each with characteristic mineralogy and refractive index behaviors. The boundaries for the five regions are depicted in Figure 23 and Figure 24. See Table 6 for summarized characteristics of Regions I-V.

Figure 23: Regional boundaries of chrysotile decomposition via optical microscopy. Boundaries are overlaid on IR graph of samples heated at 200-1000ºC for 24 hours parallel and perpendicular to the length of the fiber. IR is plotted versus temperature (˚C). Heating time of 24 hours was chosen to present the regional boundaries, although similar behavior was observed in all time increments. Boundaries of five regions are shown with dotted lines.

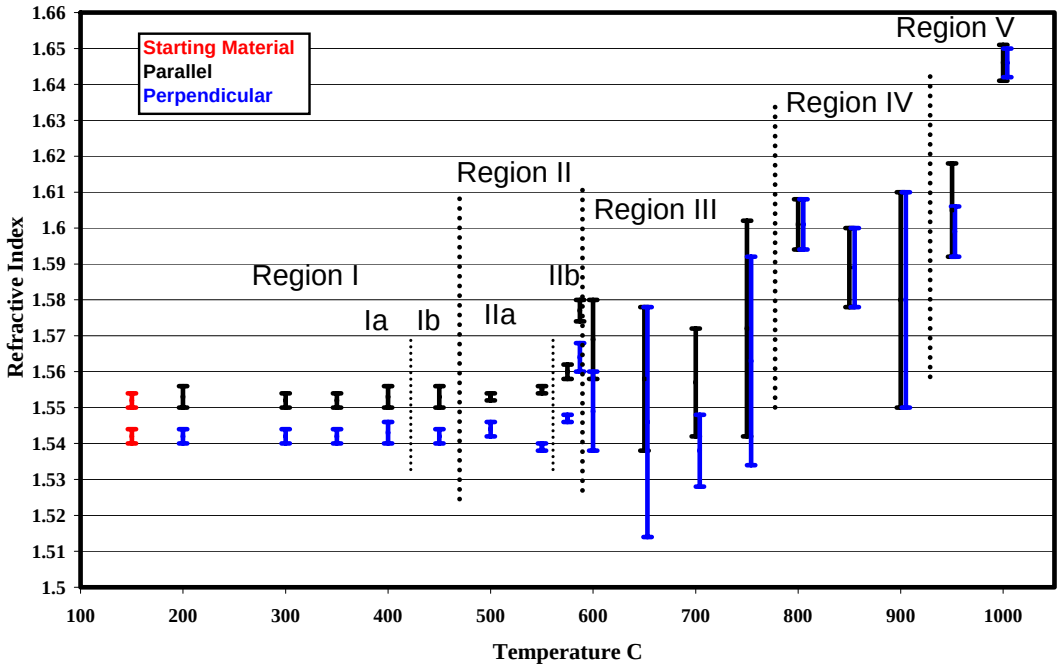

Figure 24: Regional boundaries of chrysotile decomposition via X-ray diffraction. Boundaries are overlaid on Peak Area Sums graph for chrysotile (Chr), forsterite (Fo), and enstatite (En) as a function of time and temperature. Peak area sum is plotted versus temperature (ºC). Peak Area Sum is the sum of the area under the (002), (004), and (008) peaks of chrysotile, the (020), (120), and (031) peaks of forsterite, and the (420) and (610) peaks of enstatite. The peak area sum of the starting material is depicted by a red box and labeled "starting material." Heating times include 4-24 hours. The 1 sigma uncertainty of the peak area sum is on the order of 11% and shown on the starting material. Boundaries of five regions are shown with dotted lines.

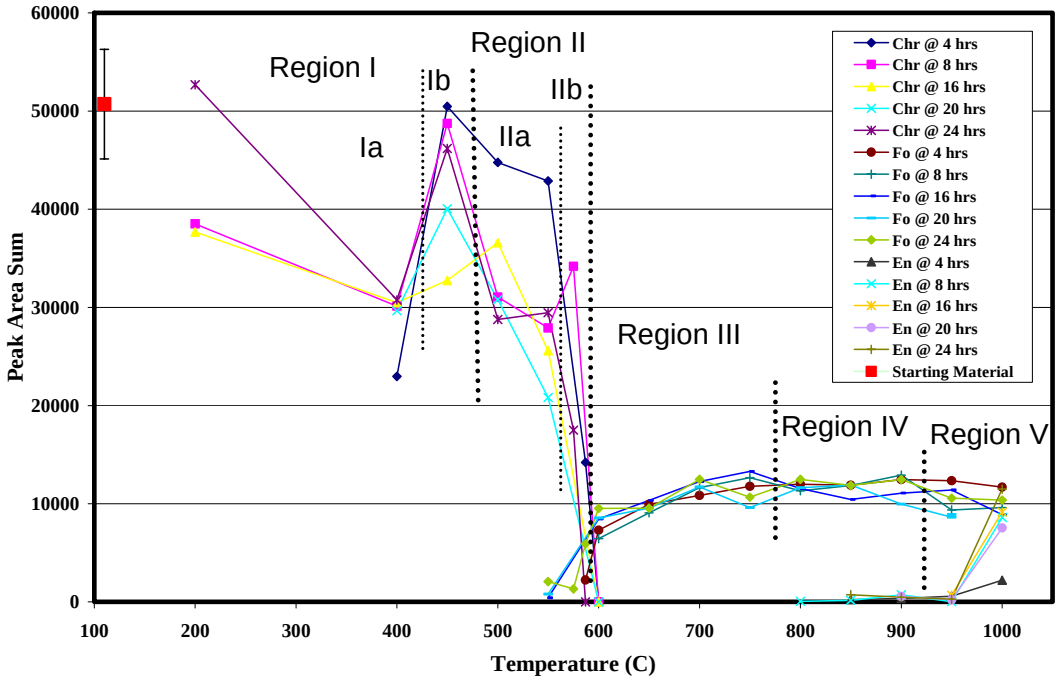

The regional boundaries and their characteristics listed in Table 6 cannot be applied to the extended heating times observed in this study. For example, forsterite was detected when the sample was heated at 500˚C for 30 days, whereas when heated at 500˚C for 4-24 hours no forsterite was detected. This would affect the boundary between regions II and III.

Table 6: Regional boundary characteristics for temperatures 200-1000˚C for 4-24 hours.

Region Ia	Minerals present: chrysotile
200-400 C	Cumulative X-ray intensity of the chrysotile pattern decreases
	No change in refractive index (IR) relative to starting material
Region Ib	Minerals present: chrysotile
450 C	Abrupt increase in cumulative X-ray intensity of the chrysotile pattern
	No change in IR relative to starting material
Region IIa	Minerals present: chrysotile, forsterite
500-550 C	Cumulative X-ray intensity of the chrysotile pattern decreases
	Initial appearance of forsterite peaks at 550 C and 16 hours
	Range of IR decreases upon passing from Region I to Region II
	IR parallel to the fibers increases while the IR perpendicular to the fibers decreases relative to region I
	Appearance of broad reflections in the 16-8Å and 3Å spacing range
Region IIb	Minerals present: chrysotile, forsterite
575-587 C	Cumulative X-ray intensity of the chrysotile pattern decreases
	Chrysotile peaks absent at 587 C and 4 hours
	Range of IR increases
	IR parallel and perpendicular to the fibers increase relative to region I
	Magnitude of minimum and maximum IR increases
Region III	Minerals present: forsterite
600-750C	Cumulative X-ray intensity of forsterite pattern increases
	Broad reflections present in the 4Å and 3Å range with peaks possibly consistent with a talc-like and tridymite-like structure
	Minimum values of IR parallel and perpendicular to the fiber are both less than that of the starting material
	Maximum values of IR parallel and perpendicular to the fiber are both greater than that of the starting material
	Range in IR is very large, up to 0.06, with large fibers having a lower IR than small fibers
Region IV	Minerals present: forsterite, enstatite
800-900 C	All broad reflections disappear
	First appearance of enstatite peak (221) at 850 C at 24 hours
	At 800 C IR both parallel and perpendicular increases from Region III and the range in both decreases
	Minimum IR decreases
	Range in IR increases
	Birefringence approaches zero
Region V	Minerals present: forsterite, enstatite
950-1000 C	X-ray intensity of enstatite pattern increases
	Minimum IR and maximum IR increases
	Highest IR observed
	Range in IR decreases from that of Region IV
	Birefringence approaches zero

Region I

Region I corresponds to the temperature range of 200-450˚C and is further divided into sub regions Ia and Ib. Region Ia includes temperatures between 200-400˚C. Within region Ia, chrysotile is present and no change in IR is observed relative to the starting material. The cumulative X-ray intensity of the chrysotile pattern, monitored by the area summation of the chosen chrysotile peaks, decreases at 400˚C. Region Ib includes temperatures at 450˚C. Within region Ib, chrysotile is still present and no change in IR is observed. An abrupt increase in the cumulative X-ray intensity of chrysotile is observed. This abrupt increase suggests recrystallization and is broadly consistent with the temperature at which Hodgson (1979) reported an increase in tensile strength; this is demonstrated in Figure 25.

Figure 25: Peak Area Sums for chrysotile (Chr) as a function of time and temperature. Peak area sum is plotted versus temperature (ºC). Peak Area Sum is the sum of the area under the (002), (004), and (008) peaks of chrysotile. The peak area sum of the starting material is depicted by a red box and labeled "starting material." Heating times are from 4 to 24 hours. Tensile strength graph of heated chrysotile asbestos adapted from Hodgson (1979) is located in the top right of the figure.

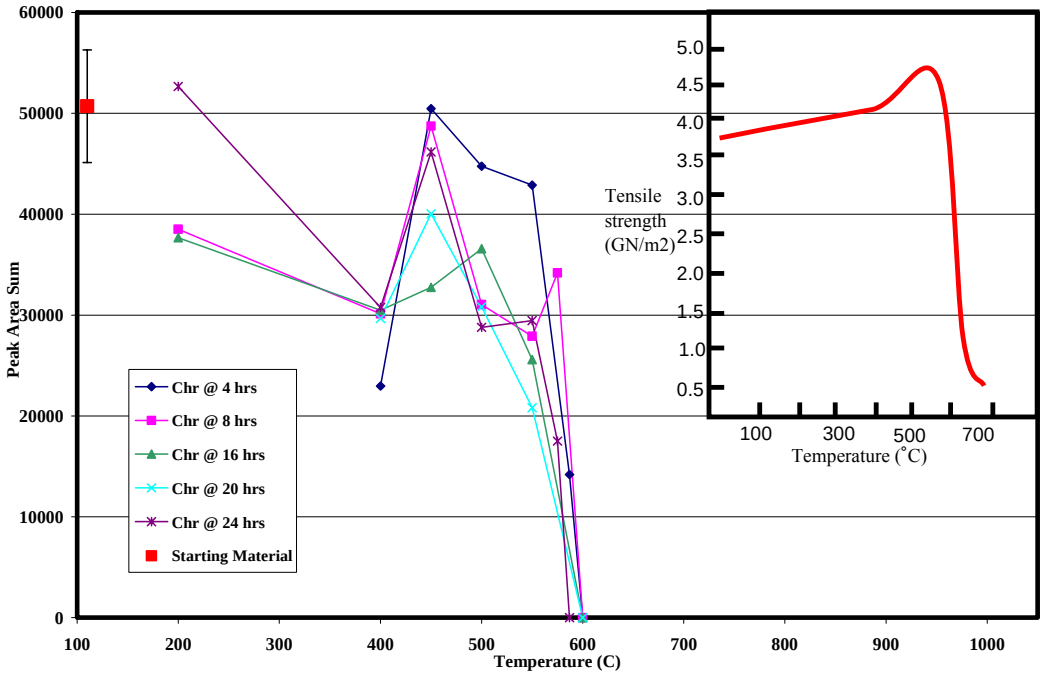

Region II

Region II corresponds to the temperature range of 500-587˚C and is further divided into sub regions IIa and IIb. Chrysotile and forsterite are both present in region II.

Region IIa includes temperatures between 500-550˚C. Within region IIa, the cumulative X-ray intensity of the chrysotile pattern decreases. The initial appearance of forsterite occurs via the 2.77Å peak when heated at 550˚C for 16 hours. IR parallel to the fibers increases while the IR perpendicular to the fibers decreases relative to region I. This decrease in IR perpendicular to the length of the fibers is the first of the three temporal areas of decrease observed within the overall trend of increasing IR as temperature increases. This decrease is consistent with the appearance of broad reflections, seen via X-ray diffraction techniques, in the 16-8Å spacing range associated with the 14Å double layer of the 7.36Å chrysotile peak. It is possible that the 16-8Å reflection is representative of disordering of the 14Å double layer of chrysotile and therefore would result in a decrease in the IR seen in region IIa.

Region IIb includes temperatures between 575-587˚C; the cumulative X-ray intensity of chrysotile decreases compared with region IIa and disappears at 587˚C after 4 hours of heating. IR measurements, parallel and perpendicular to the fiber, increase relative to region I and IIa. As temperature increases within region IIb, the range of the IR increases slightly, as does the magnitude of the maximum and minimum IR. The increase in IR observed in this region could be due to submicroscopic mineral mixture of chrysotile ± forsterite as forsterite continues to grow; forsterite has a mean IR of 1.653 compared with the starting material which has a mean IR, measured parallel to the length of the fiber, of 1.552. It is also possible that the broad reflections present in this region are a result of the dehydration of chrysotile, leading to an increase the density of the material, resulting in the slight IR increase observed in region IIb.

Region III

Region III represents the temperature range of 600-750˚C. Forsterite is present and the cumulative X-ray intensity of the forsterite pattern, monitored by the area summation of the chosen forsterite peaks, increases as temperature increases. It is within this region that variability in particle width of individual fibers is observed; fiber widths ranged from approximately 10-130 microns compared with the starting material fiber widths which ranged from approximately 70-130 microns. The lowest IR values, which are lower than the starting material, both parallel and perpendicular, are observed within region III and are characteristic of the largest particles observed. The decrease in IR relative to the starting material is the second of the three temporal areas of decrease observed within the overall trend of increasing IR as temperature increases. This decrease in IR is consistent with the appearance of broad reflections present in the 16-8Å, 4Å, and 3Å ranges. It is possible that the low IR values are due to the formation of intermediate phases of lower densities, similar to limited ordered Si rich phases which correspond with the low IR and the 4Å reflections observed in this region. The 100% and 90% intensity peaks of tridymite are 4.107Å and 4.328Å, respectively and the mean RI of tridymite is 1.471.

The magnitude of the maximum IR first decreases and then increases as temperature increases, resulting in IR values up to 0.048 greater than the starting material. The maximum IR values within this region are characteristic of the smallest particles observed. The largest range in IR value, 0.06, is observed at 750˚C. The appearance of broad reflections via X-ray diffraction analysis which, are indicative of intermediate phases, correlates with an increase in the range, or variability, of IR observed in region III. The increase in IR values relative to the starting material could be a result of the increase in density that accompanies the transition of less dense intermediate phase to forsterite with the loss of water. Also, the largest range within the maximum and minimum IR value could be a result of disorder of intermediate phases, the formation of nanoporosity formed during the dehydration of chrysotile and as forsterite grows, or submicroscopic mineral mixture of intermediate phases ± forsterite.

Region IV

Region IV corresponds to the temperature range of 800-900˚C. Forsterite is present and the cumulative X-ray intensity of the forsterite pattern remains constant as temperature increases. The initial appearance of enstatite occurs via the 3.88Å peak when heated at 800˚C for 8 hours. At 800˚C, the material is very uniform in IR, but as temperature increases, the inhomogeneity increases and the IR, especially the minimum IR, decreases dramatically. This decrease in IR is the last of the three temporal areas of decrease observed within the overall trend of increasing IR as temperature increases. By 900˚C, the minimum IR of the large particles reaches that of the starting material, thus increasing the range of the IR. All samples within region IV exhibit a birefringence which approaches zero. This suggests that as the material becomes more crystalline, it is lacking in preferred orientation. The broad reflections present in region III are no longer observed in region IV, suggesting that the dehydration is complete. One possible explanation for the lower IR observed in this region is that the initial appearance of enstatite results in the formation of intermediate, low density phases or the formation of nanoporosity; this process is favored in the larger particles. Also, submicroscopic mineral mixtures of amorphous material ± forsterite ± enstatite could account for the low minimum value of IR as well as the increased range of IR.

Region V

Region V represents the temperature range of 950-1000˚C. Forsterite and enstatite are both present. A slight decrease in the cumulative X-ray intensity of the forsterite pattern is observed as temperature increases from region IV to region V. The cumulative X-ray intensity of the enstatite pattern behaves sporadically as temperature increases. The highest cumulative X-ray intensity of the enstatite pattern was observed at 1000˚C. The range in IR decreases upon passing from region IV to region V indicating that the material is more homogeneous. The magnitude of the minimum and maximum IR increases as temperature increases and the highest IR is observed within region V where enstatite is most abundant. The highest IR, measured parallel and perpendicular to the length of the fiber, observed in region V

and in this study was 1.650 which is approximate to the mean IR of enstatite and forsterite, 1.653. It is possible that the increase in IR is a result of a decrease in the abundance of intermediate, low density phases and/or an increase in the crystalline material, evident by the highest cumulative X-ray intensity of the enstatite observed at 1000˚C. As with region IV, all samples continue to behave isotropically as would be expected from small mineral grains of random orientation compared to material observed in regions of lower temperatures.

Mineralogical Transformation within Extended Heating Times

Although the results of the extended heating durations were not discussed above, interesting correlations between the optical and X-ray diffraction results were found. Forsterite was formed and chrysotile was destroyed when the sample was heated at 500˚C for 30 days; this was the lowest temperature that forsterite was found in this study. All peaks used to monitor the growth of forsterite ((020), (120) and (031)) were present in the pattern generated from heating the sample to 500˚C for 30 days; no chrysotile peaks were present.

The IR of the sample heated at 500˚C at 30 days was significantly lower than most of the IR observed in this study. Most notably, the IR of this sample was decreased relative to the starting material. This was unexpected since X-ray diffraction analysis showed that the starting material transitioned to a mineral with a higher IR. Forsterite has a mean IR of 1.653 compared with the starting material which has a mean IR, measured parallel to the length of the fiber, of 1.552. While the optical data of the sample heated at 500˚C for 30 days was unexpected, the decrease in IR observed coupled with the formation of a new phase, forsterite, is consistent with the three temporal areas of decrease observed within the overall trend of increasing IR as temperature increases for the shorter heating times discussed above. The observed decrease could be due to the initial appearance of forsterite resulting in

the formation of intermediate, low density phases or the formation of nanoporosity. IR measurements for the sample heated to 500˚C at 30 days are displayed in Figure 9.

Chapter 6: Conclusions

This study concludes that the thermal decomposition of chrysotile is more complex than previously understood. Optical microscopy and the X-ray diffraction data track the transformation of chrysotile to forsterite and enstatite. This study suggests that:

- the optical data track the decomposition process and define the variability of the transformations;
- within the temperature range of 500-1000ºC an overall trend of increasing IR is observed;
- within the trend of increasing IR between heating times of 4-24 hours, three temporal areas of IR decrease, whether in the maximum IR or the minimum IR of the total range, is observed. The first area of decrease in IR correlates with the first appearance of broad reflections observed between 16-8Å, the second area of decrease in IR correlates with the first detection and growth of forsterite, and the third area of decrease in IR correlates with the first detection and growth of enstatite. Another decrease in IR was observed in experiments heated for 30 days; this decrease was consistent with the formation of forsterite;
- the variability observed in IR measurements is due to the loss of water content, the presence of intermediate poorly crystallized phases, formation of nanoporosity within the structure of the fiber bundles, or the presence of new mineral phases of forsterite ± enstatite;
- at 400˚C, the X-ray intensity of chrysotile decreases; at 450˚C it increases suggesting recrystallization although no change in the refractive index is observed during this process;
- broad reflections at 16-8, 4, and 3Å are interpreted to represent intermediate phases produced during chrysotile dehydration and decomposition, possibly talc and tridymite-like phases;

- complete decomposition of chrysotile occurs between 500˚C and 587˚C and is dependent on time at temperature;
- prior to the complete decomposition of chrysotile, forsterite forms, suggesting that the complete decomposition of chrysotile is triggered by forsterite nucleation;
- the optical microscopy portion of this study clearly shows that there is a relationship between particle size of the fiber and the variability observed in the IR measurement suggesting that particle size affects the decomposition rate of chrysotile. The smaller particles have higher IR values while the larger particles have lower IR values. It is possible that the smaller particles lose water at lower temperatures and faster than the larger particles, resulting in a characteristic higher IR values of the smaller particles;
- lowest temperature of forsterite formation occurs at 500°C and 720 hours;
- lowest temperature of enstatite formation occurs at 800°C and 8 hours;
- as enstatite continues to grow, a slight decrease in forsterite growth is observed at 950˚C suggesting that enstatite may grow at the expensive of forsterite;
- the sporadic appearance of enstatite between 800ºC and 950ºC suggests that enstatite has a difficult time nucleating and growing;
- throughout heating to 1000°C, the sample retains a fibrous, but not fibrillar, morphology even when chrysotile is no longer detectable.

Reports by Datta et al. (1986) and Meinhold and McKenzie (1994) suggest that the dehydration of chrysotile is a two-step process, resulting in two different dehydrated phases; named by Meinhold and McKenzie (1994) as dehyroxylate I and II. The three temporal regions of IR decrease observed, via optical microscopy, and the correlating X-ray diffraction evidence of broad reflections, forsterite formation, and enstatite formation observed in this study suggest that the dehydration is actually a three-step process. Further mineralogical and chemical analysis of samples representative of the three temporal regions would clarify this discrepancy.

This study aimed to better clarify the temperature and time decompositional boundaries of dehydration and recrystallization of chrysotile as well as reaction products which were reported inconsistently in the literature. Results from this study suggest that inconsistencies found in the literature are due to experimental methodology and particle size of the samples used in the literature. The results of this study suggest that the decompositional boundaries of chrysotile are dependent on time at temperature. For example, forsterite formed at different temperatures depending on the length of heating time. Also, this study clearly suggests that particle size has an effect on the decompositional boundaries. For any given temperature and heating time and within the range of refractive indices measured, larger fibers displayed the lowest refractive index while the smaller fibers displayed the highest refractive index. This suggests that smaller particles reacted more quickly than larger particles.

Although no actual brake material was used, this study aimed to provide information that would help to understand the characteristics of particulates released during processes such as automotive braking. The results of this study clearly suggest that the characteristics of particulates released and the formation of new mineral phases is dependent upon how long brakes are heated. It can also be suggested that the age of the brakes as well as the history of use would have an effect on the particulates released and the formation of new mineral phases. Different brake environments may also effect the transformations that take place. For instance, disc brakes and drum brakes yield different brake environments and the transformations would possibly reflect those differences. The effects of discontinuous heating were not investigated in this study. Results from this study suggest that discontinuous heating would further effect the time at temperature at which mineral transformations occur.

Appendix I: Data Summary Table

Experimental Conditions Temperature (˚C), Time (hours)		Method of encapsulation while heating	Morphology	Color	Refractive index parallel to the length of the fiber	Refractive index perpendicular to the length of the fiber	Sum of Chr peak area present: (002), (004), and (008)	Sum of Fo peak area present: (020), (120), and (031)	Sum of En peak area present: (420 and 610)
Original	0	N/A	1	white	1.554-1.550	1.544-1.540	50700	0	0
200	8	gold	1	white	1.556-1.552	1.544-1.540	38500	0	0
200	16	gold	1	white	1.554-1.550	1.544-1.540	37700	0	0
200	24	gold, slide	1	white	1.556-1.550	1.544-1.540	52700	0	0
200	240	gold	1	white	1.554-1.550	1.542-1.540	54800	0	0
300	24	slide	1	white	1.554-1.550	1.544-1.540	N/A	N/A	0
350	24	slide	1	white	1.554-1.550	1.544-1.540	N/A	N/A	0
400	4	gold	1	grey white	1.552-1.550	1.542-1.538	23000	0	0
400	8	gold	1	grey white	1.556-1.552	1.542-1.538	30100	0	0
400	16	gold	1	grey white	1.554-1.552	1.542-1.538	30500	0	0
400	20	gold	1	grey white	1.554-1.552	1.544-1.542	29700	0	0
400	24	gold, slide	1	grey white	1.556-1.550	1.546-1.540	30800	0	0
400	720	gold	1	grey white	1.556-1.548	1.542-1.536	18600	0	0
450	4	gold, slide	1	grey white	1.554-1.550	1.542-1.540	50500	0	0
450	8	gold, slide	1	grey white	1.554-1.552	1.544-1.540	48800	0	0

Appendix I Continued

Experimental Conditions Temperature (˚C), Time (hours)		Method of encapsulation while heating	Morphology	Color	Refractive index parallel to the length of the fiber	Refractive index perpendicular to the length of the fiber	Sum of Chr peak area present: (002), (004), and (008)	Sum of Fo peak area present: (020), (120), and (031)	Sum of En peak area present: (420 and 610)
450	16	gold, slide	1	grey white	1.554-1.552	1.544-1.542	32700	0	0
450	20	gold	1	grey white	1.556-1.552	1.542-1.538	40000	0	0
450	24	gold, slide	1	grey white	1.556-1.550	1.544-1.540	46200	0	0
450	48	gold	1	grey white	1.556-1.554	1.544-1.542	29500	0	0
450	240	gold	1	grey white	1.554-1.552	1.542-1.540	44000	0	0
500	4	gold	1	grey white	1.558-1.556	1.546-1.544	44800	0	0
500	8	gold	1	grey white	1.558-1.556	1.546-1.544	31100	0	0
500	16	gold	1	grey white	1.558-1.556	1.546-1.544	36600	0	0
500	20	gold	1	grey white	1.556-1.554	1.546-1.544	30800	0	0
500	24	gold	1	grey white	1.554-1.552	1.546-1.542	28800	0	0
500	720	gold	2	grey white	1.558-1.550	1.526-1.518	395	4400	0
550	4	gold	1	grey white	1.558-1.556	1.546-1.544	42900	0	0
550	8	gold	1	grey white	1.558-1.556	1.548-1.546	27900	0	0
550	16	gold	1	yellow white	1.558-1.556	1.548-1.546	25600	415	0
550	20	gold	1	yellow white	1.560-1.558	1.548-1.546	20800	782	0

Appendix I Continued

Experimental Conditions Temperature (°C), Time (hours)		Method of encapsulation while heating	Morphology	Color	Refractive index parallel to the length of the fiber	Refractive index perpendicular to the length of the fiber	Sum of Chr peak area present: (002), (004), and (008)	Sum of Fo peak area present: (020), (120), and (031)	Sum of En peak area present: (420 and 610)
550	24	gold	1	yellow white	1.556-1.554	1.540-1.538	29400	2100	0
575	8	gold	1	yellow white	1.558-1.556	1.544-1.542	34200	3400	0
575	24	gold	1	yellow white	1.562-1.558	1.548-1.546	17500	1300	0
587	4	gold	2	yellow white	1.568-1.564	1.552-1.546	14200	2200	0
587	24	gold	2	yellow white	1.580-1.574	1.568-1.560	0	5900	0
600	4	gold	1	lt. yellow orange	1.578-1.574	1.568-1.562	0	7300	0
600	8	gold	2	lt. yellow orange	1.578-1.574	1.568-1.562	0	6400	0
600	16	gold	2	lt. yellow orange	1.580-1.574	1.570-1.564	0	8400	0
600	20	gold	2	lt. yellow orange	1.584-1.570	1.572-1.564	0	8500	0
600	24	gold	2	lt. yellow orange	1.580-1.558	1.560-1.538	0	9500	0
650	4	gold	2	lt. yellow orange	1.566-1.542	1.566-1.522	0	9900	0
650	8	gold	2	lt. yellow orange	1.576-1.546	1.572-1.528	0	9100	0
650	16	gold	2	lt. yellow orange	1.582-1.554	1.548-1.540	0	10300	0
650	20	gold	2	lt. yellow orange	1.574-1.544	1.570-1.526	0	9600	0
650	24	gold	2	lt. yellow orange	1.578-1.538	1.578-1.514	0	9500	0

Appendix I Continued

Experimental Conditions Temperature (°C), Time (hours)		Method of encapsulation while heating	Morphology	Color	Refractive index parallel to the length of the fiber	Refractive index perpendicular to the length of the fiber	Sum of Chr peak area present: (002), (004), and (008)	Sum of Fo peak area present: (020), (120), and (031)	Sum of En peak area present: (420 and 610)
700	4	gold	2	lt. yellow orange	1.586-1.540	1.586-1.522	0	10800	0
700	8	gold	2	lt. yellow orange	1.582-1.550	1.582-1.538	0	11600	0
700	16	gold	2	lt. yellow orange	1.570-1.540	1.570-1.528	0	12300	0
700	20	gold	2	lt. yellow orange	1.562-1.542	1.562-1.516	0	11700	0
700	24	gold	2	lt. yellow orange	1.572-1.542	1.554-1.522	0	12500	0
750	4	gold	2	lt. yellow orange	1.586-1.542	1.586-1.524	0	11800	0
750	8	gold	2	lt. yellow orange	1.590-1.546	1.578-1.540	0	12600	0
750	16	gold	2	lt. yellow orange	1.598-1.552	1.592-1.548	0	13300	0
750	20	gold	2	lt. yellow orange	1.596-1.540	1.590-1.522	0	9600	0
750	24	gold	2	lt. yellow orange	1.602-1.542	1.592-1.534	0	10700	0
800	4	gold	2	lt. yellow orange	1.606-1.590	1.606-1.590	0	12000	0
800	8	gold	2	lt. yellow orange	1.610-1.590	1.610-1.590	0	11300	60
800	16	gold	2	lt. yellow orange	1.602-1.586	1.602-1.586	0	11500	0
800	20	gold	2	lt. yellow orange	1.598-1.590	1.590-1.576	0	11600	0
800	24	gold	2	lt. yellow orange	1.608-1.594	1.608-1.594	0	12500	0

Appendix I Continued

Experimental Conditions Temperature (°C), Time (hours)		Method of encapsulation while heating	Morphology	Color	Refractive index parallel to the length of the fiber	Refractive index perpendicular to the length of the fiber	Sum of Chr peak area present: (002), (004), and (008)	Sum of Fo peak area present: (020), (120), and (031)	Sum of En peak area present: (420 and 610)
850	4	gold	2	lt. yellow orange	1.610-1.592	1.610-1.590	0	11900	232
850	8	gold	2	lt. yellow orange	1.606-1.590	1.606-1.586	0	11800	154
850	16	gold	2	lt. yellow orange	1.598-1.574	1.598-1.574	0	10400	0
850	20	gold	2	lt. yellow orange	1.608-1.588	1.608-1.588	0	11900	0
850	24	gold	2	lt. yellow orange	1.600-1.578	1.600-1.578	0	11900	720
900	4	gold	2	lt. yellow orange	1.604-1.572	1.604-1.572	0	12400	350
900	8	gold	2	lt. yellow orange	1.612-1.558	1.612-1.558	0	12900	720
900	16	gold	2	lt. yellow orange	1.608-1.550	1.608-1.550	0	11100	0
900	20	gold	2	lt. yellow orange	1.602-1.548	1.602-1.548	0	10000	550
900	24	gold	2	lt. yellow orange	1.610-1.550	1.610-1.550	0	12400	460
950	4	gold	2	lt. yellow orange	1.620-1.558	1.620-1.550	0	12300	580
950	8	gold	2	lt. yellow orange	1.570-1.566	1.566-1.560	0	9400	10
950	16	gold	2	lt. yellow orange	1.592-1.578	1.592-1.578	0	11400	690
950	20-1	gold	2	lt. yellow orange	1.614-1.588	1.614-1.588	0	8600	220
950	20-2	gold	2	lt. yellow orange	1.616-1.590	1.616-1.590	0	8900	320

Appendix I Continued

Experimental Conditions Temperature (˚C), Time (hours)		Method of encapsulation while heating	Morphology	Color	Refractive index parallel to the length of the fiber	Refractive index perpendicular to the length of the fiber	Sum of Chr peak area present: (002), (004), and (008)	Sum of Fo peak area present: (020), (120), and (031)	Sum of En peak area present: (420 and 610)
950	24	gold	2	lt. yellow orange	1.618-1.592	1.606-1.592	0	10600	570
1000	4	gold	2	lt. orange	1.644-1.620	1.644-1.620	0	11700	2200
1000	8	gold	2	orange	1.648-1.620	1.648-1.620	0	9600	8600
1000	16	gold	2	red orange	1.650-1.638	1.650-1.638	0	8900	9100
1000	20	gold	2	red orange	1.650-1.642	1.650-1.642	0	6600	7500
1000	24-1	gold	2	red orange	1.650-1.642	1.650-1.642	0	10400	11500
1000	24-3	gold	2	red orange	1.650-1.642	1.650-1.642	0	10700	10700

Appendix II: X-ray Diffraction Data

Peak Search Report (7 Peaks, Max P/N = 14.9)
[ORIGINAL1.RD] alre1
PEAK: 29-pts/Parabolic Filter, Threshold=2.0, Cutoff=0.1%, BG=3/1.0, Peak-Top=Summit

2-Theta	d(Å)	BG	Height	I%	Area	I%	FWHM
11.82	7.481	15	489	52.9	15357	47.6	0.534
19.609	4.523	33	63	6.8	3049	9.4	0.823
24.06	3.696	37	925	100	32268	100	0.593
36.503	2.459	14	108	11.7	4136	12.8	0.651
49.601	1.836	10	79	8.5	3452	10.7	0.743
59.917	1.542	100	246	26.6	14025	43.5	0.912
63.25	1.469	13	68	7.4	2554	7.9	0.601

Peak Search Report (7 Peaks, Max P/N = 14.9)
[ORIGINAL2.RD] alre2
PEAK: 31-pts/Parabolic Filter, Threshold=2.0, Cutoff=0.1%, BG=3/1.0, Peak-Top=Summit

2-Theta	d(Å)	BG	Height	I%	Area	I%	FWHM
11.884	7.441	15	470	50.7	14830	45.9	0.536
19.64	4.516	19	100	10.8	4767	14.7	0.81
24.04	3.699	43	927	100	32327	100	0.593
36.531	2.458	12	104	11.2	4168	12.9	0.681
49.542	1.838	15	65	7	3178	9.8	0.831
59.974	1.541	22	282	30.4	17659	54.6	1.065
63.094	1.472	4	78	8.4	2994	9.3	0.614

Peak Search Report (7 Peaks, Max P/N = 13.4)
[XTA2008.RD] xta2008
PEAK: 43-pts/Parabolic Filter, Threshold=2.0, Cutoff=0.1%, BG=3/1.0, Peak-Top=Summit

2-Theta	d(Å)	BG	Height	I%	Area	I%	FWHM
12.42	7.121	17	354	47.3	11205	44.5	0.538
20.103	4.414	15	88	11.7	4753	18.9	0.918
24.66	3.607	37	749	100	25153	100	0.571
37.063	2.424	58	108	14.4	3510	14	0.553
50.081	1.820	8	67	8.9	2159	8.6	0.548
60.373	1.532	20	219	29.2	14140	56.2	1.098
63.819	1.457	8	37	4.9	1983	7.9	0.911

Appendix II Continued

Peak Search Report (7 Peaks, Max P/N = 13.4)
[XTA20016.RD]
xta20016
PEAK: 41-pts/Parabolic Filter, Threshold=2.0, Cutoff=0.1%, BG=3/1.0, Peak-Top=Summit

2-Theta	d(Å)	BG	Height	I%	Area	I%	FWHM
12.484	7.085	17	271	36.8	9158	34.6	0.574
20.284	4.374	33	59	8	2819	10.6	0.812
24.76	3.593	22	737	100	26492	100	0.611
37.063	2.424	62	96	13	3661	13.8	0.648
50.124	1.818	11	61	8.3	2029	7.7	0.565
60.464	1.530	45	200	27.1	12012	45.3	1.021
63.91	1.455	4	44	6	2810	10.6	1.086

Peak Search Report (7 Peaks, Max P/N = 15.0)
[XTA20024.RD]
xta20024
PEAK: 35-pts/Parabolic Filter, Threshold=2.0, Cutoff=0.1%, BG=3/1.0, Peak-Top=Summit

2-Theta	d(Å)	BG	Height	I%	Area	I%	FWHM
12.22	7.237	21	622	66.7	19944	66.6	0.545
19.999	4.436	12	106	11.4	5623	18.8	0.902
24.44	3.639	36	933	100	29963	100	0.546
36.882	2.435	69	86	9.2	3381	11.3	0.668
49.942	1.825	11	63	6.8	2767	9.2	0.747
60.282	1.534	32	253	27.1	16206	54.1	1.089
63.614	1.462	5	66	7.1	2136	7.1	0.55

Peak Search Report (7 Peaks, Max P/N = 15.0)
[XTA20010.RD]
xta20010d
PEAK: 39-pts/Parabolic Filter, Threshold=2.0, Cutoff=0.1%, BG=3/1.0, Peak-Top=Summit

2-Theta	d(Å)	BG	Height	I%	Area	I%	FWHM
12.38	7.144	21	453	47.2	15892	44.4	0.596
20.193	4.394	26	112	11.7	5944	16.6	0.902
24.547	3.624	60	960	100	35831	100	0.635
37.063	2.424	25	127	13.2	5324	14.9	0.713
50.033	1.822	12	71	7.4	3056	8.5	0.732
60.373	1.532	19	276	28.8	18056	50.4	1.112
63.729	1.459	11	63	6.6	2416	6.7	0.652

Appendix II Continued

Peak Search Report (6 Peaks, Max P/N = 9.5)
[4004.RD] 4004
PEAK: 41-pts/Parabolic Filter, Threshold=2.0, Cutoff=0.1%, BG=3/1.0, Peak-Top=Summit

2-Theta	d(Å)	BG	Height	I%	Area	I%	FWHM
12.402	7.131	13	217	59	7317	50.3	0.573
24.663	3.607	9	368	100	14554	100	0.672
37.039	2.425	41	39	10.6	1374	9.4	0.564
50.002	1.823	6	32	8.7	1086	7.5	0.577
60.382	1.532	46	85	23.1	4928	33.9	0.928
63.7	1.460	9	21	5.7	795	5.5	0.644

Peak Search Report (7 Peaks, Max P/N = 9.7)
[4008.RD] 4008
PEAK: 41-pts/Parabolic Filter, Threshold=2.0, Cutoff=0.1%, BG=3/1.0, Peak-Top=Summit

2-Theta	d(Å)	BG	Height	I%	Area	I%	FWHM
12.38	7.144	16	251	61.2	10098	54.3	0.684
24.66	3.607	37	410	100	18592	100	0.771
37.015	2.427	32	49	12	2075	11.2	0.72
50.002	1.823	11	36	8.8	1433	7.7	0.677
60.356	1.532	55	121	29.5	7328	39.4	1.03
63.625	1.461	9	31	7.6	1274	6.9	0.699

Peak Search Report (7 Peaks, Max P/N = 10.6)
[Xta40016.rd]
xta40016
PEAK: 45-pts/Parabolic Filter, Threshold=2.0, Cutoff=0.1%, BG=3/1.0, Peak-Top=Summit

2-Theta	d(Å)	BG	Height	I%	Area	I%	FWHM
12.38	7.144	11	325	70.5	11430	65.4	0.598
20.122	4.409	20	44	9.5	2265	13	0.875
24.482	3.633	13	461	100	17477	100	0.644
37.015	2.427	26	66	14.3	3740	21.4	0.963
50.002	1.823	7	31	6.7	1583	9.1	0.868
60.174	1.536	22	137	29.7	7842	44.9	0.973
63.757	1.458	5	34	7.4	1286	7.4	0.605

Appendix II Continued

Peak Search Report (7 Peaks, Max P/N = 10.0)
[Xta40020.rd]
xta40020
PEAK: 37-pts/Parabolic Filter, Threshold=2.0, Cutoff=0.1%, BG=3/1.0, Peak-Top=Summit

2-Theta	d(Å)	BG	Height	I%	Area	I%	FWHM
12.402	7.131	7	304	73.1	11170	65.7	0.625
20.213	4.390	24	38	9.1	1886	11.1	0.844
24.64	3.610	13	416	100	17007	100	0.695
37.015	2.427	45	41	9.9	1882	11.1	0.78
50.021	1.822	7	29	7	1483	8.7	0.869
60.359	1.532	57	99	23.8	5382	31.6	0.924
63.716	1.459	7	14	3.4	1107	6.5	1.265

Peak Search Report (7 Peaks, Max P/N = 10.7)
[XTA40024.RD]
xta40024
PEAK: 39-pts/Parabolic Filter, Threshold=2.0, Cutoff=0.1%, BG=3/1.0, Peak-Top=Summit

2-Theta	d(Å)	BG	Height	I%	Area	I%	FWHM
12.34	7.167	14	311	64.3	11159	61.2	0.61
20.103	4.414	14	48	9.9	2391	13.1	0.847
24.62	3.613	23	484	100	18229	100	0.64
36.882	2.435	86	40	8.3	1259	6.9	0.535
49.942	1.825	11	31	6.4	1369	7.5	0.707
60.402	1.531	61	106	21.9	6722	36.9	1.015
63.638	1.461	6	25	5.2	1306	7.2	0.888

Peak Search Report (7 Peaks, Max P/N = 8.3)
[XTA40030.RD]
xta40030
PEAK: 45-pts/Parabolic Filter, Threshold=2.0, Cutoff=0.1%, BG=3/1.0, Peak-Top=Summit

2-Theta	d(Å)	BG	Height	I%	Area	I%	FWHM
12.5	7.076	11	87	30.5	4241	31.5	0.829
20.485	4.332	6	32	11.2	1513	11.2	0.804
24.845	3.581	9	285	100	13480	100	0.804
37.378	2.404	32	50	17.5	2095	15.5	0.712
50.275	1.813	15	28	9.8	873	6.5	0.53
60.628	1.526	40	98	34.4	5812	43.1	1.008
64.185	1.450	5	18	6.3	974	7.2	0.866

Appendix II Continued

Peak Search Report (7 Peaks, Max P/N = 14.5)
[XXTA4504.RD]
xxta4504
PEAK: 35-pts/Parabolic Filter, Threshold=2.0, Cutoff=0.1%, BG=3/1.0, Peak-Top=Summit

2-Theta	d(Å)	BG	Height	I%	Area	I%	FWHM
12.14	7.284	25	600	68.1	19897	69.2	0.564
19.947	4.448	44	50	5.7	3415	11.9	1.161
24.399	3.645	44	881	100	28734	100	0.554
36.817	2.439	62	100	11.4	4310	15	0.733
49.829	1.828	7	63	7.2	1838	6.4	0.496
60.327	1.533	15	232	26.3	14694	51.1	1.077
63.599	1.462	12	53	6	1772	6.2	0.535

Peak Search Report (7 Peaks, Max P/N = 13.7)
[XXTA4508.RD]
xxta4508
PEAK: 35-pts/Parabolic Filter, Threshold=2.0, Cutoff=0.1%, BG=3/1.0, Peak-Top=Summit

2-Theta	d(Å)	BG	Height	I%	Area	I%	FWHM
12.36	7.155	19	623	79.3	19646	72.1	0.536
20.127	4.408	43	66	8.4	2931	10.8	0.755
24.6	3.616	32	786	100	27263	100	0.59
36.997	2.428	60	90	11.5	3977	14.6	0.751
49.98	1.823	20	45	5.7	1829	6.7	0.65
60.417	1.531	19	204	26	12250	44.9	1.021
63.619	1.461	8	49	6.2	1616	5.9	0.528

Peak Search Report (7 Peaks, Max P/N = 11.4)
[XTA45016.RD]
xta45016
PEAK: 39-pts/Parabolic Filter, Threshold=2.0, Cutoff=0.1%, BG=3/1.0, Peak-Top=Summit

2-Theta	d(Å)	BG	Height	I%	Area	I%	FWHM
12.42	7.121	13	318	59.9	11052	55.8	0.591
20.24	4.384	9	67	12.6	3293	16.6	0.836
24.62	3.613	13	531	100	19794	100	0.634
36.882	2.435	51	70	13.2	2945	14.9	0.715
49.942	1.825	11	43	8.1	1899	9.6	0.751
60.373	1.532	69	123	23.2	6632	33.5	0.863
63.655	1.461	7	36	6.8	1252	6.3	0.591

Appendix II Continued

Peak Search Report (7 Peaks, Max P/N = 12.4)
[XTA45020.RD]
xta45020
PEAK: 37-pts/Parabolic Filter, Threshold=2.0, Cutoff=0.1%, BG=3/1.0, Peak-Top=Summit

2-Theta	d(Å)	BG	Height	I%	Area	I%	FWHM
12.24	7.225	18	466	71.5	15460	68.2	0.564
20.103	4.414	18	89	13.7	4569	20.2	0.873
24.5	3.630	35	652	100	22656	100	0.591
36.92	2.433	72	108	16.6	3905	17.2	0.615
49.973	1.824	9	44	6.7	1933	8.5	0.747
60.397	1.531	65	163	25	8307	36.7	0.866
63.685	1.460	8	26	4	1623	7.2	0.999

Peak Search Report (7 Peaks, Max P/N = 13.3)
[XTA45024.RD]
xta45024
PEAK: 39-pts/Parabolic Filter, Threshold=2.0, Cutoff=0.1%, BG=3/1.0, Peak-Top=Summit

2-Theta	d(Å)	BG	Height	I%	Area	I%	FWHM
12.302	7.189	23	538	73.2	17583	65.6	0.556
20.001	4.436	11	97	13.2	5430	20.3	0.952
24.46	3.636	24	735	100	26793	100	0.62
36.861	2.436	76	79	10.7	2961	11.1	0.637
49.852	1.828	7	40	5.4	1806	6.7	0.768
60.191	1.536	46	189	25.7	12006	44.8	1.08
63.482	1.464	8	46	6.3	1532	5.7	0.566

Peak Search Report (7 Peaks, Max P/N = 9.7)
[XTA45048.RD]
xta45048
PEAK: 39-pts/Parabolic Filter, Threshold=2.0, Cutoff=0.1%, BG=3/1.0, Peak-Top=Summit

2-Theta	d(Å)	BG	Height	I%	Area	I%	FWHM
12.44	7.110	18	259	66.1	9737	53.7	0.639
20.28	4.375	18	52	13.3	2691	14.8	0.828
24.7	3.601	19	392	100	18130	100	0.786
36.791	2.441	37	83	21.2	5739	31.7	1.106
49.942	1.825	9	24	6.1	1675	9.2	1.186
60.28	1.534	72	111	28.3	6132	33.8	0.939
63.638	1.461	3	26	6.6	895	4.9	0.585

Appendix II Continued

Peak Search Report (7 Peaks, Max P/N = 11.9)
[XTA45010.RD]
xta45010d
PEAK: 41-pts/Parabolic Filter, Threshold=2.0, Cutoff=0.1%, BG=3/1.0, Peak-Top=Summit

2-Theta	d(Å)	BG	Height	I%	Area	I%	FWHM
12.14	7.284	17	536	89.5	18080	76.4	0.573
19.921	4.453	35	55	9.2	3023	12.8	0.934
24.38	3.648	30	599	100	23677	100	0.672
36.61	2.453	31	81	13.5	5030	21.2	1.056
49.67	1.834	8	45	7.5	2195	9.3	0.829
60.01	1.540	88	128	21.4	7721	32.6	1.025
63.366	1.467	10	34	5.7	1324	5.6	0.662

Peak Search Report (7 Peaks, Max P/N = 11.6)
[XTA5004.RD]
xta5004
PEAK: 39-pts/Parabolic Filter, Threshold=2.0, Cutoff=0.1%, BG=3/1.0, Peak-Top=Summit

2-Theta	d(Å)	BG	Height	I%	Area	I%	FWHM
12.12	7.296	21	499	87.2	17542	70.6	0.598
19.83	4.473	38	58	10.1	2952	11.9	0.865
24.3	3.660	31	572	100	24830	100	0.738
36.641	2.450	51	69	12.1	3240	13	0.751
49.574	1.837	6	46	8	2387	9.6	0.882
60.02	1.540	57	132	23.1	7210	29	0.874
63.185	1.470	10	31	5.4	1010	4.1	0.554

Peak Search Report (7 Peaks, Max P/N = 9.9)
[XTA5008.RD]
xta5008
PEAK: 43-pts/Parabolic Filter, Threshold=2.0, Cutoff=0.1%, BG=3/1.0, Peak-Top=Summit

2-Theta	d(Å)	BG	Height	I%	Area	I%	FWHM
12.04	7.345	14	373	87.8	13326	80.5	0.607
19.83	4.473	21	49	11.5	2281	13.8	0.791
24.365	3.650	32	425	100	16558	100	0.662
36.519	2.458	37	67	15.8	4374	26.4	1.11
49.58	1.837	13	25	5.9	1167	7	0.747
60.101	1.538	57	100	23.5	5969	36	1.015
63.185	1.470	14	25	5.9	959	5.8	0.652

Appendix II Continued

Peak Search Report (7 Peaks, Max P/N = 10.6)
[XTA50016.RD]
xta50016
PEAK: 35-pts/Parabolic Filter, Threshold=2.0, Cutoff=0.1%, BG=3/1.0, Peak-Top=Summit

2-Theta	d(Å)	BG	Height	I%	Area	I%	FWHM
12.24	7.225	11	330	68.5	13436	63.5	0.692
20.012	4.433	34	51	10.6	2950	13.9	0.983
24.456	3.637	31	482	100	21152	100	0.746
36.7	2.447	36	65	13.5	4047	19.1	1.058
49.942	1.825	6	44	9.1	1994	9.4	0.77
60.282	1.534	89	95	19.7	5845	27.6	0.984
63.67	1.460	6	36	7.5	802	3.8	0.356

Peak Search Report (7 Peaks, Max P/N = 9.6)
[XTA50020.RD]
xta50020
PEAK: 41-pts/Parabolic Filter, Threshold=2.0, Cutoff=0.1%, BG=3/1.0, Peak-Top=Summit

2-Theta	d(Å)	BG	Height	I%	Area	I%	FWHM
12.42	7.121	24	306	77.5	11385	64	0.632
20.223	4.387	30	45	11.4	2270	12.8	0.807
24.547	3.624	29	395	100	17795	100	0.766
36.791	2.441	63	49	12.4	2145	12.1	0.744
49.761	1.831	8	38	9.6	1626	9.1	0.727
60.239	1.535	48	87	22	5325	29.9	0.979
63.742	1.459	3	29	7.3	381	2.1	0.21

Peak Search Report (7 Peaks, Max P/N = 10.1)
[XTA50024.RD]
xta50024
PEAK: 33-pts/Parabolic Filter, Threshold=2.0, Cutoff=0.1%, BG=3/1.0, Peak-Top=Summit

2-Theta	d(Å)	BG	Height	I%	Area	I%	FWHM
12.16	7.272	13	327	73.2	10755	64.5	0.559
19.83	4.473	35	50	11.2	2291	13.7	0.779
24.42	3.642	40	447	100	16663	100	0.634
36.61	2.453	68	67	15	2679	16.1	0.68
49.761	1.831	11	30	6.7	1358	8.1	0.77
60.191	1.536	41	157	35.1	9980	59.9	1.081
63.457	1.465	6	34	7.6	808	4.8	0.38

Appendix II Continued

Peak Search Report (45 Peaks, Max P/N = 5.2)
[Xta50030.rd] xta50030d
PEAK: 33-pts/Parabolic Filter, Threshold=2.0, Cutoff=0.1%, BG=3/1.0, Peak-Top=Summit

2-Theta	d(Å)	BG	Height	I%	Area	I%	FWHM
17.297	5.122	1	19	16.5	522	12	0.467
19.861	4.467	6	18	15.7	577	13.2	0.545
22.839	3.890	9	43	37.4	1035	23.7	0.409
23.86	3.726	9	13	11.3	380	8.7	0.497
24.079	3.693	8	14	12.2	395	9	0.451
25.44	3.498	5	26	22.6	787	18	0.484
25.58	3.479	5	33	28.7	775	17.8	0.399
29.738	3.002	3	23	20	799	18.3	0.591
32.36	2.764	2	98	85.2	2884	66.1	0.5
35.7	2.513	7	108	93.9	3290	75.4	0.518
36.54	2.457	5	82	71.3	2401	55	0.498
38.165	2.356	8	16	13.9	236	5.4	0.251
38.165	2.356	8	16	13.9	236	5.4	0.251
39.662	2.271	7	61	53	1745	40	0.458
39.919	2.256	7	77	67	2161	49.5	0.449
40.121	2.246	4	65	56.5	2300	52.7	0.602
41.779	2.160	1	30	26.1	583	13.4	0.311
41.94	2.152	1	19	16.5	575	13.2	0.514
44.12	2.051	4	34	29.6	816	18.7	0.408
44.499	2.034	4	19	16.5	445	10.2	0.375
48.423	1.878	2	17	14.8	498	11.4	0.498
48.518	1.875	2	19	16.5	538	12.3	0.481
52.228	1.750	7	115	100	4365	100	0.645
54.883	1.671	5	26	22.6	748	17.1	0.489
55.18	1.663	6	19	16.5	585	13.4	0.523
56.004	1.641	9	34	29.6	1305	29.9	0.653
56.3	1.633	7	39	33.9	1335	30.6	0.582
56.6	1.625	5	22	19.1	826	18.9	0.601
58.601	1.574	6	21	18.3	447	10.2	0.341
58.902	1.567	7	20	17.4	425	9.7	0.361
60.22	1.535	11	36	31.3	708	16.2	0.315
60.498	1.529	11	38	33	1080	24.7	0.455
60.882	1.520	39	24	20.9	753	17.3	0.533
61.3	1.511	46	16	13.9	457	10.5	0.457

Appendix II Continued

61.681	1.503	50	27	23.5	432	9.9	0.256
61.943	1.497	54	19	16.5	433	9.9	0.387
62.559	1.484	8	76	66.1	3115	71.4	0.656
62.73	1.480	2	75	65.2	3644	83.5	0.826
64.661	1.440	2	13	11.3	295	6.8	0.386
66.86	1.398	2	54	47	2182	50	0.647
66.98	1.396	3	53	46.1	2064	47.3	0.623
67.18	1.392	1	50	43.5	2508	57.5	0.853
69.496	1.351	3	55	47.8	2247	51.5	0.695
71.44	1.319	1	25	21.7	917	21	0.587
71.66	1.315	1	30	26.1	932	21.4	0.528

Appendix II Continued

Peak Search Report (7 Peaks, Max P/N = 12.5)
[XTA5504.RD] xta5504
PEAK: 41-pts/Parabolic Filter, Threshold=2.0, Cutoff=0.1%, BG=3/1.0, Peak-Top=Summit

2-Theta	d(Å)	BG	Height	I%	Area	I%	FWHM
12.302	7.189	19	449	69.7	15750	62	0.596
20.221	4.388	30	63	9.8	2969	11.7	0.754
24.65	3.609	20	644	100	25416	100	0.671
37.018	2.426	47	76	11.8	3585	14.1	0.802
49.861	1.827	8	40	6.2	1714	6.7	0.686
60.36	1.532	71	149	23.1	7657	30.1	0.822
63.547	1.463	8	31	4.8	1510	5.9	0.828

Peak Search Report (7 Peaks, Max P/N = 9.6)
[XTA5508.RD] xta5508
PEAK: 41-pts/Parabolic Filter, Threshold=2.0, Cutoff=0.1%, BG=3/1.0, Peak-Top=Summit

2-Theta	d(Å)	BG	Height	I%	Area	I%	FWHM
12.2	7.248	17	331	78.6	11570	72.7	0.594
20.012	4.433	39	50	11.9	2456	15.4	0.835
24.44	3.639	59	421	100	15924	100	0.643
36.679	2.448	53	82	19.5	2993	18.8	0.621
49.863	1.827	10	21	5	406	2.5	0.309
60.191	1.536	42	123	29.2	6941	43.6	0.903
63.241	1.469	8	28	6.7	626	3.9	0.358

Peak Search Report (41 Peaks, Max P/N = 8.6)
[Xta55016.rd] xta55016
PEAK: 37-pts/Parabolic Filter, Threshold=2.0, Cutoff=0.1%, BG=3/1.0, Peak-Top=Summit

2-Theta	d(Å)	BG	Height	I%	Area	I%	FWHM
12.312	7.183	9	241	74.2	11280	84.9	0.749
20.2	4.392	11	58	17.8	3356	25.3	0.926
24.52	3.628	30	325	100	13283	100	0.695
32.639	2.741	4	16	4.9	415	3.1	0.415
34.821	2.574	16	71	21.8	4306	32.4	1.031
35.826	2.504	67	22	6.8	107	0.8	0.078
36.197	2.480	73	12	3.7	91	0.7	0.121
36.697	2.447	57	71	21.8	2286	17.2	0.515

Appendix II Continued

36.9	2.434	27	84	25.8	4858	36.6	0.983
37.079	2.423	27	74	22.8	3837	28.9	0.881
38.119	2.359	8	25	7.7	832	6.3	0.566
38.585	2.331	18	11	3.4	27	0.2	0.039
39.046	2.305	8	15	4.6	56	0.4	0.06
39.918	2.257	13	17	5.2	47	0.4	0.044
40.117	2.246	8	23	7.1	590	4.4	0.41
40.319	2.235	6	20	6.2	475	3.6	0.38
40.648	2.218	5	11	3.4	109	0.8	0.159
43.282	2.089	6	9	2.8	147	1.1	0.261
44.481	2.035	4	43	13.2	718	5.4	0.267
44.738	2.024	4	32	9.8	368	2.8	0.184
49.762	1.831	6	35	10.8	385	2.9	0.187
50.045	1.821	4	28	8.6	1028	7.7	0.624
52.242	1.750	8	28	8.6	956	7.2	0.58
52.355	1.746	6	30	9.2	1141	8.6	0.647
52.783	1.733	6	23	7.1	361	2.7	0.267
54.141	1.693	4	15	4.6	139	1	0.158
60.199	1.536	41	100	30.8	5112	38.5	0.818
60.487	1.529	23	106	32.6	6705	50.5	1.075
63.003	1.474	8	19	5.8	-18	-0.1	0.02
63.285	1.468	5	19	5.8	472	3.6	0.397
63.833	1.457	7	14	4.3	407	3.1	0.465
66.218	1.410	3	10	3.1	95	0.7	0.162
66.724	1.401	5	21	6.5	588	4.4	0.448
67.009	1.395	7	9	2.8	298	2.2	0.563
67.46	1.387	4	13	4	597	4.5	0.781
69.794	1.346	3	11	3.4	295	2.2	0.456
70.445	1.336	4	4	1.2	17	0.1	0.068
71.02	1.326	9	4	1.2	8	0.1	0.1
71.66	1.316	10	31	9.5	1139	8.6	0.625
72.104	1.309	6	35	10.8	1417	10.7	0.688
72.4	1.304	17	6	1.8	12	0.1	0.1

Appendix II Continued

Peak Search Report (23 Peaks, Max P/N = 8.1)
[Xta55020.rd] xta55020
PEAK: 41-pts/Parabolic Filter, Threshold=2.0, Cutoff=0.1%, BG=3/1.0, Peak-Top=Summit

2-Theta	d(Å)	BG	Height	I%	Area	I%	FWHM
12.5	7.076	13	191	69	7921	64.6	0.705
17.542	5.051	2	9	3.2	237	1.9	0.421
20.316	4.368	14	37	13.4	1988	16.2	0.913
24.8	3.587	16	277	100	12260	100	0.752
32.837	2.725	5	15	5.4	545	4.4	0.618
37.159	2.418	21	70	25.3	3795	31	0.922
39.416	2.284	6	7	2.5	153	1.2	0.35
40.325	2.235	6	12	4.3	304	2.5	0.405
44.581	2.031	3	49	17.7	836	6.8	0.29
49.683	1.834	8	17	6.1	637	5.2	0.6
50.093	1.820	7	11	4	830	6.8	1.207
52.421	1.744	6	35	12.6	1293	10.5	0.628
52.66	1.737	9	32	11.6	1181	9.6	0.627
56.46	1.629	3	9	3.2	77	0.6	0.137
60.299	1.534	38	83	30	4665	38.1	0.899
60.72	1.524	10	105	37.9	6985	57	1.064
64.462	1.444	4	8	2.9	99	0.8	0.198
66.823	1.399	6	10	3.6	574	4.7	0.918
67.391	1.388	5	12	4.3	713	5.8	0.951
68.042	1.377	6	13	4.7	55	0.4	0.068
70.021	1.343	4	13	4.7	411	3.4	0.537
71.521	1.318	7	14	5.1	788	6.4	0.901
72.163	1.308	5	22	7.9	899	7.3	0.695

Appendix II Continued

Peak Search Report (43 Peaks, Max P/N = 10.0)
[Xta55024.rd] xta55024
PEAK: 41-pts/Parabolic Filter, Threshold=2.0, Cutoff=0.1%, BG=3/1.0, Peak-Top=Summit

2-Theta	d(Å)	BG	Height	I%	Area	I%	FWHM
12.06	7.332	12	333	76.9	11970	73.1	0.611
17.379	5.099	3	10	2.3	312	1.9	0.499
20.04	4.427	15	64	14.8	3370	20.6	0.842
22.94	3.874	19	21	4.8	688	4.2	0.557
24.3	3.660	32	433	100	16380	100	0.643
32.406	2.760	4	29	6.7	1071	6.5	0.628
34.64	2.587	7	66	15.2	2389	14.6	0.615
34.838	2.573	19	48	11.1	1625	9.9	0.542
35.06	2.557	53	8	1.8	16	0.1	0.1
35.52	2.525	68	11	2.5	40	0.2	0.058
35.883	2.500	68	24	5.5	479	2.9	0.339
36.64	2.451	30	74	17.1	4758	29	1.029
36.794	2.441	21	79	18.2	4045	24.7	0.87
37.36	2.410	19	34	7.9	555	3.4	0.261
38.258	2.351	17	17	3.9	171	1	0.161
39.802	2.263	5	25	5.8	919	5.6	0.588
39.979	2.253	5	23	5.3	924	5.6	0.683
40.16	2.244	4	25	5.8	1109	6.8	0.71
41.845	2.160	3	7	1.6	111	0.7	0.254
42.041	2.147	3	10	2.3	144	0.9	0.245
44.381	2.040	7	35	8.1	752	4.6	0.365
49.561	1.838	8	18	4.2	892	5.4	0.793
49.88	1.827	5	27	6.2	1103	6.7	0.654
50.039	1.821	5	23	5.3	1080	6.6	0.798
52.139	1.753	9	36	8.3	1931	11.8	0.858
52.302	1.748	10	40	9.2	1925	11.8	0.77
52.6	1.739	9	51	11.8	2033	12.4	0.638
52.839	1.731	11	32	7.4	1830	11.2	0.972
59.701	1.548	20	81	18.7	2040	12.5	0.403
59.982	1.541	39	83	19.2	5610	34.2	1.149
60.321	1.533	46	98	22.6	5206	31.8	0.85
60.58	1.527	21	103	23.8	7383	45.1	1.219
60.92	1.520	8	102	23.6	7339	44.8	1.223
67	1.396	5	20	4.6	794	4.8	0.635

Appendix II Continued

67.34	1.390	4	30	6.9	997	6.1	0.565
67.742	1.382	7	20	4.6	109	0.7	0.087
69.341	1.354	5	18	4.2	406	2.5	0.361
69.681	1.348	4	30	6.9	798	4.9	0.452
69.793	1.346	4	13	3	850	5.2	1.112
71.28	1.322	2	24	5.5	1737	10.6	1.158
71.621	1.317	6	34	7.9	1624	9.9	0.764
71.94	1.311	3	34	7.9	2060	12.6	1.03
72.101	1.309	7	37	8.5	1589	9.7	0.687

Appendix II Continued

Peak Search Report (59 Peaks, Max P/N = 9.8)
[Xta5758.rd] xta5758
PEAK: 41-pts/Parabolic Filter, Threshold=2.0, Cutoff=0.1%, BG=3/1.0, Peak-Top=Summit

2-Theta	d(Å)	BG	Height	I%	Area	I%	FWHM
12.86	6.878	12	362	84.4	14295	77.6	0.671
20.576	4.313	39	47	11	2720	14.8	0.984
24.98	3.561	55	429	100	18416	100	0.73
35.081	2.556	11	55	12.8	2388	13	0.738
35.4	2.534	11	57	13.3	2388	13	0.712
35.605	2.519	50	22	5.1	1014	5.5	0.737
35.78	2.508	55	5	1.2	10	0.1	0.1
36.31	2.472	60	10	2.3	115	0.6	0.184
37.159	2.418	51	59	13.8	2448	13.3	0.664
37.399	2.403	27	62	14.5	4207	22.8	1.154
37.559	2.393	27	72	16.8	4357	23.7	0.968
38.379	2.343	7	39	9.1	935	5.1	0.384
38.826	2.318	7	18	4.2	405	2.2	0.36
39.039	2.305	16	12	2.8	83	0.5	0.111
39.514	2.279	9	16	3.7	220	1.2	0.22
39.786	2.264	9	11	2.6	331	1.8	0.512
40.744	2.213	10	22	5.1	69	0.4	0.05
43.379	2.084	9	19	4.4	364	2	0.307
43.902	2.061	11	23	5.4	512	2.8	0.378
44.641	2.029	11	30	7	571	3.1	0.324
46.578	1.948	6	17	4	84	0.5	0.079
46.84	1.938	6	9	2.1	57	0.3	0.101
48.911	1.861	7	16	3.7	153	0.8	0.153
49.562	1.838	7	19	4.4	342	1.9	0.288
49.64	1.835	7	18	4.2	342	1.9	0.304
49.844	1.828	7	24	5.6	1719	9.3	1.146
50.156	1.817	13	27	6.3	1274	6.9	0.802
50.339	1.811	11	34	7.9	1464	7.9	0.732
50.6	1.802	7	30	7	1606	8.7	0.857
51.02	1.789	16	5	1.2	10	0.1	0.1
51.037	1.788	15	6	1.4	21	0.1	0.056
52.4	1.745	11	19	4.4	609	3.3	0.513
52.602	1.739	11	17	4	619	3.4	0.583
52.807	1.732	12	17	4	523	2.8	0.492

Appendix II Continued

53.14	1.722	11	19	4.4	812	4.4	0.684
53.39	1.715	13	6	1.4	233	1.3	0.621
53.624	1.708	11	11	2.6	234	1.3	0.34
53.999	1.697	8	18	4.2	229	1.2	0.204
54.282	1.689	6	16	3.7	111	0.6	0.111
54.672	1.677	6	6	1.4	178	1	0.475
55.573	1.652	4	8	1.9	117	0.6	0.234
56.154	1.637	6	7	1.6	344	1.9	0.786
56.801	1.620	7	11	2.6	254	1.4	0.369
57.18	1.621	6	16	3.7	253	1.4	0.253
57.427	1.603	7	9	2.1	253	1.4	0.45
57.638	1.598	8	7	1.6	252	1.4	0.576
57.833	1.593	9	5	1.2	247	1.3	0.79
58.283	1.582	12	21	4.9	181	1	0.147
60.16	1.537	41	98	22.8	2344	12.7	0.383
60.6	1.527	71	101	23.5	5989	32.5	0.949
60.94	1.519	24	152	35.4	10259	55.7	1.08
61.28	1.511	13	124	28.9	9671	52.5	1.248
63.779	1.458	5	25	5.8	713	3.9	0.456
64.083	1.452	8	24	5.6	446	2.4	0.316
64.501	1.444	5	16	3.7	135	0.7	0.135
71.576	1.317	17	7	1.6	61	0.3	0.139
71.842	1.313	3	23	5.4	1724	9.4	1.199
72.08	1.309	9	31	7.2	1215	6.6	0.627
72.4	1.304	20	16	3.7	595	3.2	0.632

Appendix II Continued

Peak Search Report (25 Peaks, Max P/N = 7.1)
[Xta57524.rd] xta57524
PEAK: 39-pts/Parabolic Filter, Threshold=2.0, Cutoff=0.1%, BG=3/1.0, Peak-Top=Summit

2-Theta	d(Å)	BG	Height	I%	Area	I%	FWHM
12.04	7.345	11	186	79.5	6886	71.3	0.629
17.338	5.110	2	6	2.6	20	0.2	0.053
19.646	4.515	21	38	16.2	1853	19.2	0.829
22.919	3.877	16	30	12.8	581	6	0.31
24.141	3.684	35	234	100	9654	100	0.701
32.095	2.786	3	22	9.4	725	7.5	0.56
34.561	2.593	14	43	18.4	2355	24.4	0.931
35.441	2.530	56	20	8.5	274	2.8	0.219
36.405	2.466	13	78	33.3	3562	36.9	0.776
39.503	2.279	5	23	9.8	1014	10.5	0.749
39.683	2.269	4	25	10.7	753	7.8	0.512
41.781	2.160	3	15	6.4	307	3.2	0.348
43.856	2.063	6	37	15.8	883	9.1	0.406
49.602	1.836	6	26	11.1	963	10	0.63
52.1	1.754	4	44	18.8	1773	18.4	0.645
52.398	1.745	8	33	14.1	1317	13.6	0.678
56.91	1.617	2	17	7.3	193	2	0.193
60.011	1.540	80	56	23.9	3433	35.6	1.042
60.387	1.532	45	90	38.5	6522	67.6	1.232
66.769	1.400	3	20	8.5	949	9.8	0.807
67.321	1.390	6	14	6	701	7.3	0.801
69.617	1.349	2	19	8.1	491	5.1	0.439
70.962	1.327	4	21	9	116	1.2	0.088
71.401	1.320	4	29	12.4	1441	14.9	0.795
72.102	1.309	5	27	11.5	985	10.2	0.62

Appendix II Continued

Peak Search Report (50 Peaks, Max P/N = 7.1)
[Xta5874.rd] xta5875
PEAK: 31-pts/Parabolic Filter, Threshold=2.0, Cutoff=0.1%, BG=3/1.0, Peak-Top=Summit

2-Theta	d(Å)	BG	Height	I%	Area	I%	FWHM
12.1	7.309	8	142	62.8	5225	62	0.626
17.298	5.122	4	15	6.6	388	4.6	0.44
19.961	4.444	17	39	17.3	1842	21.9	0.803
23.039	3.857	21	20	8.8	366	4.3	0.311
24.32	3.657	25	226	100	8425	100	0.634
25.558	3.482	5	24	10.6	676	8	0.479
26.322	3.383	5	9	4	60	0.7	0.113
29.6	3.016	5	19	8.4	534	6.3	0.45
29.781	2.998	5	19	8.4	471	5.6	0.421
31.316	2.854	4	9	4	114	1.4	0.215
32.4	2.761	6	61	27	1474	17.5	0.411
34.461	2.600	7	29	12.8	1223	14.5	0.717
34.843	2.573	10	30	13.3	1005	11.9	0.57
35.781	2.508	24	76	33.6	1999	23.7	0.447
36.559	2.456	9	85	37.6	2805	33.3	0.561
38.245	2.351	6	26	11.5	210	2.5	0.137
39.8	2.263	4	47	20.8	1367	16.2	0.465
40.001	2.252	4	38	16.8	1350	16	0.604
40.14	2.245	4	30	13.3	1339	15.9	0.759
41.682	2.165	3	28	12.4	474	5.6	0.288
41.94	2.153	4	20	8.8	375	4.5	0.319
44.198	2.048	4	41	18.1	976	11.6	0.405
46.518	1.951	2	17	7.5	205	2.4	0.205
48.521	1.875	5	11	4.9	53	0.6	0.082
49.576	1.837	6	22	9.7	550	6.5	0.425
50.163	1.817	7	14	6.2	431	5.1	0.493
52.159	1.752	7	82	36.3	3021	35.9	0.589
52.36	1.746	7	77	34.1	2885	34.2	0.637
53.663	1.706	7	9	4	86	1	0.162
55.018	1.668	5	20	8.8	372	4.4	0.316
56.143	1.637	6	21	9.3	513	6.1	0.415
56.855	1.618	9	16	7.1	159	1.9	0.169
58.88	1.567	2	41	18.1	1462	17.4	0.606
59.6	1.550	29	45	19.9	1064	12.6	0.402

Appendix II Continued

60.1	1.538	52	75	33.2	3624	43	0.821
60.439	1.530	57	61	27	3314	39.3	0.924
60.841	1.521	38	67	29.6	4656	55.3	1.181
61.182	1.514	57	35	15.5	274	3.3	0.125
61.52	1.506	39	26	11.5	617	7.3	0.38
61.9	1.498	35	27	11.9	377	4.5	0.237
62.779	1.479	6	53	23.5	1830	21.7	0.587
66.7	1.401	3	32	14.2	417	4.9	0.208
67.059	1.394	2	47	20.8	1233	14.6	0.446
67.521	1.386	3	20	8.8	905	10.7	0.769
68.722	1.365	3	9	4	102	1.2	0.193
69.098	1.358	8	24	10.6	1664	19.8	1.179
69.52	1.351	3	43	19	1558	18.5	0.616
70.836	1.329	7	9	4	113	1.3	0.213
71.38	1.320	3	25	11.1	1549	18.4	0.991
71.84	1.313	4	38	16.8	1294	15.4	0.579

Appendix II Continued

Peak Search Report (68 Peaks, Max P/N = 6.4)
[Xta58724.rd] xta58724
PEAK: 35-pts/Parabolic Filter, Threshold=2.0, Cutoff=0.1%, BG=3/1.0, Peak-Top=Summit

2-Theta	d(Å)	BG	Height	I%	Area	I%	FWHM
17.402	5.092	6	26	15.3	646	9.5	0.398
22.96	3.870	10	68	40	1609	23.7	0.402
23.685	3.753	12	14	8.2	425	6.2	0.486
23.86	3.726	10	25	14.7	518	7.6	0.332
24.022	3.702	9	32	18.8	495	7.3	0.263
25.48	3.493	6	44	25.9	1040	15.3	0.378
25.622	3.474	4	54	31.8	1181	17.4	0.372
25.799	3.450	3	34	20	1415	20.8	0.666
29.422	3.033	6	23	13.5	232	3.4	0.161
29.626	3.013	6	28	16.5	492	7.2	0.281
29.885	2.988	9	32	18.8	788	11.6	0.394
30.117	2.965	9	26	15.3	940	13.8	0.578
32.399	2.761	5	120	70.6	3656	53.8	0.518
35.801	2.506	23	159	93.5	6801	100	0.727
36.579	2.454	4	123	72.4	3784	55.6	0.523
38.32	2.347	4	29	17.1	815	12	0.478
38.781	2.320	8	33	19.4	1071	15.7	0.519
38.959	2.310	10	29	17.1	949	14	0.556
39.921	2.256	1	111	65.3	4685	68.9	0.718
40.139	2.245	1	115	67.6	4685	68.9	0.652
41.42	2.178	5	24	14.1	258	3.8	0.172
41.661	2.166	4	42	24.7	1836	27	0.699
41.82	2.158	5	58	34.1	1311	19.3	0.384
41.94	2.152	4	41	24.1	1315	19.3	0.513
44.118	2.051	4	31	18.2	663	9.7	0.364
44.362	2.040	4	23	13.5	652	9.6	0.454
44.541	2.032	4	19	11.2	472	6.9	0.397
46.441	1.954	4	15	8.8	330	4.9	0.352
46.582	1.948	4	16	9.4	343	5	0.343
46.684	1.944	3	26	15.3	433	6.4	0.283
47.018	1.931	6	15	8.8	54	0.8	0.058
47.397	1.916	6	11	6.5	1	0	0.02
48.181	1.887	4	19	11.2	787	11.6	0.663
48.401	1.879	4	17	10	649	9.5	0.649

48.521	1.875	4	18	10.6	557	8.2	0.495
48.838	1.863	6	13	7.6	436	6.4	0.57
52.269	1.749	7	170	100	6695	98.4	0.669
52.469	1.742	13	145	85.3	6054	89	0.668
54.821	1.673	5	33	19.4	1002	14.7	0.486
54.981	1.669	6	36	21.2	965	14.2	0.456
55.896	1.644	7	21	12.4	169	2.5	0.129
56.1	1.638	11	36	21.2	1270	18.7	0.6
56.339	1.632	7	41	24.1	1769	26	0.69
56.48	1.628	7	40	23.5	1769	26	0.752
56.641	1.624	6	23	13.5	1934	28.4	1.345
56.901	1.617	4	22	12.9	2538	37.3	1.961
57.144	1.611	17	7	4.1	-84	-1.2	0.02
58.72	1.571	4	29	17.1	926	13.6	0.511
59	1.564	5	27	15.9	969	14.2	0.61
60.259	1.535	4	47	27.6	940	13.8	0.32
60.42	1.531	4	46	27.1	1228	18.1	0.427
60.58	1.527	11	42	24.7	1617	23.8	0.616
60.699	1.525	18	40	23.5	1155	17	0.462
61.042	1.517	27	50	29.4	2136	31.4	0.684
61.284	1.511	60	30	17.6	451	6.6	0.256
61.641	1.503	61	30	17.6	1550	22.8	0.827
61.715	1.502	64	30	17.6	1569	23.1	0.837
61.922	1.497	67	42	24.7	1385	20.4	0.561
62.221	1.491	57	43	25.3	2192	32.2	0.816
62.8	1.478	5	121	71.2	3714	54.6	0.522
66.442	1.406	6	24	14.1	247	3.6	0.165
67.14	1.393	2	70	41.2	2902	42.7	0.705
69.38	1.353	6	71	41.8	3036	44.6	0.684
69.586	1.350	8	68	40	2846	41.8	0.711
69.799	1.346	10	64	37.6	2783	40.9	0.696
71.339	1.321	2	28	16.5	1253	18.4	0.716
71.542	1.318	2	30	17.6	1204	17.7	0.682
71.762	1.314	3	32	18.8	1052	15.5	0.559

Appendix II Continued

Peak Search Report (57 Peaks, Max P/N = 7.6)
[Xta6004.rd] xta6004
PEAK: 33-pts/Parabolic Filter, Threshold=2.0, Cutoff=0.1%, BG=3/1.0, Peak-Top=Summit

2-Theta	d(Å)	BG	Height	I%	Area	I%	FWHM
17.429	5.084	5	39	15.7	1076	13.1	0.469
22.899	3.880	7	86	34.7	2251	27.4	0.445
23.779	3.739	9	33	13.3	751	9.1	0.364
23.919	3.717	9	45	18.1	751	9.1	0.267
24.039	3.699	9	36	14.5	751	9.1	0.355
25.38	3.506	10	48	19.4	1536	18.7	0.512
25.536	3.485	12	57	23	1442	17.5	0.43
25.66	3.469	13	46	18.5	1423	17.3	0.495
29.742	3.001	6	43	17.3	917	11.2	0.363
32.38	2.763	4	149	60.1	3968	48.3	0.453
33.76	2.653	10	3	1.2	6	0.1	0.173
35.68	2.514	30	206	83.1	6119	74.4	0.475
35.8	2.506	30	214	86.3	7493	91.2	0.595
36.441	2.464	3	167	67.3	5031	61.2	0.482
36.6	2.453	3	177	71.4	5031	61.2	0.483
38.379	2.343	4	31	12.5	955	11.6	0.524
39.781	2.260	5	109	44	3687	44.9	0.541
40.039	2.250	3	120	48.4	3917	47.7	0.555
41.8	2.159	1	66	26.6	1378	16.8	0.355
44.25	2.045	4	51	20.6	1446	17.6	0.482
44.5	2.034	6	42	16.9	1198	14.6	0.456
45.602	1.988	4	10	4	78	0.9	0.133
46.5	1.951	8	21	8.5	677	8.2	0.548
46.72	1.943	6	23	9.3	735	8.9	0.543
48.102	1.890	11	17	6.9	337	4.1	0.317
48.5	1.875	8	35	14.1	1007	12.3	0.46
48.741	1.867	7	27	10.9	993	12.1	0.625
50.392	1.809	9	11	4.4	178	2.2	0.259
50.949	1.791	13	14	5.6	245	3	0.28
52.24	1.750	15	248	100	7971	97	0.546
52.46	1.743	12	185	74.6	8220	100	0.711
54.642	1.678	5	45	18.1	1460	17.8	0.519
54.94	1.670	5	59	23.8	1505	18.3	0.434
56.1	1.638	7	55	22.2	2658	32.3	0.773

Appendix II Continued

56.28	1.633	8	61	24.6	2561	31.2	0.714
56.601	1.625	5	39	15.7	2826	34.4	1.159
56.781	1.620	4	40	16.1	2892	35.2	1.157
56.959	1.615	4	37	14.9	1142	13.9	0.525
58.661	1.572	10	45	18.1	1327	16.1	0.472
58.879	1.567	10	42	16.9	1327	16.1	0.537
59.497	1.552	28	13	5.2	91	1.1	0.112
59.759	1.546	31	13	5.2	196	2.4	0.241
60.041	1.540	21	39	15.7	924	11.2	0.379
60.14	1.537	21	41	16.5	924	11.2	0.383
60.341	1.533	21	51	20.6	1989	24.2	0.624
60.599	1.527	62	20	8.1	282	3.4	0.24
60.9	1.520	33	60	24.2	2711	33	0.723
61.142	1.514	65	29	11.7	824	10	0.483
61.538	1.506	74	36	14.5	1507	18.3	0.67
61.981	1.496	77	50	20.2	1210	14.7	0.411
62.86	1.477	10	169	68.1	5479	66.7	0.551
64.861	1.436	3	28	11.3	891	10.8	0.541
66.979	1.396	4	94	37.9	4118	50.1	0.745
67.12	1.393	8	84	33.9	3742	45.5	0.713
67.3	1.390	10	77	31	3504	42.6	0.728
69.54	1.351	13	115	46.4	3550	43.2	0.525
71.741	1.315	4	51	20.6	1591	19.4	0.53

Appendix II Continued

Peak Search Report (51 Peaks, Max P/N = 7.3)
[Xta6008.rd] xta6008
PEAK: 33-pts/Parabolic Filter, Threshold=2.0, Cutoff=0.1%, BG=3/1.0, Peak-Top=Summit

2-Theta	d(Å)	BG	Height	I%	Area	I%	FWHM
17.344	5.109	3	21	9.5	583	7.3	0.472
22.92	3.877	16	74	33.5	1737	21.8	0.376
23.064	3.850	17	65	29.4	1741	21.8	0.455
23.885	3.722	15	30	13.6	423	5.3	0.226
24.04	3.699	13	23	10.4	432	5.4	0.319
25.321	3.514	6	33	14.9	1399	17.6	0.678
25.462	3.495	6	51	23.1	1283	16.1	0.403
25.602	3.476	7	51	23.1	1420	17.8	0.473
29.642	3.011	6	26	11.8	947	11.9	0.583
29.82	2.994	5	36	16.3	1023	12.8	0.455
29.98	2.978	5	35	15.8	1048	13.2	0.509
32.354	2.765	2	144	65.2	4116	51.7	0.486
35.761	2.509	8	207	93.7	7659	96.1	0.629
36.556	2.456	5	146	66.1	3644	45.7	0.424
38.459	2.339	3	46	20.8	1863	23.4	0.688
38.944	2.311	23	24	10.9	785	9.9	0.556
39.621	2.273	5	105	47.5	4965	62.3	0.757
39.8	2.263	5	113	51.1	4962	62.3	0.703
39.98	2.253	4	128	57.9	5100	64	0.637
40.2	2.241	4	96	43.4	5779	72.5	1.023
41.8	2.159	4	60	27.1	1735	21.8	0.463
41.803	2.159	4	54	24.4	1719	21.6	0.541
44.13	2.050	5	37	16.7	1223	15.3	0.562
44.435	2.037	3	29	13.1	1326	16.6	0.777
46.463	1.953	5	27	12.2	570	7.2	0.338
46.701	1.943	3	26	11.8	807	10.1	0.528
48.561	1.873	4	32	14.5	841	10.6	0.447
48.875	1.862	5	17	7.7	418	5.2	0.418
50.315	1.812	7	6	2.7	130	1.6	0.347
50.91	1.792	8	9	4.1	288	3.6	0.512
52.27	1.749	8	221	100	7969	100	0.613
52.5	1.742	7	185	83.7	7918	99.4	0.685
54.945	1.670	4	43	19.5	1297	16.3	0.513
56.142	1.637	6	57	25.8	2293	28.8	0.684

Appendix II Continued

58.782	1.570	3	34	15.4	1140	14.3	0.57
59.056	1.563	5	24	10.9	979	12.3	0.693
60.112	1.538	4	31	14	533	6.7	0.292
60.459	1.530	4	60	27.1	1174	14.7	0.313
60.8	1.522	9	55	24.9	1460	18.3	0.425
61.101	1.515	25	71	32.1	1581	19.8	0.379
61.459	1.507	64	26	11.8	698	8.8	0.43
61.799	1.500	71	44	19.9	1321	16.6	0.48
62.081	1.494	75	51	23.1	1162	14.6	0.387
62.835	1.478	7	154	69.7	5359	67.2	0.592
64.84	1.437	3	25	11.3	882	11.1	0.6
66.983	1.396	5	79	35.7	3378	42.4	0.727
67.233	1.391	9	62	28.1	2987	37.5	0.771
67.68	1.383	4	33	14.9	241	3	0.117
69.577	1.350	6	108	48.9	3802	47.7	0.598
71.582	1.317	3	50	22.6	1569	19.7	0.502
71.818	1.313	4	49	22.2	1499	18.8	0.52

Appendix II Continued

Peak Search Report (39 Peaks, Max P/N = 8.4)
[Xta60016.rd] xta60016
PEAK: 29-pts/Parabolic Filter, Threshold=2.0, Cutoff=0.1%, BG=3/1.0, Peak-Top=Summit

2-Theta	d(Å)	BG	Height	I%	Area	I%	FWHM
17.396	5.094	5	49	16.7	1083	11.6	0.376
22.898	3.881	9	135	46.1	2537	27.2	0.319
23.941	3.714	10	48	16.4	836	9	0.296
25.559	3.482	6	73	24.9	1633	17.5	0.38
29.8	2.996	5	53	18.1	1082	11.6	0.347
32.32	2.768	4	215	73.4	4819	51.7	0.381
35.78	2.508	30	271	92.5	5965	64	0.374
36.54	2.457	6	251	85.7	6271	67.3	0.425
38.441	2.340	8	48	16.4	1026	11	0.363
38.879	2.314	8	49	16.7	1029	11	0.357
39.78	2.264	2	174	59.4	7074	75.9	0.691
40.121	2.246	3	165	56.3	4720	50.6	0.486
41.86	2.156	2	85	29	1911	20.5	0.382
44.261	2.045	4	47	16	1449	15.5	0.524
44.519	2.034	3	50	17.1	1276	13.7	0.408
46.524	1.951	5	22	7.5	698	7.5	0.539
46.837	1.938	4	24	8.2	489	5.2	0.326
48.341	1.881	5	32	10.9	887	9.5	0.443
48.599	1.872	6	29	9.9	864	9.3	0.506
51.025	1.788	7	11	3.8	224	2.4	0.346
52.26	1.749	8	293	100	9324	100	0.541
54.92	1.670	13	63	21.5	1403	15	0.379
56.14	1.637	17	72	24.6	2804	30.1	0.662
56.82	1.619	4	60	20.5	2564	27.5	0.726
58.819	1.569	2	32	10.9	481	5.2	0.256
61.082	1.516	3	42	14.3	965	10.3	0.391
61.4	1.509	5	62	21.2	1797	19.3	0.493
61.78	1.500	43	65	22.2	1901	20.4	0.468
62.021	1.495	48	66	22.5	1597	17.1	0.411
62.859	1.477	5	178	60.8	5138	55.1	0.491
63.641	1.461	8	14	4.8	89	1	0.108
64.62	1.441	6	36	12.3	1101	11.8	0.52
64.678	1.440	7	35	11.9	1065	11.4	0.517
64.956	1.434	6	30	10.2	1203	12.9	0.682

Appendix II Continued

66.981	1.396	8	93	31.7	3830	41.1	0.659
67.121	1.393	10	89	30.4	3576	38.4	0.683
67.48	1.387	3	48	16.4	1173	12.6	0.391
69.58	1.350	4	137	46.8	4288	46	0.532
71.7	1.315	3	64	21.8	1951	20.9	0.518

Appendix II Continued

Peak Search Report (40 Peaks, Max P/N = 8.4)
[Xta60020.rd] xta60020
PEAK: 31-pts/Parabolic Filter, Threshold=2.0, Cutoff=0.1%, BG=3/1.0, Peak-Top=Summit

2-Theta	d(Å)	BG	Height	I%	Area	I%	FWHM
17.442	5.080	5	32	10.9	926	9.8	0.492
22.88	3.884	11	117	39.9	2533	26.9	0.346
23.04	3.857	12	110	37.5	2563	27.2	0.396
23.867	3.725	9	50	17.1	1095	11.6	0.35
24.02	3.702	8	50	17.1	1075	11.4	0.366
25.51	3.489	7	67	22.9	1679	17.8	0.426
29.779	2.998	6	53	18.1	1281	13.6	0.387
29.921	2.984	7	50	17.1	1248	13.3	0.424
32.4	2.761	5	197	67.2	5076	53.9	0.438
35.8	2.506	25	281	95.9	8813	93.6	0.533
36.56	2.456	6	247	84.3	5605	59.5	0.386
38.262	2.350	5	47	16	3133	33.3	1.133
38.5	2.336	5	59	20.1	2341	24.9	0.675
39.059	2.304	29	20	6.8	931	9.9	0.791
39.641	2.272	10	153	52.2	6182	65.7	0.646
39.842	2.261	7	175	59.7	6406	68.1	0.622
40.08	2.248	4	141	48.1	3813	40.5	0.433
41.818	2.158	3	71	24.2	2260	24	0.541
44.423	2.038	4	55	18.8	1390	14.8	0.43
46.459	1.953	5	27	9.2	882	9.4	0.523
46.713	1.943	7	26	8.9	729	7.7	0.477
48.141	1.889	6	19	6.5	1378	14.6	1.16
48.499	1.876	4	34	11.6	1165	12.4	0.582
48.881	1.862	5	20	6.8	1138	12.1	0.91
50.927	1.792	10	21	7.2	268	2.8	0.217
52.34	1.746	11	293	100	9413	100	0.546
54.919	1.670	10	71	24.2	1712	18.2	0.41
56.16	1.636	16	76	25.9	2891	30.7	0.647
56.92	1.616	6	63	21.5	2696	28.6	0.727
58.72	1.571	2	47	16	743	7.9	0.269
60.882	1.520	0	40	13.7	679	7.2	0.289
61.261	1.512	6	61	20.8	1671	17.8	0.466
61.941	1.497	64	61	20.8	1254	13.3	0.349
62.76	1.479	12	181	61.8	5544	58.9	0.521

Appendix II Continued

64.835	1.437	5	28	9.6	1012	10.8	0.614
67	1.396	9	110	37.5	3541	37.6	0.547
67.26	1.391	9	71	24.2	3538	37.6	0.847
69.581	1.350	4	140	47.8	4621	49.1	0.561
71.501	1.318	4	50	17.1	2146	22.8	0.73
71.78	1.314	7	69	23.5	1844	19.6	0.454

Appendix II Continued

Peak Search Report (55 Peaks, Max P/N = 8.8)
[Xta60024.rd] xta60024
PEAK: 27-pts/Parabolic Filter, Threshold=2.0, Cutoff=0.1%, BG=3/1.0, Peak-Top=Summit

2-Theta	d(Å)	BG	Height	I%	Area	I%	FWHM
17.4	5.092	3	56	17.7	1081	10.3	0.328
22.935	3.874	14	143	45.1	2921	27.8	0.347
23.92	3.717	11	65	20.5	1040	9.9	0.272
25.527	3.487	6	69	21.8	2010	19.1	0.495
29.797	2.996	3	56	17.7	1343	12.8	0.408
32.36	2.764	4	239	75.4	5526	52.6	0.393
34.238	2.617	10	16	5	459	4.4	0.488
35.78	2.508	34	309	97.5	9215	87.7	0.507
36.56	2.456	0	261	82.3	6619	63	0.431
38.378	2.344	5	51	16.1	839	8	0.28
38.879	2.314	6	43	13.6	554	5.3	0.219
39.78	2.264	4	180	56.8	5386	51.3	0.509
40.1	2.247	4	150	47.3	2917	27.8	0.331
41.819	2.158	1	97	30.6	1969	18.7	0.345
44.221	2.046	9	52	16.4	1196	11.4	0.391
44.429	2.037	8	31	9.8	1335	12.7	0.732
44.62	2.029	8	29	9.1	1349	12.8	0.744
46.401	1.955	7	28	8.8	1081	10.3	0.618
46.596	1.948	7	38	12	1056	10.1	0.472
46.762	1.941	7	16	5	980	9.3	0.98
48.101	1.890	8	15	4.7	320	3	0.341
48.402	1.879	4	39	12.3	1269	12.1	0.521
48.5	1.875	6	38	12	1031	9.8	0.461
48.559	1.873	5	39	12.3	1058	10.1	0.434
48.906	1.861	6	12	3.8	226	2.2	0.301
48.977	1.858	6	11	3.5	204	1.9	0.315
49.131	1.853	11	3	0.9	6	0.1	0.204
50.522	1.805	5	18	5.7	152	1.4	0.144
51.037	1.788	9	14	4.4	156	1.5	0.189
52.3	1.748	10	317	100	10507	100	0.563
54.98	1.669	4	72	22.7	2019	19.2	0.477
56.274	1.633	5	98	30.9	3537	33.7	0.614
56.82	1.619	6	59	18.6	1760	16.8	0.477
56.981	1.615	6	43	13.6	1381	13.1	0.514

Appendix II Continued

57.6	1.599	6	10	3.2	48	0.5	0.082
57.939	1.590	10	24	7.6	101	1	0.067
58.641	1.573	12	42	13.2	1291	12.3	0.492
58.859	1.568	15	44	13.9	1188	11.3	0.459
59.464	1.553	18	16	5	81	0.8	0.081
59.96	1.542	17	32	10.1	530	5	0.282
60.36	1.532	17	50	15.8	1502	14.3	0.511
61.159	1.514	87	27	8.5	411	3.9	0.259
61.48	1.507	107	6	1.9	12	0.1	0.242
61.683	1.502	97	44	13.9	1767	16.8	0.643
61.943	1.497	107	68	21.5	1330	12.7	0.333
62.779	1.479	5	227	71.6	6854	65.2	0.513
64.918	1.435	5	31	9.8	423	4	0.232
66.96	1.396	6	110	34.7	4297	40.9	0.625
67.12	1.393	5	103	32.5	4484	42.7	0.74
67.2	1.392	7	98	30.9	4225	40.2	0.69
67.38	1.389	7	67	21.1	3748	35.7	0.895
67.919	1.379	5	16	5	95	0.9	0.101
69.5	1.351	7	167	52.7	5295	50.4	0.539
69.799	1.346	10	88	27.8	3443	32.8	0.626
71.661	1.316	6	68	21.5	1744	16.6	0.436

Appendix II Continued

Peak Search Report (48 Peaks, Max P/N = 9.6)
[Xta6504.rd] xta6504
PEAK: 29-pts/Parabolic Filter, Threshold=2.0, Cutoff=0.1%, BG=3/1.0, Peak-Top=Summit

2-Theta	d(Å)	BG	Height	I%	Area	I%	FWHM
17.38	5.098	7	52	13.9	1158	9.8	0.379
22.929	3.875	15	147	39.4	2936	24.8	0.34
23.906	3.719	10	72	19.3	1164	9.8	0.275
25.46	3.496	4	85	22.8	1972	16.6	0.371
25.56	3.482	4	93	24.9	2009	17	0.367
29.581	3.017	9	38	10.2	1074	9.1	0.452
29.762	2.999	13	61	16.4	752	6.3	0.197
29.919	2.984	7	60	16.1	1244	10.5	0.352
32.379	2.763	4	273	73.2	5842	49.3	0.364
34.761	2.579	12	23	6.2	445	3.8	0.329
35.74	2.510	28	373	100	8005	67.6	0.365
36.52	2.458	4	314	84.2	7107	60	0.385
38.419	2.341	5	73	19.6	2147	18.1	0.5
38.853	2.316	9	51	13.7	1807	15.3	0.602
39.78	2.264	5	195	52.3	7197	60.7	0.627
40.081	2.248	4	201	53.9	7277	61.4	0.579
41.768	2.161	3	117	31.4	2920	24.6	0.424
44.259	2.045	4	42	11.3	1309	11	0.53
44.441	2.037	4	35	9.4	1397	11.8	0.639
44.637	2.025	4	46	12.3	1396	11.8	0.516
46.493	1.952	6	32	8.6	824	7	0.412
46.679	1.944	5	33	8.8	845	7.1	0.435
48.503	1.875	6	35	9.4	932	7.9	0.453
50.423	1.808	3	13	3.5	176	1.5	0.23
50.996	1.789	4	20	5.4	297	2.5	0.252
52.34	1.746	6	372	99.7	11848	100	0.541
53.68	1.706	5	12	3.2	104	0.9	0.147
54.92	1.670	7	86	23.1	2285	19.3	0.452
56.16	1.636	10	103	27.6	3694	31.2	0.61
56.899	1.617	6	67	18	1308	11	0.332
57.536	1.600	9	14	3.8	77	0.6	0.088
57.879	1.592	13	13	3.5	201	1.7	0.263
58.681	1.572	15	48	12.9	1372	11.6	0.457
58.8	1.569	16	49	13.1	1287	10.9	0.447

Appendix II Continued

60.439	1.530	16	61	16.4	1834	15.5	0.511
60.999	1.518	45	67	18	2910	24.6	0.738
61.137	1.515	93	17	4.6	257	2.2	0.242
61.341	1.510	76	32	8.6	1862	15.7	0.931
61.62	1.504	79	52	13.9	3210	27.1	0.988
61.961	1.496	90	97	26	1940	16.4	0.34
62.78	1.479	5	268	71.8	7656	64.6	0.486
64.837	1.437	4	31	8.3	763	6.4	0.418
66.96	1.396	8	141	37.8	5058	42.7	0.61
67.26	1.391	9	101	27.1	4895	41.3	0.775
67.519	1.386	6	61	16.4	2948	24.9	0.773
68.264	1.373	5	13	3.5	102	0.9	0.133
69.477	1.352	5	197	52.8	6160	52	0.532
71.661	1.316	4	83	22.3	1879	15.9	0.385

Appendix II Continued

Peak Search Report (52 Peaks, Max P/N = 10.1)
[Xta6508.rd] xta6508
PEAK: 27-pts/Parabolic Filter, Threshold=2.0, Cutoff=0.1%, BG=3/1.0, Peak-Top=Summit

2-Theta	d(Å)	BG	Height	I%	Area	I%	FWHM
14.161	6.249	5	10	2.4	167	1.4	0.284
17.401	5.092	4	47	11.3	945	8.1	0.342
22.92	3.877	12	153	36.9	2659	22.7	0.295
23.921	3.717	11	77	18.6	1266	10.8	0.28
25.541	3.485	8	95	22.9	2034	17.4	0.364
29.689	3.007	14	35	8.4	817	7	0.373
29.86	2.990	10	56	13.5	1002	8.6	0.304
32.36	2.764	3	265	63.9	5473	46.8	0.351
34.383	2.606	4	27	6.5	399	3.4	0.251
35.78	2.508	26	405	97.6	9317	79.6	0.391
36.501	2.460	4	287	69.2	6556	56	0.388
38.341	2.346	4	84	20.2	2559	21.9	0.518
38.842	2.317	11	81	19.5	2007	17.1	0.421
39.76	2.265	4	183	44.1	7269	62.1	0.675
40.1	2.247	4	202	48.7	7242	61.9	0.609
41.74	2.162	3	115	27.7	2802	23.9	0.39
41.86	2.156	3	124	29.9	2799	23.9	0.384
43.685	2.070	3	13	3.1	115	1	0.15
44.261	2.045	3	56	13.5	1473	12.6	0.447
44.52	2.033	3	50	12	1486	12.7	0.476
46.522	1.950	6	33	8	808	6.9	0.392
46.701	1.943	5	24	5.8	873	7.5	0.582
48.537	1.874	4	42	10.1	1233	10.5	0.499
48.902	1.861	6	16	3.9	499	4.3	0.499
50.456	1.807	5	12	2.9	229	2	0.324
51.012	1.789	6	20	4.8	376	3.2	0.32
52.28	1.748	9	415	100	11704	100	0.479
52.559	1.740	11	199	48	5041	43.1	0.405
54.903	1.671	8	100	24.1	2283	19.5	0.388
56.18	1.636	9	125	30.1	3008	25.7	0.409
56.78	1.620	6	73	17.6	2119	18.1	0.493
57.558	1.600	5	11	2.7	82	0.7	0.127
57.937	1.590	10	15	3.6	185	1.6	0.197
58.14	1.585	11	11	2.7	187	1.6	0.289

Appendix II Continued

58.68	1.572	9	50	12	1568	13.4	0.502
58.84	1.568	12	48	11.6	1190	10.2	0.421
59.861	1.544	11	29	7	525	4.5	0.308
60.281	1.534	11	70	16.9	1719	14.7	0.417
60.66	1.525	24	61	14.7	1810	15.5	0.504
61.079	1.516	44	76	18.3	2465	21.1	0.551
61.821	1.500	82	93	22.4	3005	25.7	0.517
61.9	1.498	85	92	22.2	2696	23	0.469
62.02	1.495	86	96	23.1	2215	18.9	0.392
62.78	1.479	9	308	74.2	7604	65	0.42
64.702	1.440	3	30	7.2	898	7.7	0.479
64.841	1.437	3	40	9.6	926	7.9	0.394
66.96	1.396	7	145	34.9	5284	45.1	0.62
67.1	1.394	7	136	32.8	5286	45.2	0.622
67.459	1.387	4	88	21.2	3242	27.7	0.626
69.54	1.351	6	210	50.6	5962	50.9	0.483
70.382	1.337	4	8	1.9	71	0.6	0.151
71.7	1.315	4	95	22.9	2233	19.1	0.4

Appendix II Continued

Peak Search Report (47 Peaks, Max P/N = 10.0)
[Xta65016.rd] xta65016
PEAK: 31-pts/Parabolic Filter, Threshold=2.0, Cutoff=0.1%, BG=3/1.0, Peak-Top=Summit

2-Theta	d(Å)	BG	Height	I%	Area	I%	FWHM
17.42	5.086	7	56	13.7	1079	8.9	0.328
22.92	3.877	13	151	36.9	2928	24.1	0.33
23.94	3.714	12	74	18.1	1308	10.7	0.3
25.56	3.482	16	84	20.5	1936	15.9	0.392
29.799	2.996	8	84	20.5	3539	29.1	0.716
32.341	2.766	6	285	69.7	6321	51.9	0.377
34.041	2.632	9	10	2.4	104	0.9	0.177
35.78	2.508	30	374	91.4	9450	77.6	0.43
36.48	2.461	5	289	70.7	6966	57.2	0.41
38.28	2.349	4	75	18.3	3346	27.5	0.758
38.92	2.312	30	36	8.8	1588	13	0.75
39.729	2.267	8	187	45.7	7106	58.4	0.608
40.099	2.247	5	180	44	7370	60.5	0.696
41.801	2.159	3	124	30.3	2747	22.6	0.377
44.22	2.046	6	46	11.2	1296	10.6	0.479
44.522	2.033	5	46	11.2	1436	11.8	0.531
46.381	1.956	6	24	5.9	983	8.1	0.655
46.618	1.947	6	35	8.6	1019	8.4	0.495
46.98	1.932	7	22	5.4	654	5.4	0.476
48.322	1.882	6	30	7.3	1194	9.8	0.637
48.544	1.874	6	45	11	1189	9.8	0.449
48.797	1.865	4	24	5.9	1131	9.3	0.754
49.019	1.857	7	17	4.2	431	3.5	0.406
50.541	1.804	6	17	4.2	261	2.1	0.261
50.999	1.789	9	17	4.2	263	2.2	0.263
52.3	1.748	9	409	100	12174	100	0.506
52.64	1.737	5	187	45.7	4682	38.5	0.401
54.9	1.671	4	86	21	2017	16.6	0.399
56.24	1.634	5	103	25.2	3308	27.2	0.546
56.919	1.616	4	62	15.2	1226	10.1	0.336
58.145	1.585	9	10	2.4	271	2.2	0.461
58.712	1.571	7	52	12.7	1575	12.9	0.485
58.901	1.567	9	51	12.5	1345	11	0.448
60.441	1.530	10	71	17.4	2054	16.9	0.492

Appendix II Continued

61.172	1.514	88	23	5.6	485	4	0.358
61.74	1.501	88	57	13.9	2728	22.4	0.766
62.039	1.495	99	97	23.7	1708	14	0.299
62.82	1.478	4	267	65.3	7473	61.4	0.476
64.901	1.436	5	33	8.1	469	3.9	0.242
64.901	1.436	5	33	8.1	469	3.9	0.242
66.9	1.397	7	109	26.7	4697	38.6	0.689
67.04	1.395	5	131	32	4887	40.1	0.634
67.139	1.393	8	124	30.3	4614	37.9	0.595
67.359	1.389	7	90	22	4898	40.2	0.871
69.56	1.350	6	209	51.1	6079	49.9	0.494
71.621	1.317	3	78	19.1	2241	18.4	0.46
71.779	1.314	3	82	20	2270	18.6	0.471

Appendix II Continued

Peak Search Report (44 Peaks, Max P/N = 9.9)
[Xta65020.rd] xta65020
PEAK: 29-pts/Parabolic Filter, Threshold=2.0, Cutoff=0.1%, BG=3/1.0, Peak-Top=Summit

2-Theta	d(Å)	BG	Height	I%	Area	I%	FWHM
17.44	5.081	4	53	13.2	916	7.7	0.294
22.94	3.874	15	156	38.9	2799	23.5	0.305
23.762	3.742	3	60	15	1902	16	0.507
23.899	3.720	14	74	18.5	1263	10.6	0.29
24.001	3.705	3	73	18.2	1902	16	0.417
25.54	3.485	4	96	23.9	2034	17.1	0.36
29.606	3.015	8	30	7.5	438	3.7	0.234
29.78	2.998	8	54	13.5	917	7.7	0.272
29.939	2.982	6	47	11.7	922	7.7	0.333
32.355	2.765	2	254	63.3	5857	49.2	0.392
35.74	2.510	25	361	90	8335	70	0.393
36.534	2.458	6	292	72.8	6473	54.3	0.377
38.36	2.345	4	73	18.2	2227	18.7	0.519
38.841	2.317	9	74	18.5	2389	20.1	0.549
39.74	2.266	2	197	49.1	7259	60.9	0.59
40.119	2.246	4	183	45.6	7092	59.5	0.659
41.796	2.159	5	107	26.7	2661	22.3	0.423
44.28	2.044	5	46	11.5	1214	10.2	0.449
44.639	2.028	6	32	8	782	6.6	0.391
46.219	1.963	4	18	4.5	367	3.1	0.326
46.499	1.951	4	33	8.2	914	7.7	0.443
46.721	1.943	3	37	9.2	925	7.8	0.425
48.458	1.880	3	41	10.2	1283	10.8	0.532
48.858	1.862	5	21	5.2	917	7.7	0.699
50.442	1.808	5	19	4.7	228	1.9	0.204
50.96	1.790	7	22	5.5	393	3.3	0.304
52.26	1.750	8	401	100	11913	100	0.505
54.839	1.673	4	80	20	2123	17.8	0.425
54.999	1.668	4	83	20.7	2136	17.9	0.437
56.24	1.634	4	106	26.4	3921	32.9	0.629
56.818	1.619	3	58	14.5	2442	20.5	0.716
58.045	1.588	9	11	2.7	124	1	0.192
58.601	1.574	3	45	11.2	1548	13	0.55
58.858	1.568	6	57	14.2	1269	10.7	0.378

Appendix II Continued

60.381	1.531	8	62	15.5	1472	12.4	0.404
61.129	1.515	37	66	16.5	2658	22.3	0.685
61.868	1.498	87	81	20.2	2014	16.9	0.423
62.76	1.479	3	280	69.8	7782	65.3	0.472
64.027	1.453	4	8	2	41	0.3	0.087
64.838	1.437	4	28	7	685	5.8	0.416
66.894	1.398	6	126	31.4	4877	40.9	0.658
67.26	1.391	6	105	26.2	4851	40.7	0.785
69.481	1.352	7	202	50.4	5690	47.8	0.479
71.716	1.315	3	88	21.9	2145	18	0.414

Appendix II Continued

Peak Search Report (38 Peaks, Max P/N = 9.6)
[Xta65024.rd] xta65024
PEAK: 29-pts/Parabolic Filter, Threshold=2.0, Cutoff=0.1%, BG=3/1.0, Peak-Top=Summit

2-Theta	d(Å)	BG	Height	I%	Area	I%	FWHM
17.46	5.075	5	50	12.9	1068	9.2	0.363
22.94	3.874	10	143	36.8	2714	23.4	0.323
23.9	3.720	10	71	18.3	1125	9.7	0.269
25.561	3.482	3	83	21.3	1629	14.1	0.334
29.78	2.998	18	59	15.2	973	8.4	0.264
32.361	2.764	3	275	70.7	5760	49.7	0.356
35.76	2.509	20	389	100	8924	77	0.39
36.56	2.456	5	287	73.8	6429	55.5	0.381
38.38	2.343	5	79	20.3	1982	17.1	0.427
38.857	2.316	10	62	15.9	1545	13.3	0.424
39.78	2.264	5	192	49.4	7439	64.2	0.62
40.08	2.248	5	192	49.4	7467	64.4	0.661
41.78	2.160	3	123	31.6	2806	24.2	0.388
44.3	2.040	5	50	12.9	1175	10.1	0.4
46.581	1.948	5	30	7.7	768	6.6	0.435
46.721	1.943	5	25	6.4	756	6.5	0.484
48.52	1.875	3	44	11.3	1176	10.1	0.454
48.882	1.862	4	18	4.6	214	1.8	0.19
51.239	1.781	4	12	3.1	261	2.3	0.37
52.28	1.748	6	378	97.2	11592	100	0.521
54.88	1.672	3	102	26.2	2382	20.5	0.397
56.2	1.635	6	116	29.8	3891	33.6	0.57
56.86	1.618	2	67	17.2	1352	11.7	0.343
57.763	1.595	4	22	5.7	153	1.3	0.118
58.08	1.587	5	29	7.5	216	1.9	0.127
58.7	1.572	8	44	11.3	1215	10.5	0.442
58.84	1.568	8	43	11.1	1235	10.7	0.488
60.38	1.532	15	67	17.2	1455	12.6	0.369
61.219	1.513	91	18	4.6	726	6.3	0.645
61.94	1.497	100	103	26.5	2434	21	0.402
62.84	1.478	8	287	73.8	7965	68.7	0.472
64.837	1.437	2	24	6.2	758	6.5	0.537
67	1.396	2	122	31.4	4895	42.2	0.642
67.101	1.394	2	129	33.2	4903	42.3	0.646

Appendix II Continued

69.52	1.351	2	206	53	6346	54.7	0.524
71.719	1.315	2	77	19.8	2129	18.4	0.47

Appendix II Continued

Peak Search Report (39 Peaks, Max P/N = 10.7)
[Xta7004.rd] xta7004
PEAK: 27-pts/Parabolic Filter, Threshold=2.0, Cutoff=0.1%, BG=3/1.0, Peak-Top=Summit

2-Theta	d(Å)	BG	Height	I%	Area	I%	FWHM
17.4	5.092	4	67	14.4	1183	8.5	0.3
22.92	3.877	5	176	37.8	3134	22.6	0.303
23.861	3.726	5	97	20.9	1254	9.1	0.22
25.541	3.485	2	106	22.8	1997	14.4	0.32
29.692	3.006	6	62	13.3	1594	11.5	0.411
29.86	2.990	6	74	15.9	1535	11.1	0.353
32.34	2.766	5	327	70.3	6534	47.2	0.34
35.74	2.510	19	464	99.8	9390	67.8	0.344
36.5	2.460	4	335	72	7538	54.5	0.383
38.341	2.346	4	75	16.1	2053	14.8	0.465
38.938	2.311	23	61	13.1	1009	7.3	0.281
39.7	2.268	12	227	48.8	7863	56.8	0.589
40.06	2.249	3	209	44.9	8634	62.4	0.702
41.799	2.159	4	155	33.3	3321	24	0.364
44.221	2.046	3	41	8.8	1273	9.2	0.497
44.461	2.036	5	35	7.5	1086	7.8	0.527
44.718	2.025	5	33	7.1	1052	7.6	0.542
46.501	1.951	4	32	6.9	983	7.1	0.522
46.723	1.943	5	23	4.9	880	6.4	0.612
48.301	1.883	3	32	6.9	1356	9.8	0.678
48.541	1.874	4	60	12.9	1211	8.7	0.343
48.801	1.865	4	19	4.1	473	3.4	0.398
50.42	1.808	3	12	2.6	145	1	0.205
50.941	1.791	2	30	6.5	329	2.4	0.186
52.28	1.748	3	465	100	13843	100	0.506
54.959	1.669	5	89	19.1	2048	14.8	0.391
56.22	1.635	6	117	25.2	3798	27.4	0.552
56.821	1.619	3	82	17.6	2121	15.3	0.44
58.036	1.588	3	10	2.2	96	0.7	0.163
58.7	1.572	2	45	9.7	694	5	0.262
61.12	1.515	0	84	18.1	1320	9.5	0.267
61.959	1.490	37	128	27.5	4187	30.2	0.556
62.74	1.478	10	267	57.4	6979	50.4	0.444
64.898	1.436	5	29	6.2	969	7	0.568

Appendix II Continued

66.96	1.396	9	147	31.6	5422	39.2	0.627
67.459	1.387	2	85	18.3	4544	32.8	0.909
67.827	1.381	9	11	2.4	51	0.4	0.079
69.5	1.351	2	208	44.7	6659	48.1	0.544
71.641	1.316	1	82	17.6	2246	16.2	0.466

Appendix II Continued

Peak Search Report (44 Peaks, Max P/N = 11.5)
[Xta7008.rd] xta7008
PEAK: 27-pts/Parabolic Filter, Threshold=2.0, Cutoff=0.1%, BG=3/1.0, Peak-Top=Summit

2-Theta	d(Å)	BG	Height	I%	Area	I%	FWHM
17.42	5.087	3	67	12.4	1092	7.3	0.277
22.901	3.880	10	191	35.2	3241	21.7	0.288
23.919	3.717	9	95	17.5	1398	9.4	0.25
25.52	3.488	5	107	19.7	2105	14.1	0.334
29.8	2.996	9	90	16.6	1972	13.2	0.372
32.341	2.766	6	377	69.6	7317	49	0.33
33.978	2.636	7	18	3.3	82	0.5	0.077
35.74	2.510	20	516	95.2	11562	77.4	0.381
36.54	2.457	3	396	73.1	8112	54.3	0.348
38.319	2.347	5	60	11.1	1402	9.4	0.397
38.86	2.316	5	76	14	1237	8.3	0.277
39.74	2.266	4	228	42.1	7343	49.2	0.548
40.06	2.249	3	223	41.1	7308	48.9	0.557
41.76	2.161	1	153	28.2	2738	18.3	0.304
44.5	2.034	4	66	12.2	1592	10.7	0.41
46.321	1.959	4	24	4.4	908	6.1	0.605
46.64	1.946	4	42	7.7	969	6.5	0.392
47.34	1.919	5	13	2.4	57	0.4	0.075
48.101	1.890	8	13	2.4	176	1.2	0.217
48.54	1.874	4	51	9.4	1509	10.1	0.503
49.743	1.832	4	10	1.8	67	0.4	0.114
50.238	1.815	10	12	2.2	116	0.8	0.155
50.437	1.808	12	17	3.1	105	0.7	0.105
50.839	1.795	11	25	4.6	431	2.9	0.293
51.081	1.787	13	21	3.9	400	2.7	0.324
52.261	1.749	14	542	100	14932	100	0.468
54.959	1.669	5	123	22.7	2682	18	0.371
56.14	1.637	9	130	24	3781	25.3	0.494
56.859	1.618	3	93	17.2	2130	14.3	0.389
57.74	1.595	5	16	3	232	1.6	0.247
58.681	1.572	8	64	11.8	1400	9.4	0.35
58.813	1.569	8	62	11.4	1379	9.2	0.378
61.101	1.515	29	81	14.9	2507	16.8	0.526
61.298	1.511	38	71	13.1	1812	12.1	0.408

Appendix II Continued

61.98	1.496	98	138	25.5	2983	20	0.367
62.78	1.479	4	371	68.5	9579	64.2	0.439
63.458	1.465	4	34	6.3	383	2.6	0.192
64.86	1.436	3	41	7.6	696	4.7	0.289
66.96	1.396	2	164	30.3	6115	41	0.634
67.12	1.393	2	156	28.8	6128	41	0.629
67.319	1.390	3	127	23.4	6043	40.5	0.761
69.546	1.351	6	260	48	7278	48.7	0.476
70.464	1.335	6	14	2.6	77	0.5	0.094
71.76	1.314	6	89	16.4	2213	14.8	0.423

Appendix II Continued

Peak Search Report (46 Peaks, Max P/N = 10.5)
[Xta70016.rd] xta70016
PEAK: 31-pts/Parabolic Filter, Threshold=2.0, Cutoff=0.1%, BG=3/1.0, Peak-Top=Summit

2-Theta	d(Å)	BG	Height	I%	Area	I%	FWHM
17.441	5.081	6	58	12.6	1251	8.4	0.367
22.96	3.870	14	179	39	3729	25.1	0.354
23.96	3.711	12	89	19.4	1749	11.8	0.334
25.607	3.476	5	112	24.4	2792	18.8	0.424
29.442	3.031	7	25	5.4	415	2.8	0.266
29.7	3.006	9	59	12.9	1359	9.2	0.369
29.821	2.994	6	65	14.2	1450	9.8	0.379
32.38	2.763	4	301	65.6	7287	49.1	0.412
35.78	2.508	20	413	90	12078	81.4	0.497
36.561	2.456	3	359	78.2	8109	54.6	0.384
38.301	2.350	3	81	17.6	3024	20.4	0.635
38.9	2.313	18	66	14.4	1686	11.4	0.434
39.78	2.264	11	265	57.7	8677	58.4	0.524
40	2.252	6	220	47.9	6567	44.2	0.478
40.18	2.242	7	183	39.9	6379	43	0.558
41.86	2.156	5	153	33.3	3645	24.6	0.405
44.24	2.046	4	46	10	1512	10.2	0.559
44.501	2.034	4	47	10.2	1516	10.2	0.516
46.34	1.957	6	21	4.6	1066	7.2	0.812
46.542	1.949	6	30	6.5	1035	7	0.552
46.761	1.941	6	34	7.4	1035	7	0.517
48.478	1.876	8	43	9.4	1272	8.6	0.503
48.678	1.870	7	37	8.1	1291	8.7	0.558
48.959	1.859	7	22	4.8	851	5.7	0.619
50.365	1.810	10	17	3.7	502	3.4	0.502
51.003	1.789	13	23	5	550	3.7	0.407
52.3	1.748	15	459	100	14846	100	0.55
54.884	1.671	10	88	19.2	2283	15.4	0.441
56.199	1.635	13	108	23.5	4171	28.1	0.657
56.757	1.621	7	65	14.2	2734	18.4	0.715
57.518	1.601	6	14	3.1	67	0.5	0.077
57.992	1.589	15	9	2	61	0.4	0.108
58.755	1.570	11	42	9.2	1469	9.9	0.595

Appendix II Continued

59	1.564	11	39	8.5	1366	9.2	0.56
60.38	1.532	6	44	9.6	1010	6.8	0.367
60.599	1.527	6	49	10.7	1478	10	0.483
61.18	1.514	29	88	19.2	2470	16.6	0.477
61.44	1.508	46	79	17.2	4700	31.7	0.952
61.78	1.500	57	129	28.1	6087	41	0.755
62.005	1.496	115	91	19.8	2500	16.8	0.467
62.78	1.479	8	286	62.3	9094	61.3	0.541
67.033	1.395	6	162	35.3	6164	41.5	0.609
69.524	1.351	2	217	47.3	7474	50.3	0.586
71.561	1.317	2	74	16.1	2292	15.4	0.496
71.679	1.316	3	71	15.5	2200	14.8	0.527
71.8	1.314	3	71	15.5	2194	14.8	0.494

Appendix II Continued

Peak Search Report (46 Peaks, Max P/N = 10.9)
[Xta70020.rd] xta70020
PEAK: 29-pts/Parabolic Filter, Threshold=2.0, Cutoff=0.1%, BG=3/1.0, Peak-Top=Summit

2-Theta	d(Å)	BG	Height	I%	Area	I%	FWHM
17.439	5.081	6	55	11.2	1220	8.5	0.377
22.94	3.874	13	176	35.7	3293	22.9	0.318
23.92	3.717	11	92	18.7	1617	11.3	0.299
25.561	3.482	6	104	21.1	2235	15.6	0.365
29.621	3.013	5	41	8.3	1408	9.8	0.549
29.741	3.002	5	58	11.8	1316	9.2	0.363
29.88	2.988	4	70	14.2	1490	10.4	0.362
32.36	2.764	5	339	68.8	7205	50.2	0.361
35.8	2.506	18	493	100	12514	87.1	0.432
36.58	2.454	8	340	69	7942	55.3	0.397
38.399	2.342	8	81	16.4	2824	19.7	0.593
38.92	2.312	32	57	11.6	1339	9.3	0.399
39.78	2.264	6	225	45.6	8845	61.6	0.629
39.96	2.254	4	212	43	9052	63	0.683
40.179	2.242	4	209	42.4	9735	67.8	0.792
41.82	2.158	4	161	32.7	3758	26.2	0.397
44.279	2.044	5	55	11.2	1533	10.7	0.474
44.578	2.031	5	50	10.1	1629	11.3	0.554
46.261	1.961	4	18	3.7	1479	10.3	1.315
46.521	1.950	5	29	5.9	871	6.1	0.481
46.657	1.945	4	34	6.9	921	6.4	0.461
48.278	1.884	4	38	7.7	716	5	0.301
48.499	1.876	4	52	10.5	1411	9.8	0.434
49.059	1.855	7	10	2	322	2.2	0.515
50.982	1.790	11	20	4.1	482	3.4	0.41
52.28	1.748	14	466	94.5	14360	100	0.524
54.94	1.670	9	115	23.3	2764	19.2	0.409
55.719	1.648	11	34	6.9	229	1.6	0.108
56.26	1.634	11	135	27.4	4608	32.1	0.58
56.6	1.625	10	55	11.2	2706	18.8	0.787
56.84	1.618	3	81	16.4	2530	17.6	0.531
58.013	1.588	4	23	4.7	179	1.2	0.132
58.759	1.570	2	63	12.8	1013	7.1	0.273
61.22	1.513	3	98	19.9	2181	15.2	0.378

Appendix II Continued

61.68	1.503	16	126	25.6	5409	37.7	0.687
61.94	1.497	87	129	26.2	2700	18.8	0.356
62.8	1.478	4	309	62.7	8517	59.3	0.469
64.699	1.440	5	47	9.5	1050	7.3	0.357
64.94	1.435	3	36	7.3	1377	9.6	0.65
64.94	1.435	3	36	7.3	1377	9.6	0.65
67.04	1.395	9	160	32.5	5873	40.9	0.624
67.439	1.388	4	93	18.9	3039	21.2	0.556
69.48	1.352	6	248	50.3	7558	52.6	0.518
71.321	1.321	3	47	9.5	1571	10.9	0.535
71.581	1.317	4	74	15	2596	18.1	0.561
71.74	1.315	6	82	16.6	2297	16	0.476

Appendix II Continued

Peak Search Report (55 Peaks, Max P/N = 11.3)
[Xta70024.rd] xta70024
PEAK: 29-pts/Parabolic Filter, Threshold=2.0, Cutoff=0.1%, BG=3/1.0, Peak-Top=Summit

2-Theta	d(Å)	BG	Height	I%	Area	I%	FWHM
17.381	5.098	7	66	12.7	1180	7.9	0.304
22.94	3.874	4	185	35.6	3656	24.4	0.336
23.76	3.742	3	69	13.3	1595	10.7	0.37
23.939	3.714	4	98	18.9	1490	10	0.258
25.586	3.479	3	114	22	2329	15.6	0.347
29.78	2.998	6	83	16	1596	10.7	0.327
32.36	2.764	4	387	74.6	7637	51	0.335
35.78	2.508	18	487	93.8	11954	79.9	0.417
36.559	2.456	3	377	72.6	8549	57.1	0.385
38.3	2.348	5	92	17.7	2664	17.8	0.492
38.859	2.316	11	76	14.6	2254	15.1	0.504
39.68	2.270	5	228	43.9	9323	62.3	0.654
39.84	2.261	4	248	47.8	9397	62.8	0.606
40.08	2.248	4	247	47.6	9397	62.8	0.647
41.761	2.161	4	162	31.2	3554	23.8	0.373
44.38	2.040	5	53	10.2	1484	9.9	0.448
44.56	2.032	6	46	8.9	1370	9.2	0.506
44.924	2.016	9	5	1	5	0	0.02
45.837	1.978	5	11	2.1	124	0.8	0.192
46.159	1.965	7	17	3.3	294	2	0.277
46.481	1.952	7	36	6.9	1003	6.7	0.446
46.66	1.945	6	38	7.3	1123	7.5	0.502
47.48	1.913	7	6	1.2	-1	0	0.02
47.923	1.897	4	9	1.7	27	0.2	0.048
48.559	1.873	2	56	10.8	1252	8.4	0.38
48.899	1.861	3	14	2.7	164	1.1	0.187
48.999	1.858	5	11	2.1	-139	-0.9	0.02
50.363	1.810	2	10	1.9	64	0.4	0.109
50.899	1.792	3	20	3.9	264	1.8	0.211
51.099	1.786	4	16	3.1	249	1.7	0.265
52.3	1.748	10	519	100	14960	100	0.49
52.881	1.730	8	60	11.6	755	5	0.201
54.92	1.670	13	119	22.9	2800	18.7	0.4
56.259	1.634	10	130	25	4307	28.8	0.563

Appendix II Continued

56.66	1.623	4	75	14.5	3233	21.6	0.69
56.86	1.618	3	90	17.3	2009	13.4	0.379
57.419	1.604	2	7	1.3	54	0.4	0.123
57.526	1.601	2	5	1	58	0.4	0.186
57.645	1.598	3	6	1.2	58	0.4	0.155
57.905	1.591	4	13	2.5	5	0	0.02
57.998	1.589	4	9	1.7	58	0.4	0.11
58.098	1.586	2	6	1.2	140	0.9	0.373
58.72	1.571	1	50	9.6	944	6.3	0.321
60.422	1.531	6	16	3.1	59	0.4	0.059
61.16	1.514	1	80	15.4	1573	10.5	0.334
61.48	1.507	5	81	15.6	4205	28.1	0.831
61.98	1.496	71	136	26.2	3348	22.4	0.419
62.74	1.480	8	331	63.8	8462	56.6	0.435
64.72	1.439	4	36	6.9	851	5.7	0.378
66.146	1.412	7	7	1.3	-36	-0.2	0.02
67	1.396	5	157	30.3	5917	39.6	0.641
67.16	1.393	6	146	28.1	5770	38.6	0.632
69.5	1.351	3	253	48.7	7636	51	0.513
71.54	1.318	8	68	13.1	1997	13.3	0.47
71.798	1.314	6	89	17.1	2219	14.8	0.424

Appendix II Continued

Peak Search Report (48 Peaks, Max P/N = 10.3)
[Xta7504.rd] xta7504
PEAK: 33-pts/Parabolic Filter, Threshold=2.0, Cutoff=0.1%, BG=3/1.0, Peak-Top=Summit

2-Theta	d(Å)	BG	Height	I%	Area	I%	FWHM
17.415	5.088	4	48	11.2	1180	8.1	0.418
22.891	3.882	6	156	36.4	3469	23.8	0.378
23.9	3.720	5	86	20	2204	15.1	0.436
25.527	3.487	5	94	21.9	2297	15.7	0.415
29.866	2.989	4	68	15.9	1957	13.4	0.489
32.328	2.767	9	271	63.2	7112	48.7	0.446
34.442	2.602	10	10	2.3	55	0.4	0.094
35.76	2.510	11	399	93	10508	72	0.448
36.5	2.459	5	308	71.8	7974	54.7	0.44
38.34	2.346	4	85	19.8	3777	25.9	0.755
38.522	2.335	8	76	17.7	3425	23.5	0.721
38.879	2.314	19	56	13.1	2676	18.3	0.812
39.76	2.265	6	237	55.2	9047	62	0.611
40.042	2.250	5	224	52.2	9124	62.5	0.692
41.78	2.160	7	139	32.4	3138	21.5	0.384
44.161	2.049	4	36	8.4	1165	8	0.518
44.361	2.040	4	42	9.8	1192	8.2	0.482
44.639	2.028	4	31	7.2	1224	8.4	0.632
44.873	2.018	5	16	3.7	715	4.9	0.715
45.438	1.994	4	8	1.9	56	0.4	0.112
45.825	1.978	7	8	1.9	12	0.1	0.024
46.3	1.959	4	22	5.1	1059	7.3	0.77
46.541	1.950	5	35	8.2	977	6.7	0.447
46.761	1.941	6	25	5.8	900	6.2	0.612
48.541	1.874	4	47	11	1425	9.8	0.515
50.996	1.789	10	21	4.9	554	3.8	0.448
52.34	1.746	8	429	100	14589	100	0.578
54.94	1.670	7	89	20.7	2345	16.1	0.448
56.197	1.635	11	111	25.9	4089	28	0.626
56.621	1.624	9	64	14.9	2527	17.3	0.632
56.879	1.617	7	61	14.2	2494	17.1	0.695
57.549	1.600	6	8	1.9	45	0.3	0.09
57.94	1.590	6	9	2.1	45	0.3	0.08
58.69	1.572	3	37	8.6	880	6	0.404

Appendix II Continued

58.84	1.568	5	34	7.9	720	4.9	0.339
61.201	1.513	6	69	16.1	1688	11.6	0.416
61.54	1.506	7	97	22.6	2683	18.4	0.443
61.8	1.500	18	163	38	6292	43.1	0.618
61.94	1.497	50	135	31.5	4087	28	0.515
62.8	1.478	6	261	60.8	8457	58	0.551
63.38	1.466	3	34	7.9	375	2.6	0.176
64.558	1.442	8	19	4.4	615	4.2	0.518
64.841	1.437	2	31	7.2	814	5.6	0.446
65.161	1.430	3	17	4	-47	-0.3	0.02
67.019	1.395	2	177	41.3	5872	40.2	0.564
68.004	1.377	3	13	3	12	0.1	0.02
69.52	1.351	4	210	49	7034	48.2	0.569
71.665	1.316	3	87	20.3	2285	15.7	0.446

Appendix II Continued

Peak Search Report (59 Peaks, Max P/N = 11.2)
[Xta7508.rd] xta7508
PEAK: 29-pts/Parabolic Filter, Threshold=2.0, Cutoff=0.1%, BG=3/1.0, Peak-Top=Summit

2-Theta	d(Å)	BG	Height	I%	Area	I%	FWHM
17.408	5.090	5	62	12.3	1280	8.4	0.351
20.701	4.287	8	15	3	165	1.1	0.187
22.94	3.874	15	171	33.9	3537	23.2	0.352
23.937	3.714	15	85	16.8	1614	10.6	0.323
25.56	3.482	7	112	22.2	2412	15.8	0.366
26.698	3.336	4	31	6.1	316	2.1	0.173
29.842	2.992	4	78	15.4	1821	11.9	0.397
32.36	2.764	5	333	65.9	7830	51.3	0.4
35.78	2.508	19	462	91.5	12307	80.6	0.453
36.54	2.457	6	364	72.1	8069	52.8	0.377
38.359	2.345	5	82	16.2	3577	23.4	0.742
38.841	2.317	15	70	13.9	2791	18.3	0.678
39.72	2.267	9	234	46.3	8846	57.9	0.643
39.9	2.258	3	230	45.5	9312	61	0.648
40.12	2.246	5	241	47.7	9138	59.8	0.645
41.801	2.159	3	162	32.1	3790	24.8	0.398
44.259	2.045	6	59	11.7	1381	9	0.398
44.48	2.035	4	39	7.7	1542	10.1	0.633
44.598	2.030	4	33	6.5	1533	10	0.79
46.481	1.952	4	38	7.5	1373	9	0.578
46.661	1.945	5	42	8.3	1288	8.4	0.521
46.928	1.934	5	18	3.6	834	5.5	0.741
47.298	1.920	8	9	1.8	24	0.2	0.043
47.563	1.910	7	10	2	34	0.2	0.054
48.239	1.885	7	30	5.9	1532	10	0.817
48.4	1.879	4	43	8.5	1839	12	0.684
48.559	1.873	7	54	10.7	1481	9.7	0.466
48.74	1.867	7	27	5.3	1450	9.5	0.859
48.981	1.858	9	16	3.2	615	4	0.615
49.22	1.850	14	4	0.8	7	0	0.1
49.52	1.839	6	2	0.4	4	0	0.1
49.794	1.830	6	11	2.2	4	0	0.02
50.08	1.820	8	2	0.4	4	0	0.1
50.362	1.810	4	16	3.2	334	2.2	0.334

Appendix II Continued

50.603	1.802	4	17	3.4	410	2.7	0.41
50.882	1.793	4	19	3.8	478	3.1	0.403
51.04	1.788	7	25	5	295	1.9	0.201
52.34	1.746	5	505	100	15277	100	0.514
54.901	1.671	7	112	22.2	2192	14.3	0.333
56.2	1.635	11	122	24.2	4608	30.2	0.642
56.681	1.623	9	70	13.9	2626	17.2	0.6
56.86	1.618	3	80	15.8	2882	18.9	0.612
57.529	1.601	3	7	1.4	44	0.3	0.101
57.983	1.589	6	7	1.4	49	0.3	0.112
58.661	1.573	3	56	11.1	1207	7.9	0.345
58.88	1.567	3	51	10.1	1151	7.5	0.384
60.435	1.530	14	13	2.6	78	0.5	0.096
61.26	1.512	6	93	18.4	2547	16.7	0.466
61.9	1.498	38	158	31.3	6121	40.1	0.659
62.78	1.479	11	311	61.6	8982	58.8	0.491
63.383	1.466	3	38	7.5	831	5.4	0.372
64.541	1.443	5	37	7.3	935	6.1	0.404
64.782	1.438	3	33	6.5	989	6.5	0.509
64.918	1.435	2	34	6.7	1040	6.8	0.52
67.06	1.394	6	174	34.5	5888	38.5	0.575
67.379	1.389	8	109	21.6	3463	22.7	0.54
69.593	1.350	6	259	51.3	7942	52	0.521
71.74	1.315	3	84	16.6	2694	17.6	0.513
71.852	1.313	3	83	16.4	2828	18.5	0.579

Appendix II Continued

Peak Search Report (44 Peaks, Max P/N = 11.6)
[Xta75016.rd] xta75016
PEAK: 29-pts/Parabolic Filter, Threshold=2.0, Cutoff=0.1%, BG=3/1.0, Peak-Top=Summit

2-Theta	d(Å)	BG	Height	I%	Area	I%	FWHM
17.4	5.092	5	65	11.9	1466	9.3	0.383
22.92	3.877	13	205	37.5	3691	23.3	0.306
23.941	3.714	15	102	18.6	1589	10	0.265
25.566	3.481	5	129	23.6	2787	17.6	0.367
29.781	2.998	6	98	17.9	2209	13.9	0.383
29.921	2.984	7	91	16.6	2182	13.8	0.384
32.341	2.766	9	406	74.2	8133	51.3	0.341
35.76	2.509	10	547	100	13423	84.7	0.417
36.56	2.456	2	397	72.6	8978	56.7	0.384
38.358	2.345	2	108	19.7	4210	26.6	0.663
38.859	2.316	10	77	14.1	2563	16.2	0.566
39.721	2.267	7	265	48.4	9989	63	0.603
40.08	2.248	4	270	49.4	11402	72	0.718
41.825	2.158	2	190	34.7	3938	24.9	0.352
44.282	2.044	5	59	10.8	1648	10.4	0.447
44.499	2.034	4	63	11.5	1668	10.5	0.45
46.298	1.959	3	19	3.5	623	3.9	0.525
46.579	1.948	3	40	7.3	1035	6.5	0.44
46.741	1.942	3	36	6.6	1075	6.8	0.478
46.96	1.933	4	18	3.3	181	1.1	0.161
48.3	1.883	2	36	6.6	1384	8.7	0.615
48.514	1.875	3	54	9.9	1212	7.6	0.382
48.823	1.864	2	20	3.7	540	3.4	0.432
49.14	1.852	8	2	0.4	4	0	0.1
51.06	1.787	3	24	4.4	553	3.5	0.392
52.26	1.749	10	542	99.1	15847	100	0.497
54.78	1.674	7	112	20.5	2824	17.8	0.403
54.98	1.669	8	106	19.4	2808	17.7	0.45
56.18	1.636	12	126	23	4857	30.6	0.655
56.821	1.619	3	94	17.2	3441	21.7	0.622
57.6	1.599	4	8	1.5	29	0.2	0.058
57.932	1.590	4	14	2.6	115	0.7	0.14
58.66	1.572	4	46	8.4	942	5.9	0.328
58.84	1.568	3	52	9.5	1072	6.8	0.35

Appendix II Continued

60.356	1.532	6	12	2.2	47	0.3	0.063
61.12	1.515	81	8	1.5	16	0.1	0.1
61.329	1.510	6	91	16.6	2255	14.2	0.421
61.96	1.496	48	163	29.8	5204	32.8	0.543
62.76	1.479	10	335	61.2	8979	56.7	0.456
64.773	1.438	2	36	6.6	1160	7.3	0.548
67.052	1.395	7	172	31.4	6474	40.9	0.64
69.56	1.350	4	272	49.7	7917	50	0.495
71.66	1.316	2	94	17.2	2737	17.3	0.466
71.76	1.314	2	97	17.7	2765	17.4	0.485

Appendix II Continued

Peak Search Report (30 Peaks, Max P/N = 9.4)
[Xta75020.rd] xta75020
PEAK: 33-pts/Parabolic Filter, Threshold=2.0, Cutoff=0.1%, BG=3/1.0, Peak-Top=Summit

2-Theta	d(Å)	BG	Height	I%	Area	I%	FWHM
17.419	5.087	5	42	11.4	914	7.6	0.37
22.92	3.877	13	117	31.8	2492	20.8	0.362
23.9	3.720	10	61	16.6	1169	9.7	0.326
25.501	3.490	5	80	21.7	1766	14.7	0.375
29.859	2.990	7	60	16.3	1381	11.5	0.391
32.32	2.768	4	251	68.2	6193	51.6	0.419
35.76	2.509	22	368	100	11048	92	0.51
36.48	2.461	5	248	67.4	6247	52	0.428
38.379	2.343	6	68	18.5	3058	25.5	0.765
38.858	2.316	20	48	13	2025	16.9	0.717
40.04	2.250	4	183	49.7	7675	63.9	0.713
41.859	2.156	4	117	31.8	2788	23.2	0.405
44.159	2.049	2	34	9.2	1367	11.4	0.683
44.5	2.034	2	28	7.6	1327	11.1	0.806
46.822	1.939	3	23	6.3	887	7.4	0.656
48.594	1.872	3	31	8.4	1402	11.7	0.769
52.28	1.748	11	367	99.7	12007	100	0.556
54.961	1.669	8	89	24.2	2259	18.8	0.431
56.26	1.634	7	99	26.9	3878	32.3	0.666
56.939	1.616	2	55	14.9	1233	10.3	0.381
58.66	1.572	3	41	11.1	1206	10	0.5
60.521	1.528	3	47	12.8	1384	11.5	0.501
61.28	1.511	34	71	19.3	1637	13.6	0.392
61.981	1.496	104	85	23.1	2134	17.8	0.427
62.8	1.478	3	265	72	8013	66.7	0.514
64.937	1.435	4	24	6.5	1007	8.4	0.713
66.98	1.396	4	140	38	5592	46.6	0.679
68.16	1.375	3	10	2.7	72	0.6	0.122
69.56	1.350	5	201	54.6	6775	56.4	0.573
71.78	1.314	5	64	17.4	2127	17.7	0.565

Appendix II Continued

Peak Search Report (40 Peaks, Max P/N = 9.6)
[Xta75024.rd] xta75024
PEAK: 37-pts/Parabolic Filter, Threshold=2.0, Cutoff=0.1%, BG=3/1.0, Peak-Top=Summit

2-Theta	d(Å)	BG	Height	I%	Area	I%	FWHM
17.4	5.092	4	40	10.4	1175	9	0.499
22.88	3.884	13	123	31.9	3023	23.3	0.418
23.858	3.726	12	56	14.5	1054	8.1	0.32
25.479	3.493	4	78	20.3	1973	15.2	0.43
25.61	3.476	4	68	17.7	1940	14.9	0.456
29.702	3.005	6	63	16.4	1660	12.8	0.422
29.9	2.986	6	48	12.5	1748	13.4	0.619
32.32	2.768	6	225	58.4	6475	49.8	0.489
35.76	2.509	16	311	80.8	11689	89.9	0.639
36.54	2.457	4	245	63.6	7422	57.1	0.515
38.321	2.347	5	63	16.4	3409	26.2	0.92
38.721	2.324	11	62	16.1	2956	22.7	0.763
39.838	2.261	6	207	53.8	8076	62.1	0.663
40	2.252	6	187	48.6	8076	62.1	0.691
41.757	2.161	5	105	27.3	3114	24	0.504
44.211	2.047	4	40	10.4	1250	9.6	0.531
46.381	1.956	4	31	8.1	1027	7.9	0.53
46.639	1.946	4	26	6.8	1006	7.7	0.658
48.428	1.878	4	37	9.6	1416	10.9	0.651
52.32	1.747	15	385	100	12997	100	0.574
54.799	1.674	8	68	17.7	2054	15.8	0.513
54.941	1.670	9	66	17.1	2001	15.4	0.485
56.1	1.638	12	81	21	3639	28	0.764
56.319	1.632	8	90	23.4	4029	31	0.716
56.58	1.625	9	56	14.5	2972	22.9	0.849
56.82	1.619	3	64	16.6	3001	23.1	0.75
56.937	1.616	3	52	13.5	1988	15.3	0.65
58.56	1.575	3	37	9.6	1460	11.2	0.631
58.801	1.569	6	47	12.2	1110	8.5	0.401
60.138	1.537	2	25	6.5	678	5.2	0.461
61.332	1.510	22	74	19.2	1906	14.7	0.438
61.78	1.500	52	125	32.5	5036	38.7	0.645
62.019	1.495	95	76	19.7	3466	26.7	0.775
62.72	1.480	12	213	55.3	6978	53.7	0.557

Appendix II Continued

64.955	1.434	3	22	5.7	680	5.2	0.525
66.88	1.398	5	123	31.9	5311	40.9	0.691
67.16	1.393	6	131	34	5399	41.5	0.701
69.56	1.350	5	177	46	6375	49	0.612
71.661	1.316	5	68	17.7	1849	14.2	0.435
71.922	1.312	4	47	12.2	2399	18.5	0.868

Appendix II Continued

Peak Search Report (60 Peaks, Max P/N = 11.2)
[Xta8004.rd] xta8004
PEAK: 31-pts/Parabolic Filter, Threshold=2.0, Cutoff=0.1%, BG=3/1.0, Peak-Top=Summit

2-Theta	d(Å)	BG	Height	I%	Area	I%	FWHM
15.941	5.555	3	13	2.5	166	1.1	0.217
17.386	5.096	6	47	9.2	1190	7.5	0.405
18.288	4.847	7	7	1.4	21	0.1	0.048
19.301	4.595	2	12	2.3	85	0.5	0.113
20.518	4.325	2	16	3.1	142	0.9	0.151
22.939	3.874	10	129	25.1	2855	18.1	0.376
23.94	3.714	11	76	14.8	1500	9.5	0.336
25.64	3.472	5	96	18.7	2444	15.5	0.433
29.741	3.002	4	67	13.1	1737	11	0.415
29.88	2.988	4	70	13.6	1780	11.3	0.432
32.361	2.764	5	310	60.4	7938	50.3	0.435
35.76	2.509	12	450	87.7	11791	74.7	0.445
36.56	2.456	3	315	61.4	7051	44.7	0.381
38.34	2.346	3	81	15.8	3569	22.6	0.749
38.878	2.314	28	43	8.4	2075	13.1	0.82
39.788	2.264	3	228	44.4	8997	57	0.631
40.08	2.248	3	234	45.6	9504	60.2	0.69
41.8	2.159	3	151	29.4	3614	22.9	0.407
44.18	2.048	2	47	9.2	1526	9.7	0.552
44.578	2.031	3	39	7.6	1511	9.6	0.659
44.788	2.022	5	14	2.7	455	2.9	0.52
45.311	2.000	4	6	1.2	47	0.3	0.125
46.164	1.965	3	13	2.5	374	2.4	0.46
46.42	1.954	3	28	5.5	818	5.2	0.467
46.661	1.945	3	35	6.8	847	5.4	0.387
46.955	1.934	4	10	1.9	136	0.9	0.218
48.301	1.883	3	34	6.6	1285	8.1	0.605
48.54	1.874	4	52	10.1	1192	7.6	0.39
49.025	1.857	7	15	2.9	312	2	0.333
49.3	1.847	5	5	1	-14	-0.1	0.02
49.657	1.834	4	10	1.9	22	0.1	0.035
49.912	1.826	8	5	1	-15	-0.1	0.02
50.183	1.816	10	9	1.8	70	0.4	0.124
50.385	1.810	11	17	3.3	94	0.6	0.094

Appendix II Continued

51.057	1.787	10	27	5.3	540	3.4	0.34
52.26	1.749	12	513	100	15784	100	0.523
54.899	1.671	6	109	21.2	2699	17.1	0.421
56.22	1.635	8	130	25.3	4542	28.8	0.594
56.84	1.619	3	79	15.4	2742	17.4	0.59
58	1.589	9	19	3.7	75	0.5	0.063
58.358	1.580	4	26	5.1	551	3.5	0.339
58.621	1.574	3	47	9.2	1832	11.6	0.624
58.758	1.570	6	56	10.9	1589	10.1	0.454
58.867	1.568	6	58	11.3	1587	10.1	0.465
60.261	1.534	6	31	6	819	5.2	0.423
60.561	1.528	2	36	7	1042	6.6	0.492
61.141	1.514	16	83	16.2	1647	10.4	0.337
61.399	1.509	29	83	16.2	2140	13.6	0.413
61.88	1.498	52	174	33.9	6188	39.2	0.605
62.04	1.495	118	100	19.5	2642	16.7	0.423
62.761	1.479	7	349	68	10087	63.9	0.491
63.382	1.466	2	56	10.9	600	3.8	0.171
63.743	1.459	6	15	2.9	42	0.3	0.045
64.879	1.436	2	38	7.4	655	4.1	0.293
66.881	1.398	2	165	32.2	7079	44.8	0.686
67.101	1.394	3	173	33.7	7002	44.4	0.688
69.54	1.351	5	262	51.1	8482	53.7	0.55
71.672	1.316	5	119	23.2	2718	17.2	0.388
71.827	1.313	4	89	17.3	2384	15.1	0.429
71.958	1.311	4	59	11.5	2370	15	0.643

Appendix II Continued

Peak Search Report (54 Peaks, Max P/N = 10.7)
[Xta8008.rd] xta8008
PEAK: 31-pts/Parabolic Filter, Threshold=2.0, Cutoff=0.1%, BG=3/1.0, Peak-Top=Summit

2-Theta	d(Å)	BG	Height	I%	Area	I%	FWHM
17.46	5.075	8	46	9.5	1003	6.6	0.371
20.606	4.307	3	17	3.5	381	2.5	0.381
20.621	4.304	3	20	4.1	382	2.5	0.325
22.901	3.880	11	140	29	2960	19.3	0.359
23.94	3.714	12	76	15.7	1370	9	0.306
25.58	3.480	4	110	22.8	2414	15.8	0.373
28.242	3.157	5	9	1.9	63	0.4	0.119
29.78	2.998	9	71	14.7	1712	11.2	0.386
29.94	2.982	9	59	12.2	1734	11.3	0.5
32.38	2.763	10	311	64.4	7344	48	0.401
35.78	2.508	16	426	88.2	10313	67.4	0.412
36.58	2.454	6	321	66.5	7808	51	0.414
38.359	2.345	6	92	19	2056	13.4	0.38
38.94	2.311	22	69	14.3	1851	12.1	0.456
39.721	2.267	10	216	44.7	8434	55.1	0.625
39.9	2.258	6	208	43.1	8748	57.2	0.673
40.099	2.247	7	219	45.3	8656	56.6	0.672
41.815	2.159	7	155	32.1	3571	23.3	0.392
44.2	2.047	8	52	10.8	1543	10.1	0.504
44.36	2.040	8	44	9.1	1564	10.2	0.569
44.618	2.029	6	44	9.1	1868	12.2	0.679
44.804	2.021	8	18	3.7	516	3.4	0.459
46.42	1.954	7	28	5.8	1008	6.6	0.576
46.659	1.945	5	42	8.7	1169	7.6	0.445
46.821	1.939	6	25	5.2	994	6.5	0.676
48.069	1.891	12	7	1.4	-33	-0.2	0.02
48.339	1.881	7	34	7	1211	7.9	0.57
48.521	1.875	5	46	9.5	1412	9.2	0.522
48.781	1.865	6	29	6	1365	8.9	0.753
49.101	1.854	8	12	2.5	665	4.3	0.887
49.645	1.835	7	6	1.2	94	0.6	0.251
49.88	1.827	8	11	2.3	85	0.6	0.124
50.381	1.810	7	20	4.1	526	3.4	0.447
51.04	1.788	8	35	7.2	1265	8.3	0.614

Appendix II Continued

52.34	1.746	22	483	100	15302	100	0.539
54.98	1.669	11	109	22.6	2652	17.3	0.414
56.24	1.634	14	133	27.5	4370	28.6	0.559
56.8	1.620	7	72	14.9	2476	16.2	0.55
57.02	1.614	7	53	11	1534	10	0.492
58.081	1.587	6	26	5.4	443	2.9	0.29
58.36	1.580	6	26	5.4	1219	8	0.75
58.78	1.570	10	59	12.2	1629	10.6	0.469
58.92	1.566	10	46	9.5	1490	9.7	0.518
60.42	1.531	6	37	7.7	678	4.4	0.312
61.34	1.510	27	87	18	2295	15	0.448
61.96	1.496	56	159	32.9	6005	39.2	0.642
62.86	1.477	10	308	63.8	8817	57.6	0.487
64.917	1.435	5	30	6.2	740	4.8	0.419
66.981	1.396	5	152	31.5	6197	40.5	0.652
67.12	1.393	4	158	32.7	6308	41.2	0.679
67.36	1.389	8	133	27.5	5952	38.9	0.716
69.6	1.350	7	269	55.7	8199	53.6	0.518
71.64	1.316	5	77	15.9	2725	17.8	0.566
71.82	1.313	5	91	18.8	2728	17.8	0.51

Appendix II Continued

Peak Search Report (36 Peaks, Max P/N = 10.8)
[Xta80016.rd] xta80016
PEAK: 33-pts/Parabolic Filter, Threshold=2.0, Cutoff=0.1%, BG=3/1.0, Peak-Top=Summit

2-Theta	d(Å)	BG	Height	I%	Area	I%	FWHM
17.399	5.093	8	47	9.9	1038	6.7	0.375
20.561	4.316	7	11	2.3	341	2.2	0.496
22.92	3.877	13	135	28.4	3196	20.6	0.402
23.879	3.723	12	67	14.1	1448	9.3	0.367
25.56	3.482	4	91	19.1	2616	16.8	0.489
29.681	3.007	7	63	13.2	2017	13	0.512
29.86	2.990	7	70	14.7	2025	13	0.492
32.36	2.764	10	279	58.6	7315	47	0.446
35.72	2.512	14	389	81.7	10199	65.6	0.446
36.52	2.458	5	312	65.5	8324	53.5	0.454
38.34	2.346	9	65	13.7	2376	15.3	0.621
38.939	2.311	13	47	9.9	2249	14.5	0.813
39.898	2.258	8	176	37	6672	42.9	0.644
41.8	2.159	3	126	26.5	3187	20.5	0.43
44.219	2.046	8	54	11.3	1835	11.8	0.578
44.421	2.038	8	53	11.1	1808	11.6	0.546
44.62	2.029	8	47	9.9	1734	11.2	0.59
46.52	1.950	7	32	6.7	990	6.4	0.495
46.66	1.945	6	31	6.5	1103	7.1	0.605
48.498	1.876	5	47	9.9	1580	10.2	0.571
49.044	1.856	11	16	3.4	57	0.4	0.057
51.155	1.784	7	22	4.6	505	3.2	0.39
52.32	1.747	9	476	100	15549	100	0.555
54.94	1.670	10	110	23.1	2887	18.6	0.446
56.2	1.635	12	113	23.7	4523	29.1	0.68
56.917	1.616	5	64	13.4	4031	25.9	1.071
58.08	1.587	14	13	2.7	108	0.7	0.133
58.76	1.570	9	55	11.6	1539	9.9	0.476
61.301	1.511	21	89	18.7	1878	12.1	0.359
61.979	1.496	115	104	21.8	2635	16.9	0.431
62.8	1.478	14	304	63.9	9589	61.7	0.536
64.68	1.440	4	38	8	866	5.6	0.387
67.04	1.395	6	168	35.3	6423	41.3	0.65
67.457	1.387	5	91	19.1	3908	25.1	0.73

69.5	1.351	7	243	51.1	8107	52.1	0.567
71.7	1.315	4	84	17.6	2748	17.7	0.556

Appendix II Continued

Peak Search Report (36 Peaks, Max P/N = 10.3)
[Xta80020.rd] xta80020
PEAK: 31-pts/Parabolic Filter, Threshold=2.0, Cutoff=0.1%, BG=3/1.0, Peak-Top=Summit

2-Theta	d(Å)	BG	Height	I%	Area	I%	FWHM
17.322	5.115	5	36	8.4	1042	7	0.492
20.724	4.283	7	12	2.8	227	1.5	0.322
22.88	3.884	16	131	30.4	3099	20.7	0.402
23.899	3.720	12	68	15.8	1409	9.4	0.352
25.459	3.496	3	89	20.6	2658	17.8	0.508
25.56	3.482	3	87	20.2	2663	17.8	0.49
29.855	2.990	4	59	13.7	2030	13.6	0.585
32.36	2.764	10	267	61.9	7493	50.1	0.477
35.68	2.514	18	355	82.4	10911	73	0.522
36.44	2.464	4	313	72.6	7663	51.2	0.416
38.36	2.345	4	126	29.2	3339	22.3	0.451
38.88	2.314	20	33	7.7	1152	7.7	0.593
39.78	2.264	0	215	49.9	7590	50.7	0.6
40.06	2.249	22	144	33.4	5544	37.1	0.616
41.8	2.159	1	129	29.9	2891	19.3	0.381
44.599	2.030	10	233	54.1	4843	32.4	0.353
45.162	2.010	13	15	3.5	249	1.7	0.282
46.48	1.952	13	34	7.9	985	6.6	0.464
46.718	1.943	11	35	8.1	1086	7.3	0.527
48.354	1.881	5	36	8.4	1105	7.4	0.522
48.6	1.872	4	40	9.3	1181	7.9	0.472
50.944	1.791	6	11	2.6	194	1.3	0.3
52.26	1.749	10	431	100	14956	100	0.59
54.94	1.670	8	93	21.6	2734	18.3	0.5
56.26	1.634	7	107	24.8	4594	30.7	0.73
56.852	1.618	4	51	11.8	406	2.7	0.135
58.76	1.570	7	53	12.3	1595	10.7	0.512
60.301	1.534	4	27	6.3	710	4.7	0.447
61.151	1.514	25	70	16.2	1308	8.7	0.318
61.88	1.498	67	138	32	4844	32.4	0.597
62.78	1.479	14	275	63.8	9119	61	0.564
64.92	1.435	3	74	17.2	1732	11.6	0.398
66.9	1.397	7	151	35	6135	41	0.691
67.18	1.392	7	142	32.9	6118	40.9	0.689

69.5	1.351	8	228	52.9	7835	52.4	0.584
71.7	1.315	4	82	19	2586	17.3	0.536

Appendix II Continued

Peak Search Report (46 Peaks, Max P/N = 10.9)
[Xta80024.rd] xta80024
PEAK: 33-pts/Parabolic Filter, Threshold=2.0, Cutoff=0.1%, BG=3/1.0, Peak-Top=Summit

2-Theta	d(Å)	BG	Height	I%	Area	I%	FWHM
17.425	5.085	7	56	11.6	1230	7.7	0.373
20.82	4.263	5	15	3.1	483	3	0.547
22.941	3.874	16	163	33.7	3622	22.6	0.378
23.945	3.713	12	75	15.5	1569	9.8	0.356
25.442	3.498	2	93	19.3	2857	17.8	0.492
25.579	3.480	2	110	22.8	2857	17.8	0.442
25.68	3.466	2	95	19.7	2820	17.6	0.475
26.683	3.338	3	20	4.1	299	1.9	0.239
26.865	3.316	3	20	4.1	314	2	0.267
29.803	2.995	6	78	16.1	2120	13.2	0.435
32.36	2.764	12	320	66.3	7633	47.6	0.406
35.759	2.509	12	457	94.6	11918	74.2	0.443
36.58	2.454	3	375	77.6	8494	52.9	0.385
38.381	2.343	6	80	16.6	3076	19.2	0.654
38.879	2.314	14	68	14.1	2598	16.2	0.65
39.036	2.306	22	53	11	2104	13.1	0.635
39.78	2.264	4	234	48.4	9829	61.2	0.672
40.14	2.245	5	228	47.2	9745	60.7	0.727
41.84	2.157	5	155	32.1	3830	23.9	0.42
44.179	2.048	6	40	8.3	1527	9.5	0.649
44.481	2.035	6	43	8.9	1495	9.3	0.556
46.681	1.944	6	43	8.9	1131	7	0.421
48.38	1.880	3	40	8.3	1489	9.3	0.596
48.56	1.873	3	52	10.8	1397	8.7	0.457
48.98	1.858	5	20	4.1	912	5.7	0.73
50.465	1.807	9	10	2.1	122	0.8	0.207
51.002	1.789	10	26	5.4	560	3.5	0.345
52.3	1.748	11	483	100	16052	100	0.565
54.921	1.670	4	98	20.3	2622	16.3	0.455
56.24	1.634	8	120	24.8	3948	24.6	0.559
56.82	1.619	7	75	15.5	2190	13.6	0.496
57.488	1.602	6	9	1.9	5	0	0.02
58.003	1.589	13	14	2.9	118	0.7	0.143
58.3	1.581	6	23	4.8	772	4.8	0.537

Appendix II Continued

58.621	1.574	4	65	13.5	2194	13.7	0.54
58.74	1.571	5	72	14.9	2178	13.6	0.514
58.981	1.565	11	45	9.3	1328	8.3	0.472
60.36	1.532	4	37	7.7	667	4.2	0.306
61.2	1.513	19	99	20.5	1959	12.2	0.317
61.401	1.509	30	95	19.7	2344	14.6	0.419
61.94	1.497	60	163	33.7	5978	37.2	0.623
62.8	1.478	15	324	67.1	10038	62.5	0.527
64.839	1.437	2	41	8.5	920	5.7	0.381
67.04	1.395	2	178	36.9	6705	41.8	0.64
69.579	1.350	6	243	50.3	7901	49.2	0.553
71.664	1.316	5	84	17.4	2744	17.1	0.555

Appendix II Continued

Peak Search Report (47 Peaks, Max P/N = 11.8)
[Xta8504.rd] xta8504
PEAK: 29-pts/Parabolic Filter, Threshold=2.0, Cutoff=0.1%, BG=3/1.0, Peak-Top=Summit

2-Theta	d(Å)	BG	Height	I%	Area	I%	FWHM
17.36	5.104	4	59	10.4	1207	7.5	0.348
20.661	4.295	4	10	1.8	226	1.4	0.384
22.841	3.890	9	163	28.6	3063	19	0.319
23.88	3.723	9	91	16	1376	8.5	0.257
25.501	3.490	3	111	19.5	2423	15	0.371
28.039	3.180	3	13	2.3	232	1.4	0.303
29.84	2.992	10	76	13.3	1802	11.2	0.403
32.379	2.763	12	338	59.3	7615	47.3	0.383
33.398	2.681	7	11	1.9	98	0.6	0.151
35.74	2.510	9	472	82.8	12331	76.5	0.444
36.5	2.460	4	384	67.4	8072	50.1	0.357
38.419	2.341	5	85	14.9	2791	17.3	0.558
38.86	2.316	11	85	14.9	2219	13.8	0.444
39.721	2.267	5	267	46.8	9270	57.5	0.59
40.12	2.246	5	240	42.1	9265	57.5	0.656
41.78	2.160	5	158	27.7	3736	23.2	0.402
44.241	2.046	4	47	8.2	1316	8.2	0.476
44.5	2.034	6	39	6.8	1264	7.8	0.551
44.638	2.028	4	32	5.6	1752	10.9	0.931
46.423	1.954	8	29	5.1	622	3.9	0.343
46.64	1.946	4	37	6.5	1105	6.9	0.508
48.38	1.880	4	49	8.6	1519	9.4	0.496
48.541	1.874	4	55	9.6	1541	9.6	0.476
50.188	1.816	8	10	1.8	159	1	0.27
50.682	1.800	10	19	3.3	569	3.5	0.479
50.931	1.792	12	30	5.3	667	4.1	0.378
52.28	1.748	13	570	100	16116	100	0.481
54.9	1.671	8	122	21.4	2703	16.8	0.377
55.46	1.655	11	6	1.1	12	0.1	0.032
56.1	1.638	12	121	21.2	4440	27.6	0.624
56.641	1.624	9	76	13.3	2882	17.9	0.607
56.879	1.618	3	84	14.7	2218	13.8	0.449
57.2	1.609	11	3	0.5	6	0	0.227
57.483	1.602	7	9	1.6	71	0.4	0.134

Appendix II Continued

57.961	1.590	4	14	2.5	214	1.3	0.245
58.158	1.585	2	16	2.8	385	2.4	0.409
58.738	1.571	1	58	10.2	1286	8	0.377
61.201	1.513	1	102	17.9	2229	13.8	0.372
61.92	1.497	39	171	30	5964	37	0.593
62.8	1.478	10	317	55.6	9176	56.9	0.492
63.357	1.467	3	41	7.2	994	6.2	0.412
63.903	1.456	6	11	1.9	58	0.4	0.09
64.759	1.438	2	37	6.5	1020	6.3	0.469
67.02	1.395	5	175	30.7	6337	39.3	0.616
67.355	1.389	5	89	15.6	4230	26.2	0.808
69.56	1.350	4	281	49.3	8333	51.7	0.504
71.681	1.316	5	90	15.8	2579	16	0.487

Appendix II Continued

Peak Search Report (53 Peaks, Max P/N = 10.9)
[Xta8508.rd] xta8508
PEAK: 31-pts/Parabolic Filter, Threshold=2.0, Cutoff=0.1%, BG=3/1.0, Peak-Top=Summit

2-Theta	d(Å)	BG	Height	I%	Area	I%	FWHM
17.38	5.098	6	58	11.8	1328	8.5	0.389
20.481	4.333	5	16	3.3	254	1.6	0.27
20.714	4.285	4	14	2.8	284	1.8	0.345
22.88	3.884	14	155	31.5	3252	20.9	0.357
23.92	3.717	13	77	15.7	1529	9.8	0.338
25.502	3.490	4	104	21.1	2681	17.2	0.438
28.241	3.157	4	8	1.6	75	0.5	0.159
29.747	3.001	6	71	14.4	1830	11.8	0.412
29.88	2.988	6	73	14.8	1793	11.5	0.418
30.958	2.886	12	11	2.2	79	0.5	0.122
32.36	2.764	13	324	65.9	7261	46.7	0.381
35.76	2.509	15	453	92.1	10717	69	0.402
36.52	2.458	4	357	72.6	8512	54.8	0.405
38.239	2.352	6	76	15.4	3680	23.7	0.775
38.4	2.342	4	89	18.1	3667	23.6	0.7
38.899	2.313	17	73	14.8	2719	17.5	0.633
39.82	2.262	5	252	51.2	9331	60	0.629
40.06	2.249	4	223	45.3	9890	63.6	0.71
41.8	2.159	5	154	31.3	3772	24.3	0.416
44.241	2.046	3	49	10	1394	9	0.484
44.532	2.033	3	38	7.7	1705	11	0.763
46.224	1.962	5	23	4.7	536	3.4	0.373
46.596	1.948	5	38	7.7	1038	6.7	0.464
46.799	1.940	5	30	6.1	1026	6.6	0.547
48.201	1.886	8	25	5.1	885	5.7	0.566
48.539	1.874	8	57	11.6	1477	9.5	0.441
49.033	1.856	11	12	2.4	638	4.1	0.851
49.557	1.838	12	5	1	10	0.1	0.205
49.802	1.829	13	6	1.2	26	0.2	0.069
50.269	1.814	10	22	4.5	562	3.6	0.434
50.54	1.804	22	3	0.6	6	0	0.207
50.9	1.792	20	19	3.9	576	3.7	0.485
51.021	1.788	21	19	3.9	564	3.6	0.505
52.32	1.747	18	492	100	15543	100	0.537

Appendix II Continued

54.9	1.671	5	109	22.2	2473	15.9	0.386
56.12	1.638	7	117	23.8	4746	30.5	0.69
56.76	1.621	2	75	15.2	3433	22.1	0.732
56.88	1.617	2	69	14	3527	22.7	0.869
57.519	1.601	6	15	3	64	0.4	0.068
58.021	1.588	15	7	1.4	175	1.1	0.4
58.667	1.572	6	51	10.4	1931	12.4	0.644
58.88	1.567	9	45	9.1	1484	9.5	0.528
60.459	1.530	6	31	6.3	491	3.2	0.269
61.261	1.512	24	93	18.9	2156	13.9	0.394
61.84	1.499	47	155	31.5	6443	41.5	0.665
62	1.496	117	95	19.3	2652	17.1	0.475
62.8	1.478	5	319	64.8	9753	62.7	0.52
64.895	1.436	2	23	4.7	856	5.5	0.633
67.08	1.394	2	171	34.8	6503	41.8	0.646
67.499	1.386	4	89	18.1	2634	16.9	0.503
69.6	1.350	5	254	51.6	8145	52.4	0.545
71.621	1.316	4	82	16.7	2475	15.9	0.483
71.859	1.313	75	15.2	2472	15.9	0.56	

Appendix II Continued

Peak Search Report (34 Peaks, Max P/N = 10.3)
[Xta85016.rd] xta85016
PEAK: 33-pts/Parabolic Filter, Threshold=2.0, Cutoff=0.1%, BG=3/1.0, Peak-Top=Summit

2-Theta	d(Å)	BG	Height	I%	Area	I%	FWHM
17.362	5.104	6	41	9.5	989	6.8	0.41
20.562	4.316	5	14	3.2	379	2.6	0.433
22.96	3.870	7	118	27.3	2644	18.2	0.381
23.862	3.726	7	62	14.4	1385	9.5	0.38
25.58	3.480	4	75	17.4	2004	13.8	0.454
29.699	3.006	3	55	12.7	1551	10.7	0.451
29.878	2.988	4	56	13	1488	10.2	0.452
32.34	2.766	9	248	57.4	6789	46.7	0.465
35.76	2.509	7	356	82.4	12478	85.8	0.596
36.479	2.461	5	248	57.4	6612	45.5	0.453
38.3	2.348	3	70	16.2	3079	21.2	0.748
38.879	2.314	12	63	14.6	2450	16.9	0.661
39.68	2.270	8	165	38.2	8335	57.3	0.808
39.999	2.252	3	210	48.6	8752	60.2	0.708
41.8	2.159	4	122	28.2	3598	24.8	0.501
44.28	2.044	4	60	13.9	1731	11.9	0.462
44.52	2.033	5	50	11.6	1671	11.5	0.568
46.301	1.959	3	25	5.8	1167	8	0.747
46.611	1.947	4	27	6.3	1071	7.4	0.674
48.38	1.880	3	33	7.6	1206	8.3	0.585
48.561	1.873	2	46	10.6	1250	8.6	0.462
52.32	1.747	7	432	100	14536	100	0.572
54.919	1.670	11	75	17.4	2511	17.3	0.569
56.28	1.633	14	106	24.5	3993	27.5	0.64
56.907	1.617	2	49	11.3	681	4.7	0.236
58.709	1.571	3	30	6.9	688	4.7	0.367
58.861	1.568	2	31	7.2	798	5.5	0.438
61.18	1.514	0	73	16.9	1582	10.9	0.368
61.94	1.497	34	141	32.6	5163	35.5	0.622
62.74	1.480	12	287	66.4	8593	59.1	0.509
64.681	1.440	3	33	7.6	881	6.1	0.454
67	1.396	6	150	34.7	6321	43.5	0.716
69.54	1.351	2	236	54.6	8060	55.4	0.581
71.78	1.314	3	74	17.1	1984	13.6	0.456

Appendix II Continued

Peak Search Report (45 Peaks, Max P/N = 11.2)
[Xta85020.rd]
xta85020
PEAK: 31-pts/Parabolic Filter, Treshold=2.0, Cutoff=0.1%, BG=3/1.0, Peak-Top=Summit

2-Theta	d(Å)	BG	Height	I%	Area	I%	FWHM
17.421	5.086	6	53	10.3	1098	6.8	0.352
20.621	4.304	5	14	2.7	290	1.8	0.352
22.92	3.877	12	160	31.2	3242	20	0.344
23.959	3.711	11	79	15.4	1560	9.6	0.336
25.5	3.490	5	105	20.5	2580	15.9	0.393
25.6	3.477	6	109	21.2	2482	15.3	0.387
29.661	3.009	4	58	11.3	1689	10.4	0.466
29.84	2.992	4	79	15.4	1694	10.4	0.365
32.38	2.763	6	345	67.3	7557	46.5	0.372
35.78	2.508	16	446	86.9	10569	65.1	0.403
36.56	2.456	5	336	65.5	8745	53.9	0.442
38.42	2.341	4	87	17	3847	23.7	0.752
38.899	2.313	33	62	12.1	2174	13.4	0.596
39.82	2.262	4	242	47.2	9311	57.3	0.616
39.98	2.253	4	227	44.2	9308	57.3	0.656
40.14	2.245	4	215	41.9	9308	57.3	0.736
41.84	2.157	4	159	31	3706	22.8	0.396
44.279	2.044	4	56	10.9	1645	10.1	0.499
44.557	2.032	5	53	10.3	1564	9.6	0.472
46.4	1.955	3	31	6	1069	6.6	0.552
46.639	1.946	3	42	8.2	1088	6.7	0.414
46.821	1.939	3	22	4.3	1161	7.2	0.844
48.298	1.883	5	29	5.7	1414	8.7	0.78
48.579	1.873	3	51	9.9	1410	8.7	0.47
49.049	1.856	12	8	1.6	-109	-0.7	0.02
49.28	1.848	7	3	0.6	6	0	0.204
49.818	1.829	5	6	1.2	43	0.3	0.115
50.038	1.821	6	13	2.5	84	0.5	0.103
50.399	1.809	9	18	3.5	467	2.9	0.441
50.941	1.791	11	25	4.9	760	4.7	0.486
51.162	1.784	12	21	4.1	812	5	0.619
52.261	1.749	12	513	100	16237	100	0.538
54.94	1.670	4	124	24.2	2953	18.2	0.405
56.179	1.636	11	122	23.8	4522	27.8	0.63

Appendix II Continued

56.824	1.619	3	77	15	2835	17.5	0.626
58.024	1.588	8	14	2.7	103	0.6	0.125
58.9	1.567	6	45	8.8	887	5.5	0.335
61.261	1.512	4	92	17.9	1973	12.2	0.365
61.94	1.497	39	172	33.5	5869	36.1	0.58
62.82	1.478	7	342	66.7	9552	58.8	0.475
64.782	1.438	4	48	9.4	934	5.8	0.331
66.96	1.396	6	174	33.9	6506	40.1	0.636
67.333	1.390	3	104	20.3	3713	22.9	0.607
69.48	1.352	5	262	51.1	8114	50	0.526
71.719	1.315	4	100	19.5	2557	15.7	0.435

Appendix II Continued

Peak Search Report (48 Peaks, Max P/N = 11.2)
[Xta85024.rd] xta85024
PEAK: 31-pts/Parabolic Filter, Threshold=2.0, Cutoff=0.1%, BG=3/1.0, Peak-Top=Summit

2-Theta	d(Å)	BG	Height	I%	Area	I%	FWHM
17.34	5.110	5	52	10.1	1306	8.2	0.427
20.719	4.284	3	96	18.6	799	5	0.141
22.96	3.870	13	134	26	3039	19.2	0.386
23.92	3.717	14	78	15.1	1622	10.2	0.354
25.56	3.482	6	106	20.6	2603	16.4	0.417
28.142	3.168	4	15	2.9	352	2.2	0.375
29.879	2.988	10	72	14	1599	10.1	0.378
31.041	2.879	16	21	4.1	372	2.3	0.283
32.301	2.769	14	302	58.6	7531	47.5	0.424
35.78	2.508	13	437	84.9	12930	81.6	0.503
36.5	2.460	3	322	62.5	8029	50.6	0.424
38.38	2.343	3	76	14.8	3677	23.2	0.822
38.919	2.312	34	44	8.5	1863	11.8	0.72
39.78	2.264	7	218	42.3	8698	54.9	0.638
39.98	2.253	4	229	44.5	9052	57.1	0.672
41.821	2.158	6	163	31.7	3699	23.3	0.386
42.663	2.118	6	9	1.7	62	0.4	0.117
44.26	2.045	6	46	8.9	1455	9.2	0.538
44.46	2.036	6	39	7.6	1375	8.7	0.564
46.64	1.946	4	32	6.2	968	6.1	0.514
46.877	1.937	4	27	5.2	939	5.9	0.556
48.42	1.878	2	45	8.7	1525	9.6	0.576
48.701	1.868	2	43	8.3	1683	10.6	0.626
48.962	1.859	5	24	4.7	217	1.4	0.145
49.241	1.849	3	14	2.7	53	0.3	0.061
49.565	1.838	6	8	1.6	-10	-0.1	0.02
49.75	1.831	6	7	1.4	63	0.4	0.144
50.436	1.808	17	7	1.4	25	0.2	0.057
50.721	1.798	7	28	5.4	1034	6.5	0.591
51.039	1.788	7	38	7.4	1034	6.5	0.463
52.26	1.749	18	515	100	15852	100	0.523
54.901	1.671	6	124	24.1	2780	17.5	0.381
56.24	1.634	8	126	24.5	4341	27.4	0.586
56.918	1.616	5	64	12.4	1121	7.1	0.298

Appendix II Continued

58.002	1.589	9	11	2.1	133	0.8	0.206
58.601	1.574	4	42	8.2	1699	10.7	0.647
58.841	1.568	7	55	10.7	1264	8	0.391
60.38	1.532	4	30	5.8	664	4.2	0.376
61.082	1.516	18	81	15.7	2798	17.7	0.587
61.301	1.511	24	91	17.7	2355	14.9	0.44
61.92	1.497	102	109	21.2	3232	20.4	0.504
62.8	1.478	3	323	62.7	10075	63.6	0.53
64.938	1.435	4	31	6	548	3.5	0.301
66.98	1.396	5	174	33.8	6355	40.1	0.621
67.26	1.391	6	128	24.9	6302	39.8	0.788
69.56	1.350	7	247	48	8095	51.1	0.557
71.483	1.319	3	58	11.3	2445	15.4	0.717
71.78	1.314	3	91	17.7	2460	15.5	0.46

Appendix II Continued

Peak Search Report (37 Peaks, Max P/N = 11.1)
[Xta9004.rd] xta9004
PEAK: 31-pts/Parabolic Filter, Threshold=2.0, Cutoff=0.1%, BG=3/1.0, Peak-Top=Summit

2-Theta	d(Å)	BG	Height	I%	Area	I%	FWHM
17.379	5.098	7	48	9.5	1079	6.6	0.382
20.622	4.303	4	14	2.8	280	1.7	0.34
21.564	4.118	3	8	1.6	60	0.4	0.127
22.88	3.884	11	145	28.7	3316	20.3	0.389
23.959	3.711	11	79	15.6	1375	8.4	0.296
25.54	3.485	3	103	20.4	2463	15.1	0.407
29.819	2.994	4	83	16.4	1855	11.4	0.38
31.136	2.870	9	22	4.4	354	2.2	0.274
32.38	2.763	8	324	64.2	8054	49.4	0.423
35.82	2.505	12	457	90.5	13853	85	0.515
36.559	2.456	7	318	63	7862	48.2	0.42
38.337	2.346	3	72	14.3	3609	22.1	0.852
38.88	2.314	34	38	7.5	1750	10.7	0.783
39.86	2.260	2	249	49.3	9412	57.8	0.605
40.099	2.247	2	211	41.8	10355	63.5	0.834
41.86	2.156	2	150	29.7	3753	23	0.425
44.101	2.052	4	41	8.1	1366	8.4	0.566
44.43	2.037	3	30	5.9	1387	8.5	0.786
46.58	1.948	4	46	9.1	1072	6.6	0.396
48.48	1.876	4	43	8.5	1511	9.3	0.597
50.96	1.791	12	27	5.3	708	4.3	0.446
52.26	1.749	11	505	100	16295	100	0.549
54.9	1.671	5	118	23.4	2795	17.2	0.403
56.319	1.632	5	129	25.5	5105	31.3	0.673
56.96	1.615	5	74	14.7	1510	9.3	0.347
58.04	1.588	3	17	3.4	120	0.7	0.12
58.7	1.572	3	44	8.7	841	5.2	0.306
58.881	1.567	3	42	8.3	889	5.5	0.36
61.24	1.512	0	91	18	1962	12	0.367
61.9	1.498	20	184	36.4	7219	44.3	0.667
62.82	1.478	7	342	67.7	9318	57.2	0.463
64.561	1.442	3	31	6.1	970	6	0.532
64.938	1.435	3	32	6.3	918	5.6	0.488
66.901	1.397	7	159	31.5	6616	40.6	0.666

Appendix II Continued

67.16	1.393	5	179	35.4	6841	42	0.65
69.6	1.350	6	288	57	8219	50.4	0.485
71.8	1.314	2	88	17.4	2604	16	0.503

Appendix II Continued

Peak Search Report (52 Peaks, Max P/N = 12.0)
[Xta9008.rd] xta9008
PEAK: 27-pts/Parabolic Filter, Threshold=2.0, Cutoff=0.1%, BG=3/1.0, Peak-Top=Summit

2-Theta	d(Å)	BG	Height	I%	Area	I%	FWHM
17.402	5.092	5	58	9.8	1265	7.8	0.371
20.639	4.300	4	18	3.1	228	1.4	0.215
22.921	3.877	11	189	32.1	3301	20.4	0.297
23.9	3.720	10	98	16.6	1570	9.7	0.272
25.54	3.485	5	120	20.4	2500	15.4	0.354
27.999	3.184	8	15	2.5	420	2.6	0.448
29.8	2.996	14	81	13.8	1883	11.6	0.395
31.138	2.870	18	17	2.9	305	1.9	0.305
32.379	2.763	7	401	68.1	8350	51.6	0.354
34.634	2.588	7	10	1.7	101	0.6	0.172
35.78	2.508	8	549	93.2	11644	71.9	0.361
36.54	2.457	6	406	68.9	8414	52	0.352
38.36	2.345	7	100	17	2886	17.8	0.491
38.861	2.316	15	93	15.8	2087	12.9	0.381
39.76	2.265	6	248	42.1	9250	57.1	0.634
40.1	2.247	6	264	44.8	9250	57.1	0.596
41.82	2.158	7	197	33.4	3788	23.4	0.327
42.689	2.116	6	10	1.7	141	0.9	0.24
44.28	2.044	7	52	8.8	1643	10.1	0.537
44.579	2.031	5	60	10.2	1825	11.3	0.517
46.614	1.947	5	46	7.8	1290	8	0.477
46.779	1.940	6	36	6.1	1170	7.2	0.52
47.075	1.929	8	9	1.5	205	1.3	0.364
48.321	1.882	5	33	5.6	1329	8.2	0.644
48.481	1.876	5	61	10.4	1353	8.4	0.377
48.861	1.862	5	20	3.4	740	4.6	0.592
49.803	1.829	6	14	2.4	86	0.5	0.104
50.413	1.809	16	12	2	150	0.9	0.213
50.942	1.791	16	33	5.6	686	4.2	0.333
51.138	1.785	19	18	3.1	566	3.5	0.535
52.3	1.748	16	589	100	16188	100	0.467
54.94	1.670	4	134	22.8	2766	17.1	0.351
56.22	1.635	4	167	28.4	4038	24.9	0.411
56.88	1.617	6	83	14.1	1730	10.7	0.354

Appendix II Continued

57.961	1.590	11	16	2.7	180	1.1	0.191
58.66	1.572	7	60	10.2	1804	11.1	0.511
58.8	1.569	10	57	9.7	1426	8.8	0.4
58.999	1.564	9	38	6.5	1431	8.8	0.603
59.634	1.549	6	9	1.5	59	0.4	0.111
60.341	1.533	5	35	5.9	643	4	0.312
61.14	1.514	24	93	15.8	2170	13.4	0.397
61.3	1.511	24	93	15.8	2170	13.4	0.373
61.94	1.497	95	153	26	3808	23.5	0.423
62.8	1.478	7	390	66.2	10292	63.6	0.449
63.401	1.466	4	54	9.2	769	4.8	0.242
64.099	1.452	5	11	1.9	78	0.5	0.121
64.84	1.437	3	44	7.5	929	5.7	0.359
66.941	1.397	3	183	31.1	6582	40.7	0.611
67.459	1.387	3	119	20.2	5367	33.2	0.767
68.16	1.375	4	25	4.2	193	1.2	0.131
69.54	1.351	1	306	52	8271	51.1	0.46
71.721	1.315	2	91	15.4	2260	14	0.422

Appendix II Continued

Peak Search Report (49 Peaks, Max P/N = 11.2)
[Xta90016.rd] xta90016
PEAK: 31-pts/Parabolic Filter, Threshold=2.0, Cutoff=0.1%, BG=3/1.0, Peak-Top=Summit

2-Theta	d(Å)	BG	Height	I%	Area	I%	FWHM
17.419	5.087	7	53	10.4	1096	7.2	0.352
22.92	3.877	13	145	28.4	2885	19	0.338
23.92	3.717	11	77	15.1	1601	10.5	0.353
25.461	3.496	6	93	18.2	2350	15.4	0.404
25.579	3.480	6	96	18.8	2345	15.4	0.415
29.663	3.009	10	52	10.2	1722	11.3	0.53
29.82	2.994	11	64	12.5	1627	10.7	0.432
29.939	2.982	12	60	11.7	1588	10.4	0.423
32.379	2.763	13	329	64.4	7097	46.6	0.367
35.76	2.509	12	456	89.2	10295	67.6	0.384
36.58	2.454	7	319	62.4	7740	50.8	0.412
38.339	2.346	6	78	15.3	2848	18.7	0.621
38.922	2.312	33	57	11.2	1202	7.9	0.358
39.76	2.265	6	218	42.7	8700	57.2	0.678
40.139	2.245	6	250	48.9	8700	57.2	0.592
41.88	2.155	6	161	31.5	3660	24	0.386
44.092	2.052	8	42	8.2	1640	10.8	0.664
44.36	2.040	8	45	8.8	1620	10.6	0.576
44.661	2.027	9	37	7.2	1522	10	0.699
46.223	1.962	9	21	4.1	1117	7.3	0.851
46.541	1.950	8	36	7	1178	7.7	0.524
46.76	1.941	8	29	5.7	1054	6.9	0.618
48.122	1.889	8	17	3.3	229	1.5	0.216
48.34	1.881	3	39	7.6	1420	9.3	0.583
48.58	1.873	3	51	10	1417	9.3	0.472
49.863	1.827	2	9	1.8	63	0.4	0.112
50.34	1.811	7	11	2.2	298	2	0.461
50.96	1.791	11	19	3.7	435	2.9	0.366
51.119	1.785	11	28	5.5	530	3.5	0.322
52.32	1.747	14	511	100	15223	100	0.506
53.983	1.697	8	11	2.2	124	0.8	0.192
54.899	1.671	8	121	23.7	3347	22	0.47
56.26	1.634	27	130	25.4	4440	29.2	0.581
56.86	1.618	27	75	14.7	2817	18.5	0.639

Appendix II Continued

57.959	1.590	27	14	2.7	256	1.7	0.293
58.179	1.584	25	12	2.3	592	3.9	0.789
58.74	1.571	4	66	12.9	2161	14.2	0.524
58.98	1.565	4	60	11.7	2161	14.2	0.612
61.18	1.514	20	92	18	1617	10.6	0.281
61.399	1.509	26	92	18	2490	16.4	0.46
61.868	1.498	47	163	31.9	6423	42.2	0.67
62.059	1.494	106	90	17.6	3013	19.8	0.536
62.8	1.478	11	320	62.6	8979	59	0.477
64.72	1.439	3	40	7.8	1034	6.8	0.439
67.06	1.394	7	175	34.2	6293	41.3	0.611
67.199	1.392	5	149	29.2	6471	42.5	0.695
67.478	1.387	3	103	20.2	4027	26.5	0.665
69.56	1.350	2	284	55.6	7716	50.7	0.462
71.772	1.314	6	68	13.3	1968	12.9	0.463

Appendix II Continued

Peak Search Report (38 Peaks, Max P/N = 10.5)
[Xta90020.rd] xta90020
PEAK: 33-pts/Parabolic Filter, Threshold=2.0, Cutoff=0.1%, BG=3/1.0, Peak-Top=Summit

2-Theta	d(Å)	BG	Height	I%	Area	I%	FWHM
17.381	5.098	4	37	8.2	1008	6.8	0.463
20.479	4.333	5	11	2.4	332	2.2	0.483
22.628	3.926	13	57	12.7	1006	6.8	0.282
22.92	3.877	16	110	24.5	2317	15.6	0.358
23.881	3.723	13	57	12.7	998	6.7	0.298
25.539	3.485	3	85	18.9	2058	13.9	0.412
28.221	3.160	3	13	2.9	347	2.3	0.454
29.861	2.990	3	48	10.7	1464	9.9	0.519
31.099	2.873	8	16	3.6	205	1.4	0.218
32.38	2.763	8	266	59.2	6639	44.7	0.424
35.78	2.508	14	361	80.4	11747	79.1	0.553
36.52	2.458	4	257	57.2	6959	46.9	0.46
38.361	2.344	4	70	15.6	3094	20.8	0.751
38.999	2.308	33	37	8.2	1422	9.6	0.653
39.795	2.263	6	183	40.8	7657	51.6	0.669
40.06	2.249	4	180	40.1	7823	52.7	0.739
41.76	2.161	3	141	31.4	3494	23.5	0.421
43.959	2.058	3	38	8.5	1204	8.1	0.539
44.26	2.045	4	29	6.5	952	6.4	0.525
44.558	2.032	3	18	4	1208	8.1	1.141
46.539	1.950	4	32	7.1	857	5.8	0.428
46.701	1.943	4	33	7.3	873	5.9	0.45
48.322	1.882	3	32	7.1	983	6.6	0.491
48.56	1.873	2	38	8.5	1038	7	0.464
51.099	1.786	5	13	2.9	292	2	0.382
52.32	1.747	6	449	100	14850	100	0.562
54.94	1.670	7	107	23.8	2537	17.1	0.403
56.18	1.636	5	116	25.8	4259	28.7	0.624
56.94	1.615	4	52	11.6	1200	8.1	0.392
58.898	1.567	7	34	7.6	1282	8.6	0.641
61.181	1.514	20	90	20	2675	18	0.505
61.979	1.496	125	73	16.3	1820	12.3	0.424
62.78	1.479	8	307	68.4	9301	62.6	0.515
64.855	1.436	1	23	5.1	708	4.8	0.523

Appendix II Continued

67.08	1.394	3	156	34.7	6015	40.5	0.655
67.498	1.387	3	81	18	4451	30	0.934
69.58	1.350	3	232	51.7	7909	53.3	0.58
71.779	1.314	3	70	15.6	2449	16.5	0.595

Appendix II Continued

Peak Search Report (53 Peaks, Max P/N = 11.4)
[Xta90024.rd] xta90024
PEAK: 27-pts/Parabolic Filter, Threshold=2.0, Cutoff=0.1%, BG=3/1.0, Peak-Top=Summit

2-Theta	d(Å)	BG	Height	I%	Area	I%	FWHM
17.419	5.087	8	56	10.5	1198	7.6	0.364
22.838	3.891	13	212	39.8	3427	21.6	0.275
22.981	3.867	14	158	29.6	3938	24.9	0.399
23.979	3.708	13	93	17.4	1633	10.3	0.299
25.54	3.485	9	110	20.6	2298	14.5	0.355
28.174	3.165	5	15	2.8	148	0.9	0.168
29.801	2.996	9	80	15	1615	10.2	0.343
29.998	2.976	10	53	9.9	1612	10.2	0.487
31.059	2.877	16	19	3.6	316	2	0.283
32.36	2.764	6	357	67	7826	49.4	0.373
34.442	2.602	11	12	2.3	93	0.6	0.132
35.8	2.506	19	503	94.4	12324	77.8	0.417
36.535	2.457	6	339	63.6	7749	48.9	0.389
38.38	2.343	7	72	13.5	1527	9.6	0.361
38.88	2.314	10	55	10.3	1129	7.1	0.349
39.701	2.268	8	184	34.5	6354	40.1	0.553
39.863	2.260	5	194	36.4	7249	45.8	0.635
40.079	2.248	5	200	37.5	7163	45.2	0.609
41.8	2.159	2	159	29.8	3460	21.8	0.37
43.302	2.088	6	13	2.4	77	0.5	0.101
44.26	2.045	9	63	11.8	1933	12.2	0.522
44.52	2.033	10	50	9.4	1870	11.8	0.598
46.52	1.951	7	37	6.9	914	5.8	0.395
46.729	1.942	6	35	6.6	931	5.9	0.452
48.495	1.876	5	46	8.6	1288	8.1	0.476
48.719	1.868	5	38	7.1	1621	10.2	0.683
49.022	1.857	7	25	4.7	255	1.6	0.163
50.321	1.812	14	16	3	178	1.1	0.178
50.542	1.804	16	13	2.4	171	1.1	0.224
50.857	1.794	10	25	4.7	1040	6.6	0.666
51.039	1.788	8	35	6.6	1161	7.3	0.564
52.3	1.748	10	533	100	15837	100	0.505
54.003	1.697	4	10	1.9	56	0.4	0.095
54.961	1.670	7	127	23.8	2764	17.5	0.37

Appendix II Continued

56.161	1.636	9	147	27.6	3887	24.5	0.45
56.821	1.619	5	83	15.6	2024	12.8	0.415
57.63	1.598	6	6	1.1	26	0.2	0.069
58.119	1.586	7	13	2.4	157	1	0.205
58.602	1.574	5	29	5.4	855	5.4	0.472
58.812	1.569	5	44	8.3	842	5.3	0.325
61.2	1.513	7	90	16.9	2087	13.2	0.394
61.681	1.503	14	129	24.2	6282	39.7	0.779
62.019	1.495	95	128	24	2884	18.2	0.383
62.82	1.478	16	324	60.8	8775	55.4	0.46
63.361	1.467	5	46	8.6	785	5	0.273
63.717	1.459	14	16	3	94	0.6	0.1
64.881	1.436	4	46	8.6	1102	7	0.407
66.94	1.397	2	180	33.8	7394	46.7	0.698
67.206	1.392	4	122	22.9	6904	43.6	0.962
67.543	1.386	5	80	15	4643	29.3	0.987
68.198	1.374	4	15	2.8	175	1.1	0.198
69.599	1.350	5	292	54.8	8494	53.6	0.495
71.751	1.314	7	85	15.9	2428	15.3	0.486

Appendix II Continued

Peak Search Report (45 Peaks, Max P/N = 11.2)
[Xta9504.rd] xta9504
PEAK: 33-pts/Parabolic Filter, Threshold=2.0, Cutoff=0.1%, BG=3/1.0, Peak-Top=Summit

2-Theta	d(Å)	BG	Height	I%	Area	I%	FWHM
17.411	5.089	7	44	8.6	1106	6.9	0.427
20.844	4.258	3	11	2.1	90	0.6	0.139
22.94	3.874	2	137	26.7	3451	21.6	0.428
23.961	3.711	5	79	15.4	1954	12.2	0.42
25.541	3.485	6	100	19.5	2664	16.7	0.453
28.197	3.163	4	16	3.1	202	1.3	0.202
29.7	3.006	5	52	10.1	1631	10.2	0.502
29.917	2.984	6	61	11.9	1618	10.1	0.451
31.22	2.863	13	14	2.7	373	2.3	0.453
32.402	2.761	11	297	57.8	7784	48.7	0.446
35.8	2.506	16	430	83.7	13581	84.9	0.537
36.552	2.456	4	318	61.9	7614	47.6	0.407
38.4	2.342	4	77	15	3584	22.4	0.791
38.839	2.317	12	66	12.8	2984	18.7	0.769
39.039	2.305	40	32	6.2	1605	10	0.803
39.8	2.263	6	224	43.6	9018	56.4	0.644
40.1	2.247	3	228	44.4	9853	61.6	0.735
41.82	2.158	3	139	27	3944	24.7	0.482
44.139	2.050	5	41	8	1295	8.1	0.537
44.551	2.032	4	29	5.6	1508	9.4	0.884
46.585	1.948	7	26	5.1	1059	6.6	0.692
46.899	1.936	8	21	4.1	1141	7.1	0.869
47.147	1.926	7	15	2.9	26	0.2	0.028
48.162	1.888	6	20	3.9	436	2.7	0.349
48.539	1.874	3	46	8.9	1395	8.7	0.516
48.819	1.864	5	28	5.4	1175	7.3	0.671
50.542	1.804	10	11	2.1	-128	-0.8	0.02
50.899	1.793	13	15	2.9	274	1.7	0.311
52.34	1.746	15	514	100	15994	100	0.529
54.96	1.669	12	102	19.8	2694	16.8	0.449
56.219	1.635	16	111	21.6	4329	27.1	0.663
56.879	1.617	5	61	11.9	1483	9.3	0.413
58.66	1.572	3	46	8.9	1561	9.8	0.543
58.901	1.567	6	50	9.7	1346	8.4	0.458

Appendix II Continued

61.18	1.514	4	92	17.9	1800	11.3	0.313
61.415	1.508	10	97	18.9	2738	17.1	0.48
61.84	1.499	32	158	30.7	6812	42.6	0.69
62.103	1.493	113	86	16.7	2506	15.7	0.495
62.8	1.478	9	295	57.4	9425	58.9	0.543
64.898	1.436	1	30	5.8	704	4.4	0.399
67.065	1.394	3	174	33.9	6840	42.8	0.668
67.437	1.388	4	97	18.9	4564	28.5	0.8
69.58	1.350	6	263	51.2	8360	52.3	0.54
71.739	1.315	3	79	15.4	2743	17.2	0.59
71.92	1.312	3	75	14.6	2742	17.1	0.585

Appendix II Continued

Peak Search Report (44 Peaks, Max P/N = 9.7)
[Xta9508.rd] xta9508
PEAK: 39-pts/Parabolic Filter, Threshold=2.0, Cutoff=0.1%, BG=3/1.0, Peak-Top=Summit

2-Theta	d(Å)	BG	Height	I%	Area	I%	FWHM
17.419	5.087	6	29	7.4	836	5.6	0.49
19.725	4.497	6	5	1.3	83	0.6	0.266
20.375	4.355	6	6	1.5	147	1	0.392
20.664	4.295	6	6	1.5	147	1	0.392
22.88	3.884	9	79	20.3	2215	14.7	0.477
23.898	3.720	9	45	11.5	973	6.5	0.368
25.52	3.488	3	71	18.2	1931	12.8	0.462
29.779	2.998	4	39	10	1222	8.1	0.533
31.021	2.880	10	5	1.3	10	0.1	0.1
32.36	2.764	7	195	50	6307	41.9	0.55
35.76	2.509	16	290	74.4	15036	100	0.881
36.34	2.470	3	205	52.6	8686	57.8	0.678
36.561	2.456	3	204	52.3	6977	46.4	0.581
38.48	2.338	7	61	15.6	2796	18.6	0.779
38.92	2.312	41	23	5.9	830	5.5	0.577
39.788	2.264	2	164	42.1	8023	53.4	0.832
41.82	2.158	3	106	27.2	3321	22.1	0.533
44.16	2.049	4	46	11.8	1243	8.3	0.459
44.362	2.040	4	31	7.9	1238	8.2	0.639
44.58	2.031	3	14	3.6	835	5.6	0.954
46.5	1.951	3	27	6.9	800	5.3	0.474
46.72	1.943	2	23	5.9	838	5.6	0.619
48.34	1.881	3	40	10.3	1133	7.5	0.453
48.561	1.873	4	32	8.2	1000	6.7	0.531
52.24	1.750	17	390	100	14227	94.6	0.62
54.86	1.672	7	79	20.3	2510	16.7	0.54
55.92	1.643	9	105	26.9	3668	24.4	0.559
56.241	1.634	8	102	26.2	4172	27.7	0.695
56.439	1.629	6	70	17.9	4374	29.1	1.062
56.901	1.617	3	47	12.1	631	4.2	0.228
58.541	1.576	6	38	9.7	1358	9	0.572
58.781	1.570	6	44	11.3	1356	9	0.493
58.938	1.566	6	28	7.2	1341	8.9	0.814
61.221	1.513	22	76	19.5	2041	13.6	0.457

Appendix II Continued

61.876	1.498	67	108	27.7	4397	29.2	0.692
62.68	1.481	13	232	59.5	8507	56.6	0.587
62.92	1.476	6	250	64.1	9022	60	0.613
64.902	1.436	1	24	6.2	730	4.9	0.517
67	1.396	3	140	35.9	6399	42.6	0.731
67.24	1.391	8	139	35.6	5892	39.2	0.721
69.68	1.348	4	211	54.1	7470	49.7	0.602
71.481	1.319	3	42	10.8	2093	13.9	0.797
71.622	1.316	2	54	13.8	2200	14.6	0.652
71.858	1.313	2	69	17.7	2216	14.7	0.546

Appendix II Continued

Peak Search Report (44 Peaks, Max P/N = 11.3)
[Xta95016.rd] xta95016
PEAK: 33-pts/Parabolic Filter, Threshold=2.0, Cutoff=0.1%, BG=3/1.0, Peak-Top=Summit

2-Theta	d(Å)	BG	Height	I%	Area	I%	FWHM
17.399	5.093	5	45	8.6	1095	6.8	0.414
20.501	4.329	5	13	2.5	347	2.2	0.427
22.9	3.880	8	134	25.7	3048	19	0.387
23.901	3.720	9	85	16.3	1261	7.8	0.252
25.461	3.496	2	91	17.5	2379	14.8	0.418
25.579	3.480	3	93	17.9	2306	14.3	0.422
28.044	3.179	4	14	2.7	317	2	0.385
29.76	3.000	3	66	12.7	1654	10.3	0.426
31.122	2.871	7	19	3.6	370	2.3	0.312
32.341	2.766	6	315	60.5	7255	45.1	0.392
35.72	2.512	14	419	80.4	10788	67.1	0.438
36.58	2.454	3	319	61.2	7578	47.1	0.404
38.3	2.348	3	73	14	2057	12.8	0.479
38.978	2.309	40	30	5.8	1267	7.9	0.718
40.04	2.250	7	203	39	8571	53.3	0.718
41.86	2.156	5	145	27.8	3494	21.7	0.41
44.08	2.053	5	39	7.5	1553	9.7	0.677
44.5	2.034	3	46	8.8	1622	10.1	0.564
44.596	2.030	3	31	6	1624	10.1	0.891
46.56	1.949	4	35	6.7	1093	6.8	0.5
46.761	1.941	4	30	5.8	1046	6.5	0.593
48.468	1.877	4	45	8.6	1446	9	0.546
49.022	1.857	10	10	1.9	86	0.5	0.138
49.565	1.838	6	13	2.5	35	0.2	0.043
49.797	1.830	6	10	1.9	44	0.3	0.07
50.342	1.811	5	23	4.4	1586	9.9	1.172
50.659	1.800	7	23	4.4	1162	7.2	0.808
50.959	1.791	7	31	6	1134	7.1	0.585
51.159	1.784	19	15	2.9	534	3.3	0.605
52.34	1.747	13	521	100	16080	100	0.525
54.98	1.669	4	113	21.7	2763	17.2	0.416
56.22	1.635	7	128	24.6	4420	27.5	0.587
56.88	1.618	2	72	13.8	2737	17	0.646
58.86	1.568	6	60	11.5	1823	11.3	0.517

Appendix II Continued

60.499	1.529	3	41	7.9	988	6.1	0.41
61.22	1.513	19	96	18.4	2587	16.1	0.458
61.999	1.496	114	103	19.8	2624	16.3	0.433
62.82	1.478	8	316	60.7	8532	53.1	0.459
63.576	1.462	2	25	4.8	583	3.6	0.396
64.918	1.435	1	42	8.1	813	5.1	0.329
67.08	1.394	3	164	31.5	6344	39.5	0.658
67.436	1.388	3	89	17.1	5303	33	1.013
69.66	1.349	5	254	48.8	7735	48.1	0.518
71.8	1.314	2	85	16.3	2659	16.5	0.532

Appendix II Continued

Peak Search Report (52 Peaks, Max P/N = 9.1)
[950201.rd] 950201
PEAK: 31-pts/Parabolic Filter, Threshold=2.0, Cutoff=0.1%, BG=3/1.0, Peak-Top=Summit

2-Theta	d(Å)	BG	Height	I%	Area	I%	FWHM
17.361	5.104	6	37	10.9	828	7.3	0.38
20.7	4.287	4	14	4.1	449	3.9	0.545
22.88	3.884	13	104	30.5	2334	20.5	0.382
23.88	3.723	14	55	16.1	930	8.2	0.287
25.501	3.490	3	70	20.5	1791	15.8	0.409
25.62	3.474	4	69	20.2	1730	15.2	0.426
29.702	3.005	5	41	12	1353	11.9	0.528
29.821	2.994	5	51	15	1366	12	0.455
31.001	2.882	9	15	4.4	225	2	0.255
32.34	2.766	9	213	62.5	5448	47.9	0.435
35.74	2.510	7	290	85	8122	71.4	0.476
36.54	2.457	3	242	71	6093	53.6	0.428
38.36	2.345	3	52	15.2	2464	21.7	0.806
38.839	2.317	7	52	15.2	2167	19.1	0.708
40.06	2.249	2	164	48.1	6992	61.5	0.725
41.801	2.159	3	115	33.7	2835	24.9	0.419
44.239	2.046	4	51	15	1167	10.3	0.389
44.46	2.036	3	32	9.4	1258	11.1	0.629
44.678	2.027	3	22	6.5	1095	9.6	0.796
46.186	1.964	3	16	4.7	181	1.6	0.181
46.579	1.948	3	24	7	702	6.2	0.468
46.759	1.941	3	22	6.5	684	6	0.529
48.541	1.874	3	32	9.4	1025	9	0.545
48.821	1.864	4	13	3.8	905	8	1.114
48.936	1.860	5	11	3.2	865	7.6	1.258
49.819	1.829	4	10	2.9	62	0.5	0.099
50.42	1.808	11	5	1.5	10	0.1	0.1
50.981	1.790	10	21	6.2	409	3.6	0.331
52.32	1.747	9	341	100	11368	100	0.567
54.919	1.671	5	67	19.6	1777	15.6	0.451
56.181	1.636	9	76	22.3	2828	24.9	0.633
56.82	1.619	3	54	15.8	2289	20.1	0.721
57.994	1.589	8	17	5	146	1.3	0.146
58.7	1.572	3	44	12.9	1319	11.6	0.51

Appendix II Continued

58.899	1.567	5	30	8.8	1018	9	0.543
59.403	1.555	4	10	2.9	37	0.3	0.059
60.301	1.534	2	23	6.7	435	3.8	0.303
60.558	1.528	2	27	7.9	666	5.9	0.395
61.18	1.514	20	61	17.9	1036	9.1	0.289
61.721	1.502	29	106	31.1	5085	44.7	0.768
61.84	1.500	36	102	29.9	4550	40	0.714
62.019	1.495	82	63	18.5	2090	18.4	0.564
62.78	1.479	7	219	64.2	6812	59.9	0.529
63.441	1.465	2	32	9.4	506	4.5	0.253
63.883	1.456	5	10	2.9	51	0.4	0.082
64.52	1.443	6	15	4.4	378	3.3	0.403
64.818	1.437	3	21	6.2	519	4.6	0.42
65.059	1.432	2	13	3.8	569	5	0.7
66.979	1.396	5	113	33.1	4218	37.1	0.635
67.962	1.378	7	10	2.9	18	0.2	0.029
69.6	1.350	2	180	52.8	5885	51.8	0.556
71.656	1.316	3	58	17	1807	15.9	0.53

Appendix II Continued

Peak Search Report (39 Peaks, Max P/N = 9.8)
[950202.rd] 950202
PEAK: 31-pts/Parabolic Filter, Threshold=2.0, Cutoff=0.1%, BG=3/1.0, Peak-Top=Summit

2-Theta	d(Å)	BG	Height	I%	Area	I%	FWHM
17.42	5.087	5	48	12.2	977	8.4	0.346
20.563	4.316	4	11	2.8	270	2.3	0.393
22.941	3.874	12	130	33.2	2447	21.1	0.32
23.939	3.714	10	68	17.3	1170	10.1	0.292
25.56	3.482	5	85	21.7	1951	16.8	0.39
29.74	3.002	5	43	11	1197	10.3	0.445
29.86	2.990	5	45	11.5	1181	10.2	0.446
30.965	2.886	6	12	3.1	322	2.8	0.429
32.38	2.763	7	242	61.7	5478	47.2	0.385
35.76	2.509	10	306	78.1	7276	62.7	0.404
36.52	2.458	4	251	64	6042	52	0.409
38.399	2.342	4	62	15.8	2659	22.9	0.729
38.958	2.310	27	34	8.7	1205	10.4	0.603
39.82	2.262	4	172	43.9	6527	56.2	0.607
40.119	2.246	4	156	39.8	6526	56.2	0.711
41.84	2.157	4	132	33.7	2778	23.9	0.358
44.101	2.052	5	42	10.7	1279	11	0.518
44.597	2.030	5	27	6.9	1691	14.6	1.065
46.633	1.946	4	23	5.9	774	6.7	0.572
48.54	1.874	4	41	10.5	1192	10.3	0.494
51.041	1.788	18	16	4.1	333	2.9	0.354
52.3	1.748	12	392	100	11612	100	0.504
54.959	1.669	4	78	19.9	1943	16.7	0.423
56.181	1.636	7	91	23.2	3084	26.6	0.576
56.878	1.618	4	57	14.5	1142	9.8	0.341
57.48	1.602	6	4	1	8	0.1	0.1
58.022	1.588	4	12	3.1	152	1.3	0.215
58.501	1.576	3	26	6.6	1088	9.4	0.67
58.72	1.571	3	38	9.7	1090	9.4	0.459
58.94	1.566	3	32	8.2	1080	9.3	0.574
61.269	1.512	20	64	16.3	1462	12.6	0.388
61.959	1.496	76	85	21.7	2107	18.1	0.421
62.8	1.478	4	223	56.9	6463	55.7	0.493
64.86	1.436	3	22	5.6	592	5.1	0.457

Appendix II Continued

67.12	1.393	4	124	31.6	4826	41.6	0.662
67.52	1.386	4	51	13	3158	27.2	1.053
69.54	1.351	4	190	48.5	5954	51.3	0.533
71.321	1.321	2	31	7.9	887	7.6	0.458
71.719	1.315	1	60	15.3	1823	15.7	0.517

Appendix II Continued

Peak Search Report (46 Peaks, Max P/N = 11.5)
[Xta95024.rd] xta95024
PEAK: 31-pts/Parabolic Filter, Threshold=2.0, Cutoff=0.1%, BG=3/1.0, Peak-Top=Summit

2-Theta	d(Å)	BG	Height	I%	Area	I%	FWHM
17.36	5.104	6	53	9.8	1013	6.9	0.325
20.785	4.270	4	12	2.2	376	2.6	0.533
22.899	3.880	7	162	30.1	3033	20.6	0.318
23.9	3.720	6	77	14.3	1313	8.9	0.29
25.52	3.488	2	98	18.2	2337	15.9	0.405
28.162	3.166	4	11	2	302	2.1	0.439
29.72	3.004	4	61	11.3	1560	10.6	0.409
29.86	2.990	4	68	12.6	1560	10.6	0.39
31.116	2.872	9	11	2	271	1.8	0.419
32.34	2.766	8	312	57.9	6514	44.3	0.355
35.76	2.509	10	422	78.3	9637	65.6	0.388
36.54	2.457	3	384	71.2	8198	55.8	0.363
38.32	2.347	3	75	13.9	2452	16.7	0.556
38.859	2.316	28	50	9.3	1055	7.2	0.359
39.72	2.267	6	239	44.3	8625	58.7	0.577
40.1	2.247	5	232	43	8717	59.3	0.639
41.82	2.158	4	158	29.3	3142	21.4	0.338
44.041	2.054	2	38	7.1	1494	10.2	0.629
44.241	2.046	2	38	7.1	1493	10.2	0.668
44.46	2.036	2	39	7.2	1494	10.2	0.651
44.699	2.026	3	24	4.5	2141	14.6	1.427
46.624	1.946	5	31	5.8	701	4.8	0.362
48.54	1.874	3	53	9.8	1399	9.5	0.449
48.721	1.868	3	26	4.8	1341	9.1	0.825
49.041	1.856	6	9	1.7	442	3	0.786
49.643	1.835	3	10	1.9	87	0.6	0.148
50.214	1.815	3	10	1.9	566	3.9	0.962
50.362	1.810	3	10	1.9	602	4.1	0.963
50.986	1.790	3	20	3.7	575	3.9	0.489
52.3	1.748	6	539	100	14692	100	0.463
54.96	1.669	7	121	22.4	2494	17	0.35
56.24	1.634	7	128	23.7	3411	23.2	0.453
56.8	1.620	3	81	15	2496	17	0.524
58.02	1.588	7	15	2.8	179	1.2	0.203

Appendix II Continued

58.721	1.571	5	55	10.2	1726	11.7	0.502
58.92	1.566	5	56	10.4	1545	10.5	0.469
60.301	1.534	4	26	4.8	507	3.5	0.331
61.22	1.513	21	87	16.1	2135	14.5	0.417
62.021	1.495	87	133	24.7	3705	25.2	0.474
62.8	1.478	11	342	63.5	8576	58.4	0.426
64.941	1.435	2	38	7.1	889	6.1	0.398
67.02	1.395	4	178	33	5999	40.8	0.573
67.48	1.387	8	89	16.5	4578	31.2	0.874
68.102	1.376	4	14	2.6	101	0.7	0.123
69.58	1.350	4	254	47.1	7413	50.5	0.496
71.821	1.313	4	103	19.1	2747	18.7	0.453

Appendix II Continued

Peak Search Report (43 Peaks, Max P/N = 11.8)
[Xta10004.rd] xta10004
PEAK: 27-pts/Parabolic Filter, Threshold=2.0, Cutoff=0.1%, BG=3/1.0, Peak-Top=Summit

2-Theta	d(Å)	BG	Height	I%	Area	I%	FWHM
17.34	5.110	6	58	10.4	1201	8	0.352
20.28	4.375	4	14	2.5	381	2.5	0.435
20.62	4.304	5	11	2	198	1.3	0.306
22.86	3.887	7	152	27.2	3005	20	0.336
23.92	3.717	6	74	13.2	1377	9.2	0.316
25.5	3.490	3	111	19.9	2412	16.1	0.369
28.079	3.175	6	40	7.2	1043	7	0.443
29.821	2.994	6	73	13.1	1503	10	0.35
31	2.882	9	54	9.7	1159	7.7	0.365
32.34	2.766	7	379	67.8	7477	49.9	0.335
35.74	2.510	13	480	85.9	10360	69.1	0.367
36.54	2.457	3	379	67.8	8156	54.4	0.366
38.342	2.346	10	74	13.2	1709	11.4	0.393
38.899	2.313	16	58	10.4	1197	8	0.351
39.78	2.264	10	213	38.1	7532	50.2	0.601
40.1	2.247	9	216	38.6	7368	49.2	0.58
41.8	2.159	0	151	27	2896	19.3	0.326
44.2	2.047	4	38	6.8	1254	8.4	0.561
44.516	2.034	5	31	5.5	1241	8.3	0.681
46.539	1.950	6	35	6.3	1154	7.7	0.528
46.702	1.943	6	44	7.9	1123	7.5	0.434
48.5	1.875	2	58	10.4	1204	8	0.353
50.582	1.803	1	13	2.3	309	2.1	0.404
50.96	1.790	2	22	3.9	413	2.8	0.319
52.34	1.746	5	559	100	14990	100	0.456
54.94	1.670	5	125	22.4	2619	17.5	0.356
56.24	1.634	8	162	29	4188	27.9	0.439
56.862	1.618	9	92	16.5	2272	15.2	0.42
57.961	1.590	8	17	3	181	1.2	0.181
58.919	1.566	9	44	7.9	1119	7.5	0.432
60.5	1.529	5	35	6.3	903	6	0.439
61.24	1.512	24	102	18.2	1979	13.2	0.33
61.98	1.496	85	156	27.9	4476	29.9	0.488
62.859	1.477	16	377	67.4	9016	60.1	0.407

Appendix II Continued

63.52	1.463	4	47	8.4	885	5.9	0.32
64.981	1.434	3	32	5.7	777	5.2	0.413
67.1	1.394	2	197	35.2	6290	42	0.543
67.48	1.387	5	107	19.1	2792	18.6	0.444
69.66	1.349	5	298	53.3	7560	50.4	0.431
70.516	1.334	3	9	1.6	60	0.4	0.113
71.74	1.315	3	98	17.5	3192	21.3	0.521
71.859	1.313	3	91	16.3	3184	21.2	0.595

Appendix II Continued

Peak Search Report (40 Peaks, Max P/N = 11.7)
[Xta10008.rd] xta10008
PEAK: 25-pts/Parabolic Filter, Threshold=2.0, Cutoff=0.1%, BG=3/1.0, Peak-Top=Summit

2-Theta	d(Å)	BG	Height	I%	Area	I%	FWHM
17.38	5.098	5	57	10.2	981	7.7	0.293
20.241	4.384	4	24	4.3	581	4.5	0.387
22.9	3.880	7	155	27.8	2364	18.5	0.259
23.92	3.717	6	93	16.7	1424	11.1	0.26
25.52	3.488	5	106	19	1919	15	0.308
26.695	3.337	9	33	5.9	321	2.5	0.165
28.14	3.169	12	157	28.2	3964	31	0.429
29.798	2.996	6	67	12	1228	9.6	0.312
30.9	2.891	4	231	41.5	4639	36.3	0.341
32.36	2.764	11	379	68	6257	49	0.281
35.76	2.509	18	506	90.8	10551	82.6	0.354
36.56	2.456	4	377	67.7	6723	52.6	0.303
38.36	2.345	11	65	11.7	1038	8.1	0.271
38.879	2.314	15	63	11.3	825	6.5	0.223
39.76	2.265	10	205	36.8	6063	47.5	0.503
40.1	2.247	8	233	41.8	3875	30.3	0.283
41.821	2.158	1	165	29.6	2674	20.9	0.276
44.041	2.054	9	42	7.5	1501	11.7	0.608
44.601	2.030	11	35	6.3	1420	11.1	0.649
45.818	1.979	17	38	6.8	1364	10.7	0.61
46.66	1.945	7	45	8.1	983	7.7	0.371
48.5	1.875	3	56	10.1	1227	9.6	0.372
50.4	1.809	4	25	4.5	1712	13.4	1.096
50.601	1.802	5	35	6.3	1533	12	0.701
50.861	1.794	6	42	7.5	1398	10.9	0.533
52.339	1.747	7	557	100	12776	100	0.39
54.96	1.669	7	129	23.2	2046	16	0.27
56.2	1.635	5	200	35.9	5294	41.4	0.45
56.919	1.616	5	92	16.5	2711	21.2	0.501
58.839	1.568	3	44	7.9	927	7.3	0.358
60.46	1.530	0	52	9.3	912	7.1	0.298
61.201	1.513	18	81	14.5	2190	17.1	0.46
61.98	1.496	41	184	33	5894	46.1	0.545
62.76	1.479	26	341	61.2	7289	57.1	0.363

Appendix II Continued

63.559	1.463	4	76	13.6	1828	14.3	0.409
64.9	1.436	2	49	8.8	704	5.5	0.244
67.02	1.395	2	175	31.4	5380	42.1	0.523
67.479	1.387	5	97	17.4	3732	29.2	0.654
69.6	1.350	6	296	53.1	6820	53.4	0.392
71.66	1.316	3	100	18	2838	22.2	0.482

Appendix II Continued

Peak Search Report (45 Peaks, Max P/N = 9.9)
[Xt100016.rd] xt100016
PEAK: 29-pts/Parabolic Filter, Threshold=2.0, Cutoff=0.1%, BG=3/1.0, Peak-Top=Summit

2-Theta	d(Å)	BG	Height	I%	Area	I%	FWHM
17.36	5.104	4	37	9.3	993	8.8	0.456
20.121	4.410	7	13	3.3	355	3.1	0.464
22.94	3.874	4	106	26.7	2199	19.5	0.353
23.861	3.726	4	54	13.6	1011	9	0.318
25.598	3.477	2	78	19.6	1606	14.2	0.35
28.199	3.162	11	156	39.3	4764	42.2	0.519
29.86	2.990	5	50	12.6	837	7.4	0.285
30.88	2.893	4	195	49.1	4384	38.9	0.382
32.321	2.768	8	256	64.5	5709	50.6	0.379
33.2	2.696	4	29	7.3	446	4	0.261
33.2	2.696	4	29	7.3	446	4	0.261
35.72	2.512	17	338	85.1	8617	76.4	0.433
36.599	2.453	3	296	74.6	6712	59.5	0.385
38.32	2.347	3	66	16.6	2638	23.4	0.679
39	2.308	33	36	9.1	765	6.8	0.361
39.821	2.262	27	161	40.6	5733	50.8	0.605
40.099	2.247	10	171	43.1	7019	62.2	0.657
41.821	2.158	7	113	28.5	2221	19.7	0.334
44.116	2.051	2	38	9.6	1051	9.3	0.47
44.618	2.029	2	23	5.8	1134	10.1	0.838
45.721	1.983	3	56	14.1	1833	16.2	0.524
45.981	1.972	7	41	10.3	2091	18.5	0.867
46.52	1.950	3	32	8.1	780	6.9	0.39
46.721	1.943	3	31	7.8	780	6.9	0.428
48.519	1.875	7	42	10.6	913	8.1	0.37
50.72	1.798	9	39	9.8	1488	13.2	0.649
50.979	1.790	10	32	8.1	1185	10.5	0.63
52.34	1.746	7	397	100	11282	100	0.483
54.96	1.669	6	88	22.2	1507	13.4	0.291
56.22	1.635	4	163	41.1	5407	47.9	0.564
56.701	1.622	7	70	17.6	2591	23	0.592
56.94	1.616	5	78	19.6	1603	14.2	0.349
58.058	1.587	3	25	6.3	285	2.5	0.194
58.801	1.569	3	44	11.1	1002	8.9	0.387

Appendix II Continued

60.34	1.533	0	34	8.6	640	5.7	0.32
61.382	1.509	30	70	17.6	1620	14.4	0.393
61.999	1.496	41	162	40.8	7777	68.9	0.816
62.76	1.479	38	235	59.2	5340	47.3	0.386
63.5	1.464	2	68	17.1	1790	15.9	0.447
64.839	1.437	2	35	8.8	704	6.2	0.342
67.06	1.394	5	132	33.2	4185	37.1	0.539
67.499	1.386	8	59	14.9	2692	23.9	0.776
68.296	1.372	10	19	4.8	327	2.9	0.293
69.56	1.350	7	201	50.6	5712	50.6	0.483
71.8	1.314	2	109	27.5	3305	29.3	0.515

Appendix II Continued

Peak Search Report (52 Peaks, Max P/N = 9.0)
[100020.rd] 100020
PEAK: 31-pts/Parabolic Filter, Threshold=2.0, Cutoff=0.1%, BG=3/1.0, Peak-Top=Summit

2-Theta	d(Å)	BG	Height	I%	Area	I%	FWHM
17.349	5.107	4	22	6.2	603	6.2	0.466
20.12	4.410	4	14	4	446	4.6	0.542
20.58	4.312	5	9	2.5	402	4.1	0.715
22.861	3.887	6	73	20.6	1718	17.7	0.4
23.93	3.716	4	30	8.5	649	6.7	0.368
25.578	3.480	2	46	13	1486	15.3	0.549
28.1	3.173	12	112	31.6	3883	40	0.589
29.821	2.994	5	30	8.5	704	7.3	0.399
30.92	2.890	6	140	39.5	3645	37.6	0.443
32.32	2.768	11	164	46.3	4333	44.6	0.449
35.719	2.512	12	236	66.7	7941	81.8	0.572
36.499	2.460	5	189	53.4	5014	51.7	0.451
38.357	2.345	5	47	13.3	1351	13.9	0.489
38.841	2.317	13	37	10.5	1807	18.6	0.781
39.038	2.305	39	22	6.2	628	6.5	0.485
39.911	2.257	8	140	39.5	5966	61.5	0.724
41.82	2.158	6	76	21.5	1841	19	0.412
43.194	2.093	2	14	4	71	0.7	0.086
43.981	2.057	4	34	9.6	762	7.9	0.381
44.378	2.042	4	16	4.5	1216	12.5	1.292
44.577	2.031	5	18	5.1	1031	10.6	0.916
45.402	1.996	12	10	2.8	242	2.5	0.387
45.681	1.984	14	28	7.9	628	6.5	0.359
45.86	1.977	15	37	10.5	633	6.5	0.291
46.119	1.967	6	29	8.2	1689	17.4	0.932
46.368	1.957	16	12	3.4	303	3.1	0.404
46.579	1.948	14	15	4.2	191	2	0.216
46.779	1.940	12	15	4.2	188	1.9	0.213
48.361	1.880	4	21	5.9	646	6.7	0.492
48.523	1.875	4	20	5.6	681	7	0.545
48.641	1.870	5	21	5.9	623	6.4	0.475
50.64	1.801	5	31	8.8	1137	11.7	0.587
50.82	1.795	5	29	8.2	1086	11.2	0.637
52.319	1.747	6	286	80.8	9705	100	0.577

Appendix II Continued

54.979	1.669	8	58	16.4	1290	13.3	0.378
56.26	1.634	10	125	35.3	4169	43	0.567
56.921	1.616	33	354	100	1830	18.9	0.088
57.268	1.607	4	20	5.6	175	1.8	0.149
58.939	1.566	8	39	11	696	7.2	0.303
60.26	1.534	2	42	11.9	754	7.8	0.305
61.323	1.510	30	66	18.6	1729	17.8	0.445
61.94	1.497	51	142	40.1	4853	50	0.581
62.779	1.479	29	181	51.1	5182	53.4	0.487
63.64	1.461	3	55	15.5	1556	16	0.481
65.023	1.433	2	17	4.8	362	3.7	0.362
67.06	1.394	2	107	30.2	3668	37.8	0.583
68.378	1.371	5	13	3.7	146	1.5	0.191
69.64	1.349	4	186	52.5	5789	59.6	0.529
71.441	1.319	3	55	15.5	2655	27.4	0.772
71.7	1.315	4	80	22.6	2587	26.7	0.517
71.9	1.312	6	66	18.6	2298	23.7	0.592

Appendix II Continued

Peak Search Report (44 Peaks, Max P/N = 12.1)
[1000241.rd] 1000241
PEAK: 25-pts/Parabolic Filter, Threshold=2.0, Cutoff=0.1%, BG=3/1.0, Peak-Top=Summit

2-Theta	d(Å)	BG	Height	I%	Area	I%	FWHM
17.361	5.104	5	57	9.7	948	7.4	0.283
20.26	4.380	5	25	4.3	488	3.8	0.312
22.899	3.880	9	164	27.9	2354	18.3	0.244
23.939	3.714	6	106	18	1497	11.7	0.24
25.54	3.485	3	103	17.5	1818	14.2	0.3
28.12	3.171	13	232	39.5	5710	44.5	0.418
29.8	2.996	6	72	12.2	1331	10.4	0.314
30.88	2.893	5	331	56.3	5776	45	0.297
32.36	2.764	10	423	71.9	7068	55	0.284
33.201	2.696	3	35	6	911	7.1	0.442
35.779	2.508	16	525	89.3	11263	87.7	0.365
36.56	2.456	2	432	73.5	6947	54.1	0.273
38.321	2.347	11	75	12.8	916	7.1	0.208
38.918	2.312	16	79	13.4	866	6.7	0.186
39.72	2.268	13	199	33.8	6281	48.9	0.537
40.081	2.248	10	252	42.9	4192	32.6	0.283
41.88	2.155	4	173	29.4	2430	18.9	0.239
44.577	2.031	17	40	6.8	1370	10.7	0.582
45.82	1.979	23	64	10.9	1934	15.1	0.514
46.62	1.947	5	57	9.7	1312	10.2	0.391
46.858	1.937	3	28	4.8	442	3.4	0.253
48.501	1.875	5	53	9	988	7.7	0.317
50.42	1.808	8	43	7.3	1936	15.1	0.72
50.64	1.801	8	51	8.7	1809	14.1	0.568
50.96	1.790	9	42	7.1	1517	11.8	0.578
52.32	1.747	3	588	100	12840	100	0.371
52.601	1.738	4	208	35.4	6122	47.7	0.471
54.98	1.669	3	136	23.1	1954	15.2	0.244
56.2	1.635	5	244	41.5	4892	38.1	0.341
56.821	1.619	6	102	17.3	2335	18.2	0.389
57.961	1.590	7	30	5.1	575	4.5	0.326
58.74	1.571	7	55	9.4	1146	8.9	0.354

Appendix II Continued

60.34	1.533	3	54	9.2	1613	12.6	0.508
61.24	1.512	41	71	12.1	1248	9.7	0.299
61.999	1.496	64	206	35	7336	57.1	0.605
62.76	1.479	34	334	56.8	6247	48.7	0.318
63.62	1.461	6	100	17	2150	16.7	0.366
64.86	1.436	5	39	6.6	460	3.6	0.201
67.02	1.395	1	191	32.5	4225	32.9	0.376
67.48	1.387	3	106	18	2058	16	0.33
68.201	1.373	9	32	5.4	384	3	0.204
69.58	1.350	7	276	46.9	6413	49.9	0.395
71.64	1.316	4	115	19.6	3645	28.4	0.507
71.82	1.313	6	116	19.7	3362	26.2	0.493

Appendix II Continued

Peak Search Report (46 Peaks, Max P/N = 11.7)
[1000243.rd] 1000243
PEAK: 25-pts/Parabolic Filter, Threshold=2.0, Cutoff=0.1%, BG=3/1.0, Peak-Top=Summit

2-Theta	d(Å)	BG	Height	I%	Area	I%	FWHM
17.401	5.092	4	60	10.7	1071	8.4	0.303
20.321	4.367	4	27	4.8	479	3.8	0.302
22.941	3.873	8	164	29.1	2355	18.5	0.244
23.961	3.711	7	99	17.6	1500	11.8	0.258
25.64	3.472	4	109	19.4	2073	16.3	0.323
28.199	3.162	11	216	38.4	4903	38.4	0.386
29.819	2.994	4	69	12.3	1194	9.4	0.294
30.96	2.886	4	308	54.7	5846	45.8	0.323
32.419	2.760	8	444	78.9	7308	57.3	0.28
33.28	2.690	2	36	6.4	689	5.4	0.325
35.8	2.506	13	563	100	10510	82.4	0.317
36.58	2.454	3	368	65.4	6428	50.4	0.297
38.36	2.345	4	99	17.6	1693	13.3	0.291
38.94	2.311	25	70	12.4	832	6.5	0.202
39.78	2.264	11	184	32.7	7030	55.1	0.65
40.14	2.245	3	271	48.1	7745	60.7	0.486
41.88	2.155	3	180	32	2836	22.2	0.268
44.2	2.047	2	32	5.7	422	3.3	0.224
44.558	2.032	2	38	6.7	494	3.9	0.221
45.72	1.983	3	42	7.5	1413	11.1	0.538
45.92	1.975	9	44	7.8	1430	11.2	0.553
46.478	1.952	12	21	3.7	806	6.3	0.614
46.679	1.944	5	43	7.6	801	6.3	0.317
48.56	1.873	4	66	11.7	1196	9.4	0.308
48.862	1.862	5	15	2.7	606	4.8	0.646
49.018	1.857	6	15	2.7	451	3.5	0.481
49.621	1.836	8	8	1.4	128	1	0.256
50.1	1.819	15	5	0.9	10	0.1	0.1
51.037	1.788	10	39	6.9	1217	9.5	0.53
52.34	1.747	6	553	98.2	12753	100	0.392
55.02	1.668	4	115	20.4	1875	14.7	0.277
56.24	1.634	4	217	38.5	4647	36.4	0.364
56.84	1.619	4	81	14.4	1963	15.4	0.412
58.02	1.588	6	27	4.8	475	3.7	0.299

Appendix II Continued

58.718	1.571	7	43	7.6	1027	8.1	0.406
58.98	1.565	6	51	9.1	1026	8	0.342
60.419	1.531	4	60	10.7	1698	13.3	0.481
61.22	1.513	39	77	13.7	1668	13.1	0.368
61.98	1.496	106	131	23.3	3432	26.9	0.445
62.82	1.478	35	341	60.6	6806	53.4	0.339
63.56	1.463	4	89	15.8	2034	15.9	0.389
64.959	1.434	2	27	4.8	491	3.9	0.309
67.04	1.395	4	168	29.8	4184	32.8	0.423
67.519	1.386	6	88	15.6	2744	21.5	0.53
69.62	1.349	3	292	51.9	7053	55.3	0.411
71.72	1.315	4	107	19	3341	26.2	0.531

Appendix III: X-ray Diffraction Patterns with Corresponding Reference Patterns used for Mineral Phase Identification

1. X-ray diffraction pattern of unheated starting material, chrysotile from Thetford, Canada indexed by using 10-381 reference pattern diffraction file for chrysotile from the International Center for Diffraction Data (1994). Miller indices correspond to both diffraction patterns.

	Unheated Thetford Chrysotile, <65º 2-Theta		10-381 Chrysotile PDF Reference Pattern 25 ºC, <65º 2-Theta	
Miller Indices	d-spacing (Å)	I (%)	d-spacing (Å)	I (%)
002	7.481	47.6	7.36	100
020	4.523	9.4	4.58	50
004	3.696	100	3.66	80
202	2.459	12.8	2.456	65
008	1.836	10.7	1.829	30
060	1.542	43.5	1.536	65
0.0.10	1.469	7.9	1.465	30

2. X-ray diffraction pattern of sample heated at 450ºC for 4 hours indexed by using 10-381 reference pattern diffraction file for chrysotile from the International Center for Diffraction Data (1994). Miller indices correspond to both diffraction patterns.

	Thetford Chrysotile heated at 450 ºC for 4 hours, <65º 2-Theta		10-381 Chrysotile PDF Reference Pattern 25 ºC, <65º 2-Theta	
Miller Indices	d-spacing (Å)	I (%)	d-spacing (Å)	I (%)
002	7.284	69.2	7.36	100
020	4.448	11.9	4.58	50
004	3.645	100	3.66	80
202	2.439	15	2.456	65
008	1.829	6.4	1.829	30
060	1.533	51.1	1.536	65
0.0.10	1.462	6.2	1.465	30

Appendix III Continued

3. X-ray diffraction pattern of sample heated at 650ºC for 24 hours indexed by using reference pattern 34-189 reference pattern diffraction file for forsterite from the International Center for Diffraction Data (1994). Miller indices correspond to both diffraction patterns.

	Thetford Chrysotile heated at 650 ºC for 24 hours, <50º 2-Theta		34-189 Forsterite PDF Reference Pattern 25 ºC, <50º 2-Theta	
Miller Indices	d-spacing (Å)	I (%)	d-spacing (Å)	I (%)
020	5.075	9.2	5.102	22
011	missing		4.307	4
120	3.874	23.4	3.881	76
101	3.720	9.7	3.722	25
111	3.482	14.1	3.496	26
021	missing		3.477	22
121	missing		3.006	14
200	2.998	8.4	2.991	18
031	2.764	49.7	2.765	66
131	2.509	77	2.5097	83
211	2.456	55.5	2.4567	100
140	2.343	17.1	2.3456	13
012	2.316	13.3	2.315	13
221	2.264	64.2	2.2673	57
041	2.248	64.4	2.247	37
112	2.160	24.2	2.1589	23
231	2.043	10.1	2.0303	7
032	1.948	6.6	1.9497	6
240	1.943	6.5	1.9407	5
051	1.875	10.1	1.8744	8
202	1.862	1.8	1.8608	3

Appendix III Continued

4. X-ray diffraction pattern of sample heated at 1000ºC for 20 hours indexed by using the 22-714 reference pattern diffraction file for enstatite from the International Center for Diffraction Data (1994). Miller indices correspond to both diffraction patterns.

	Thetford Chrysotile heated at 1000 ºC for 20 hours, <50º 2-Theta		22-714 Enstatite PDF Reference Pattern 25 ºC, <50º 2-Theta	
Miller Indices	d-spacing (Å)	I (%)	d-spacing (Å)	I (%)
020	*5.107*	*6.2*	*Forsterite*	
210	missing		6.33	2
020	4.410	4.6	4.43	4
011	*4.312*	*4.1*	*Forsterite*	
211	missing		4.03	2
121	missing		3.31	6
120	*3.8868*	*17.7*	*Forsterite*	
101	*3.716*	*6.7*	*Forsterite*	
021	*3.480*	*15.3*	*Forsterite*	
420	3.173	40	3.18	100
030	2.994	7.3	2.946	16
610	2.890	37.6	2.878	55
511	missing		2.832	10
031	*2.768*	*44.6*	*Forsterite*	
421	missing		2.71	10
131	missing		2.54	25
131	*2.512*	*81.8*	*Forsterite*	
100	*2.460*	*51.7*	*Forsterite*	
710	missing		2.497	18
430	missing		2.477	18
302	missing		2.386	2
331	missing		2.364	2
140	*2.345*	*13.9*	*Forsterite*	
701	missing		2.32	2
012	*2.317*	*18.6*	*Forsterite*	
	2.305	6.5	?	
800	missing		2.283	2
621	2.257	61.5	2.257	4
022	missing		2.239	4
112	*2.158*	*19*	*Forsterite*	
630	2.093	0.7	2.116	12

Appendix III Continued

4. Continued

	Thetford Chrysotile heated at 1000 ºC for 20 hours, <50º 2-Theta		22-714 Enstatite PDF Reference Pattern 25 ºC, <50º 2-Theta	
322	missing		2.1	12
721	2.057	7.9	2.06	6
	2.042	12.5	?	
820	2.031	10.6	2.025	8
	1.996	2.5	?	
440	1.984	6.5	1.988	10
	1.977	6.5	?	
631	1.967	17.4	1.961	12
	1.957	3.1	?	
032	*1.948*	*2*	*Forsterite*	
240	*1.940*	*1.9*	*Forsterite*	
341	missing		1.929	2
901	1.880	6.7	1.888	4
051	*1.875*	*7*	*Forsterite*	
920	missing		1.841	4
	1.870	6.4	?	
830	1.801	11.7	1.803	2

Appendix IV: X-ray Diffraction Uncertainty

Four X-ray diffraction analyses were conducted on chrysotile heated at 400˚C for 24 hours. This experimental condition was chosen so that no other mineral interference occurred. The sample was repacked for each trial. The four diffraction patterns are located in Table 1a-b below.

Table 1a: Diffraction Patterns of the four trial of chrysotile heated at 400˚C for 24 hours.

Peak Search Report (7 Peaks, Max
P/N = 10.7)
[XTA40024.RD]
xta40024
PEAK: 39-pts/Parabolic Filter, Threshold=2.0,
Cutoff=0.1%, BG=3/1.0, Peak-Top=Summit

2-Theta	d(A)	BG	Height	I%	Area	I%	FWHM
12.34	7.167	14	311	64.3	11159	61.2	0.61
20.103	4.414	14	48	9.9	2391	13.1	0.847
24.62	3.613	23	484	100	18229	100	0.64
36.882	2.435	86	40	8.3	1259	6.9	0.535
49.942	1.825	11	31	6.4	1369	7.5	0.707
60.402	1.531	61	106	21.9	6722	36.9	1.015
63.638	1.461	6	25	5.2	1306	7.2	0.888

Peak Search Report (7 Peaks, Max
P/N = 14.9)
[RE40024.RD]
re40024
PEAK: 39-pts/Parabolic Filter, Threshold=2.0,
Cutoff=0.1%, BG=3/1.0, Peak-Top=Summit

2-Theta	d(A)	BG	Height	I%	Area	I%	FWHM
12.319	7.179	25	626	67.1	19985	66.7	0.543
20	4.436	19	105	11.3	5820	19.4	0.942
24.52	3.628	48	933	100	29969	100	0.546
36.973	2.429	43	112	12	3908	13	0.593
49.942	1.825	3	62	6.6	2863	9.6	0.785
60.282	1.534	90	140	15	8832	29.5	1.009
63.547	1.463	9	59	6.3	1714	5.7	0.494

Appendix IV Continued

Table 1b.

Peak Search Report (7 Peaks, Max
P/N = 11.8)
[3X40024.RD]
3x40024
PEAK: 43-pts/Parabolic Filter, Threshold=2.0,
Cutoff=0.1%, BG=3/1.0, Peak-Top=Summit

2-Theta	d(A)	BG	Height	I%	Area	I%	FWHM
12.2	7.249	18	371	61.6	13933	57.6	0.638
19.921	4.453	41	50	8.3	2485	10.3	0.845
24.5	3.630	45	602	100	24180	100	0.683
36.791	2.441	46	83	13.8	3849	15.9	0.788
49.919	1.825	11	56	9.3	1819	7.5	0.52
60.282	1.534	18	185	30.7	11895	49.2	1.093
63.547	1.463	4	43	7.1	1702	7	0.633

Peak Search Report (7 Peaks, Max
P/N = 10.6)
[40024X4.RD]
40024x4
PEAK: 41-pts/Parabolic Filter, Threshold=2.0,
Cutoff=0.1%, BG=3/1.0, Peak-Top=Summit

2-Theta	d(A)	BG	Height	I%	Area	I%	FWHM
12.3	7.190	12	184	39	6921	33.5	0.639
20.217	4.389	14	48	10.2	2448	11.8	0.867
24.64	3.610	20	472	100	20666	100	0.744
36.882	2.435	24	76	16.1	4210	20.4	0.942
49.942	1.825	11	37	7.8	1822	8.8	0.837
60.373	1.532	16	204	43.2	14928	72.2	1.244
63.729	1.459	7	43	9.1	2237	10.8	0.884

Absolute Uncertainty of the Peak Area Sum

Using the sums of the area under the peaks for each trial listed above, the sum, mean, standard deviation, and standard deviation of the mean was taken. Calculations conclude a 68% chance that a new measurement would fall within 57155 +/- 12,000 and 68% chance that the mean of any additional 4 measurements would fall within 57,155 +/- 6,400. See Table 2 below.

Appendix IV Continued

Table 2: Uncertainty calculations for the Peak Area Sums

Calculation	XTA40024hrs	RE40024hrs	3X40024	4X40024hrs
Sums	42435	73091	59863	53232
Mean	57155.25			
Standard Deviation	12823.91			
Standard Deviation of Mean	6411.95			

Relative Uncertainty of the Peak Area Sum

Dividing the standard deviation of the mean by the mean of the sums results in the 1 sigma relative uncertainty in the peak area sums to be on the order of 11%. See the calculation below.

$$(6411.95/57155.25)* 100 = 11.0\%$$

Uncertainty of 2-Theta (º) and of d-spacing (Å) values

The absolute error (standard deviation of the mean, 1sigma) for 2-theta values is on the order of 0.05 and appears to be independent of 2-theta from 2-theta values in the general range of 10-65º.

The absolute error (standard deviation of the mean, 1 sigma) for the d-spacing values do vary from a high of 0.02 at d-spacings near 7.3Å to a low of 0.001 at d-spacings near 1.5Å. To be conservative, an average d-spacing error of 0.01 has been applied to 0.01. This has the effect of reducing the number of significant figures at lower d-spacings, but does not affect any of the results presented in this work.

To prevent rounding errors, one extra figure was carried beyond the last significant digit.

Appendix V: Broad Reflections

Characteristics of the broad reflections are listed below. Information provided includes the experimental condition of time and temperature, the dimensions (Å), shape, height, and possible mineral or structural associations.

Experiment (˚C, hrs)	Maximum, Minimum and Center Dimension (Å)	Maximum Height (counts)	Possible Mineral or Structural Association
500, 720	15.896-10.81, asymetrical	11	14 A- double layer of Chr (002)
	7.97-6.62, centered at 7.21	5	Disordered chrysotile or part of double layer sheet pattern
	4.66-4.17, centered at 4.32	18	possibly tridymite
550, 20	14.139-10.208, centered at 11.798	3	14 Å- double layer of Chr (002)
	3.286-2.856, centered at 3.051	7	Talc
575, 24	15.5-9.772, asymetrical	9	14 Å- double layer of Chr (002)
587, 4	16.0-10.075, asymetrical	9	14 Å- double layer of Chr (002)
587, 24	16.0-8.801, centered at 10.861	10	14 Å- double layer of Chr (002), Talc
	4.68-4.2, centered at 4.4	15	Talc
600, 4	15.5-8.9, asymetrical	7	Talc
	4.795-4.185, centered at 4.49	15	Talc
	3.386-3.055, centered at 3.212	17	Talc

Appendix V Continued

Experiment (˚C, hrs)	Maximum, Minimum and Center Dimension (Å)	Maximum Height (counts)	Possible Mineral or Structural Association
600, 8	15.061-8.723, centered at 10.983	11	Talc
	4.772-4.115, centered at 4.429	15	Talc
600, 16	14.50-8.073, centered at 10.624	12	Talc
	4.77-4.22, asymetrical	17	Talc
600, 20	4.792-4.22, centered at 4.44	18	Talc
	3.397-3.064, centered at 3.202	18	Talc
600, 24	16.0-8.7, asymetrical	15	Talc
	4.7262-4.149, centered at 4.469	20	Talc
	3.409-3.065, centered at 3.202	16	Talc
650, 4	14.831-8.35, centered at 10.861	18	Talc
	4.771-4.09, centered at 4.42	31	Talc
	3.319-3.065, centered at 3.192	26	Talc
650, 8	14.83-8.646, centered at 10.624	17	Talc
	4.681-4.185, centered at 4.429	17	Talc
	3.36-3.065, centered at 3.202	20	Talc
650 at 16	14.609-8.646, centered at 10.398	15	Talc
	4.749-4.132, asymetrical	20	Talc
	3.329-3.037, asymetrical	63	Talc
650 at 20	12.702-8.723, centered at 10.398	12	Talc
	4.681-4.09, asymetrical	19	Talc
	3.409-3.07, asymetrical	17	Talc

Appendix V Continued

Experiment (˚C, hrs)	Maximum, Minimum and Center Dimension (Å)	Maximum Height (counts)	Possible Mineral or Structural Association
650 at 24	14.183-8.279, centered at 10.624	11	Talc
	4.726-4.203, centered at 4.469	15	Talc
	3.341-3.065, asymetrical	27	Talc
700 at 4	14.183-10.041, centered at 10.861	14	Talc
	4.726-4.115, asymetrical	21	Talc
	3.363-3.046, asymetrical	17	Talc
700 at 8	14.831-8.141, centered at 10.516	11	Talc
	4.681-4.081, asymetrical	12	Talc
	3.352-3.046, asymetrical	13	Talc
700 at 16	14.183-8.645, asymetrical	10	Talc
	4.79-4.167, asymetrical	14	Talc
	3.352-3.064, asymetrical	16	Talc
700 at 20	14.183-9.046, asymetrical	12	Talc
	4.749-4.257, asymetrical	19	Talc
700 at 24	4.795-4.257, asymetrical	18	Talc
	3.34-3.065, asymetrical	13	Talc
750 at 20	4.749-4.2029, centered at 4.49	10	Talc
	3.3633-3.093, asymetrical	13	Talc
750 at 24	15.061-8.882, centered at 11.109	17	Talc
	4.8187-4.1674, centered at 4.409	7	Talc
	3.363-3.065, asymetrical	23	Talc

Appendix VI: Broad Reflections Images

Diffraction patterns containing regions of broad X-ray reflections are shown below. Diffraction patterns were produced using Material Data Jade Software: Jade 5.

Experiment: 500˚C for 30 days

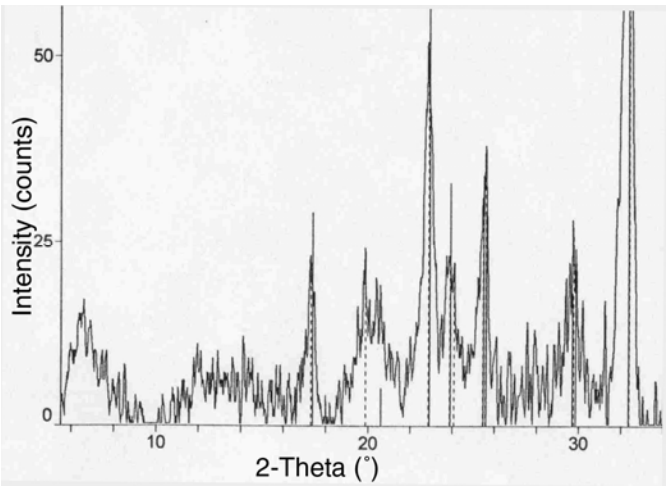

Experiment: 550˚C for 20 hours

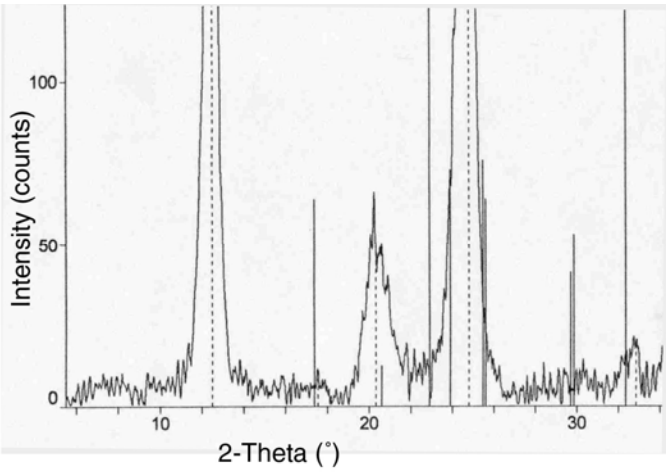

Appendix VI Continued

Experiment: 575˚C for 24 hours

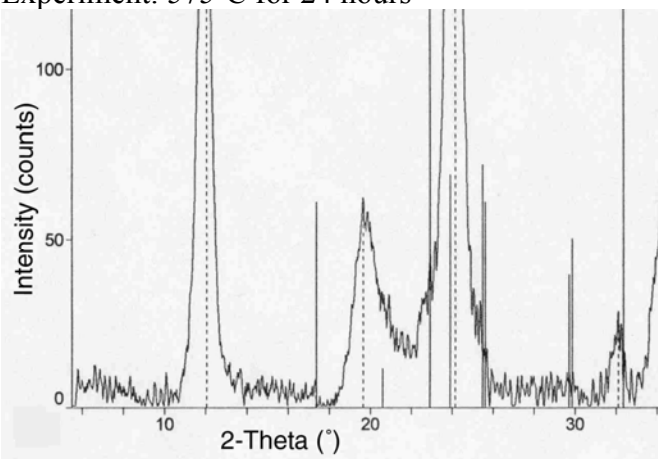

Experiment: 587˚C for 4 hours

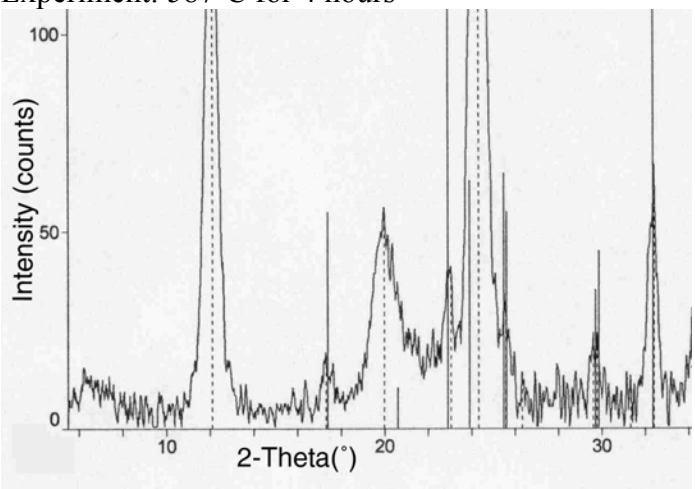

Experiment: 587˚C for 24 hours

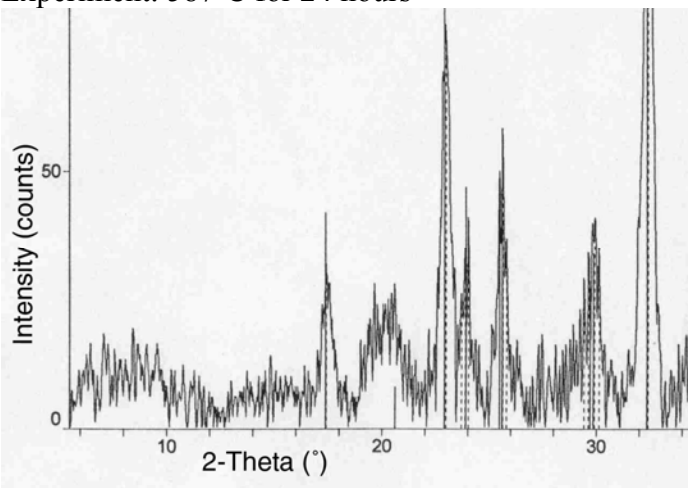

Appendix VI Continued

Experiment: 600˚C for 4 hours

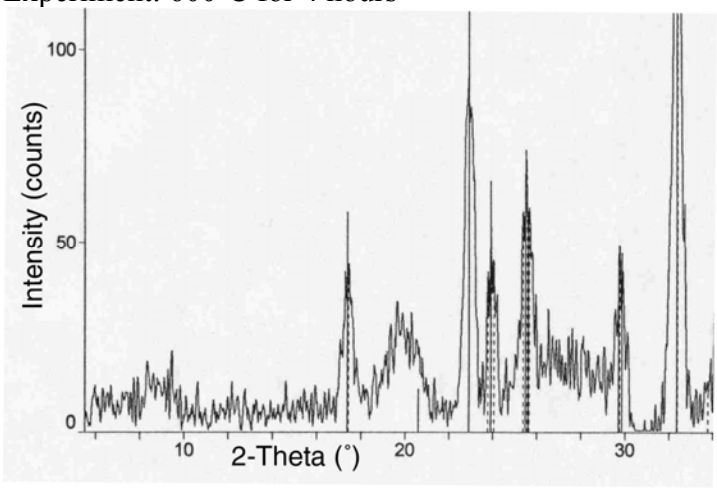

Experiment: 600˚C for 8 hours

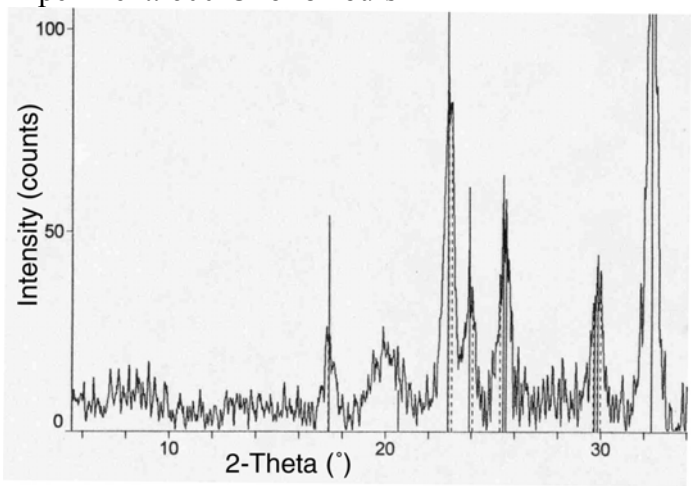

Experiment: 600˚C for 16 hours

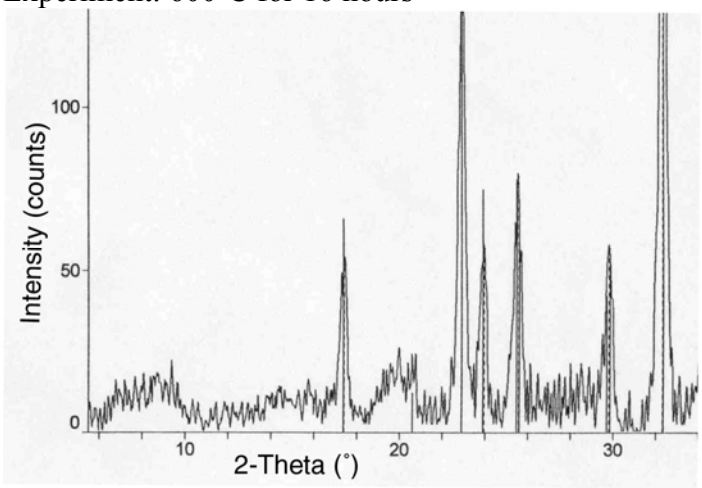

Appendix VI Continued

Experiment: 600˚C for 20 hours

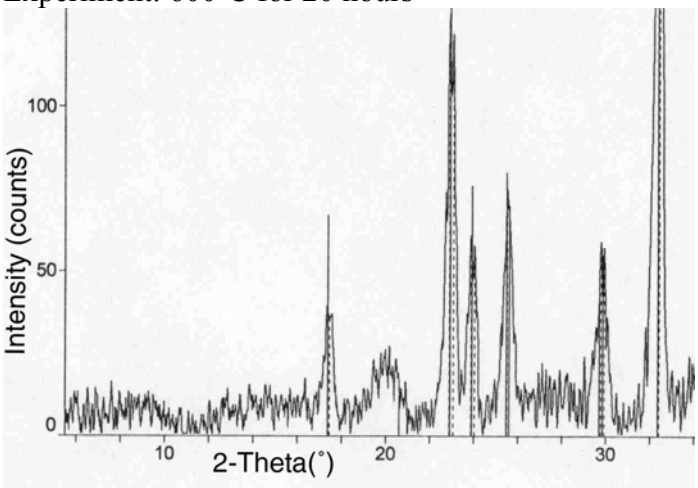

Experiment: 600˚C for 24 hours

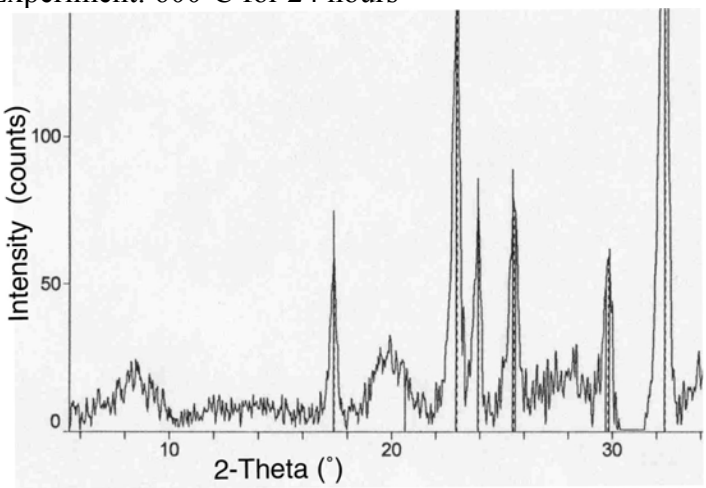

Experiment: 650˚C for 4 hours

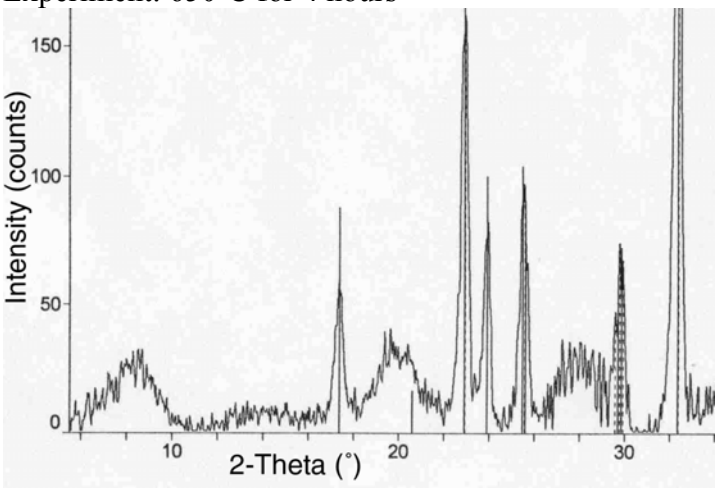

Appendix VI Continued

Experiment: 650˚C for 8 hours

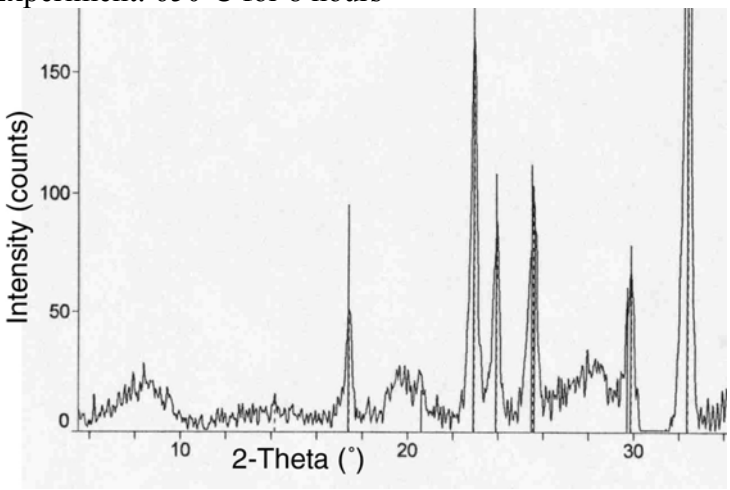

Experiment: 650˚C for 16 hours

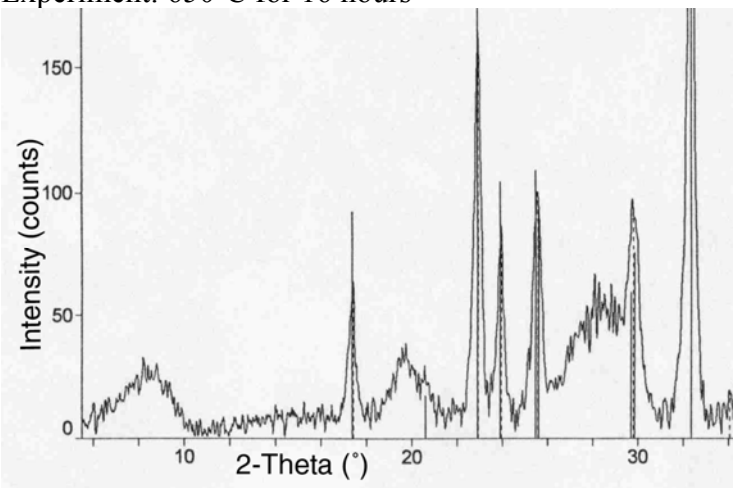

Experiment: 650˚C for 20 hours

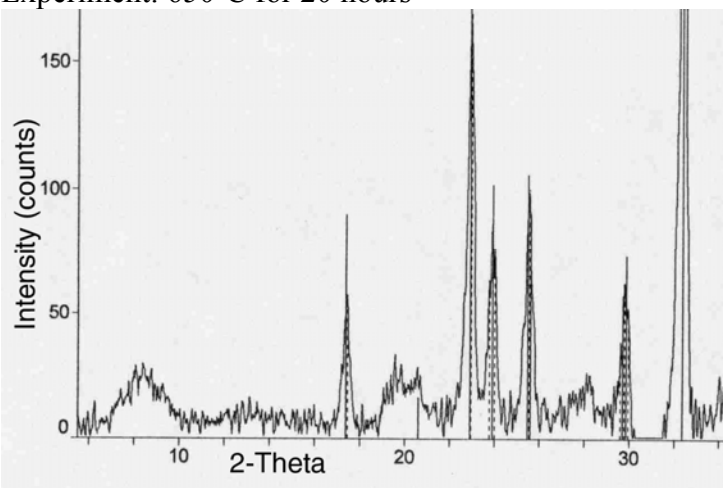

Appendix VI Continued

Experiment: 650˚C for 24 hours

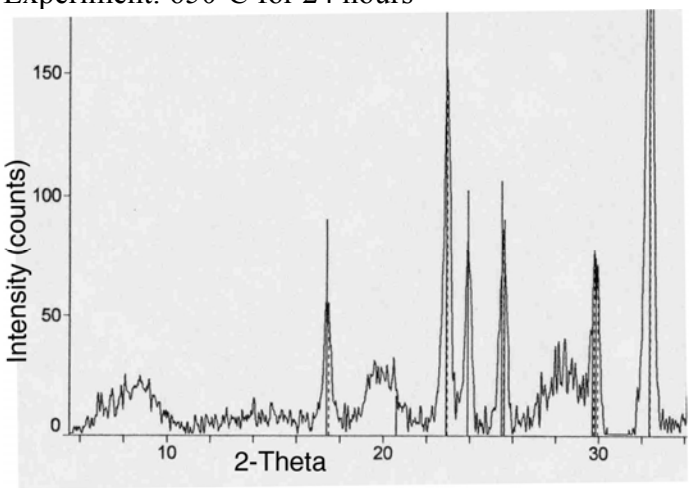

Experiment: 700˚C for 4 hours

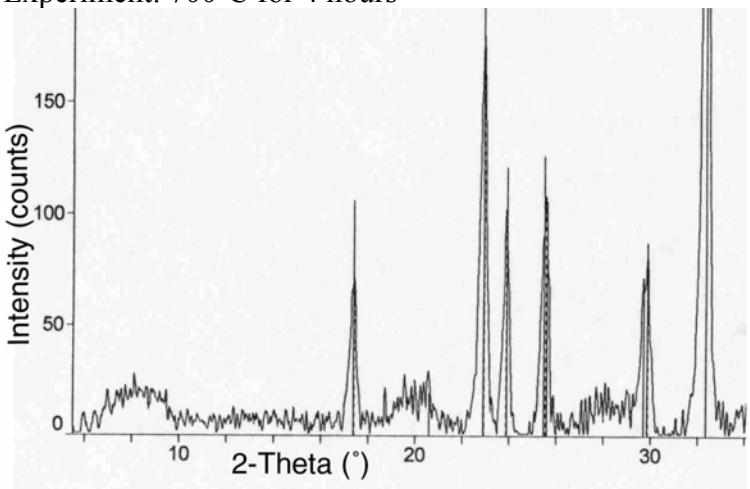

Experiment: 700˚C for 8 hours

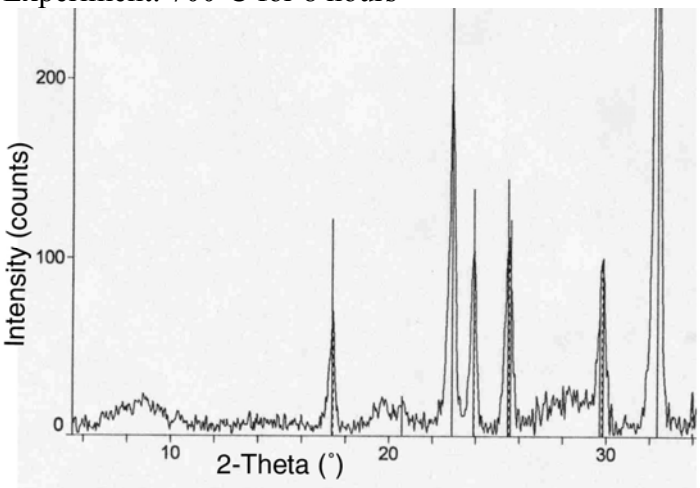

Appendix VI Continued

Experiment: 700˚C for 16 hours

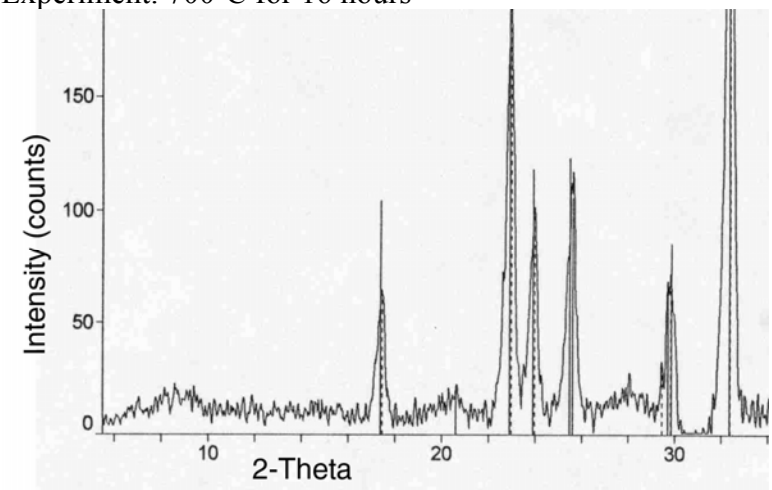

Experiment: 700˚C for 20 hours

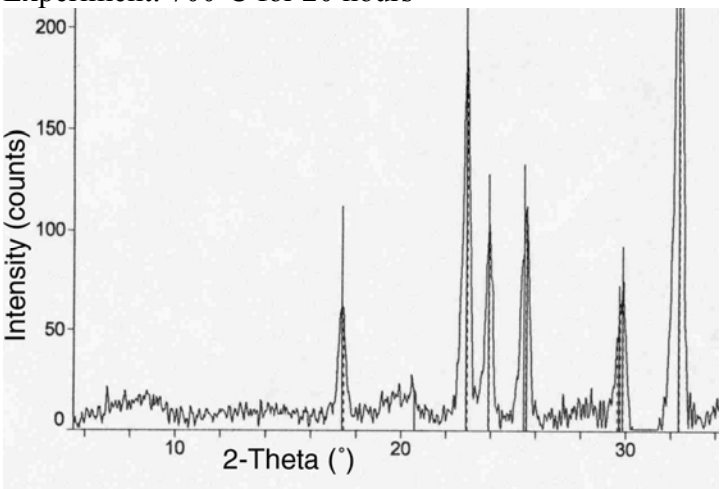

Experiment: 700˚C for 24 hours

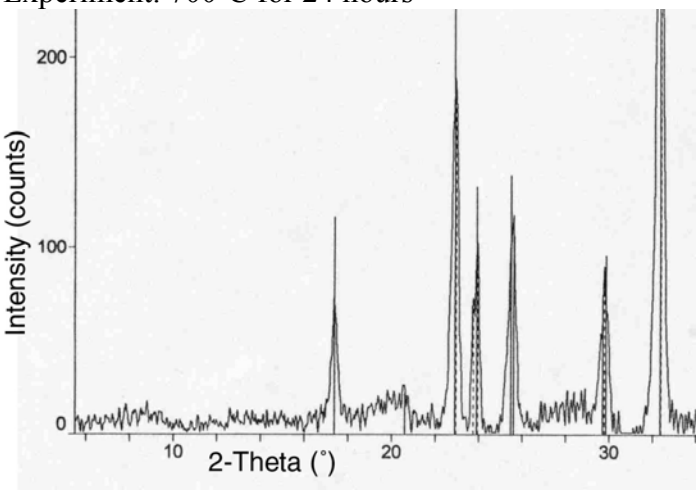

Appendix VI Continued

Experiment: 750˚C for 20 hours

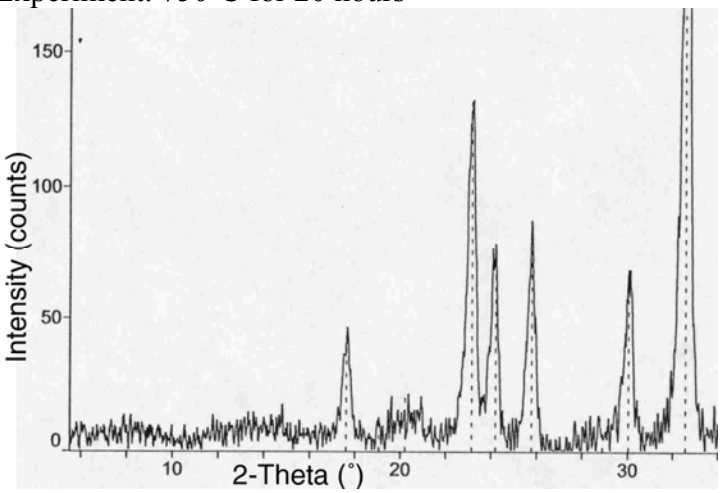

Experiment: 750˚C for 24 hours

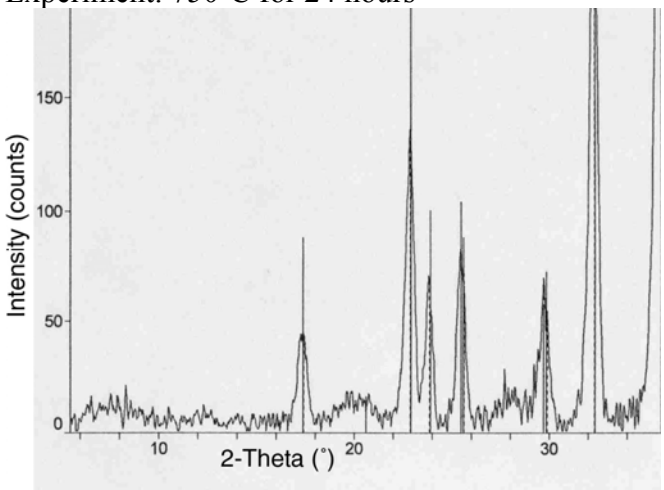

Bibliography

Ball, M.C and Taylor, H. F. W. (1963) The dehydration of chrysotile in air and under hydrothermal conditions. *Min. Mag*. 33, 467-482.

Berman, R. G., Engi, M., Greenwood, H. J. and Brown, T. H. (1986) Derivation of internally consistent thermodynamic data by the technique of mathematical programming: a review with application to the system MgO-SiO_2-H_2O. *J. Petrol*. **27**, 1331-1364.

Benarde, Melvin A. (1990) Adverse Health Effects of Asbestos. In *Asbestos: The Hazardous Fiber* (ed. Melvin A. Benarde). CRC Press, Inc., Boca Raton, FL.

Bloss, F. Donald. (1994) *Crystallography and Crystal Chemistry*. Mineralogical Society of America, Washington, DC.

Brindley, G. W. and Hayami, R. (1965) Mechanism for the formation of forsterite and enstatite from serpentine. *Min. Mag*. 35, 189-195.

Brindley, G. W. and Zussman, J. (1957) A Structural Study of the Thermal Transformation of Serpentine Minerals to Forsterite. *Am. Mineral*. **42**, 461-474.

Cattaneo, A., Gualtieri, A. F., and Artioli, G. (2003) Kinetic study of the dehydroxylation of chrysotile asbestos with temperature by in situ XRPD. *Phys. Chem. Minerals.* **30**, 177-183.

Datta, A. K. Samantary, B. K., Bhattacherjee, S. (1986) Thermal transformation in chrysotile asbestos. *Bull. Mater. Sci*. **8** (4), 497-503.

Deer, W. A., Howie, R. A., and Zussman, J. (1966) *An Introduction to the Rock Forming Minerals*. Longmans Green and Co LTD, London.

de Souza Santos, H. and Yada, K. (1979) Thermal Transformation of Chrysotile Studied by High Resolution Electron Microscopy. *Clays and Clay Mineral.* **27** (3), 161-174.

Dunnington, J. (1988) Linking Chrysotile Asbestos with Mesothelioma. *Am. J. Ind. Med*. **14**, 205.

Earnest, D. J., Candela, P. A., Wylie, A. G., Crummett, C. D., and Frank, M. R. (2004) Synchrotron Radiation Study of the Kinetics of Dehydration of Chrysotile Fiber. American Geophysical Union Fall 2004 Meeting. Abstract #V23C-06.

Faust, George T. and Fahey, Joseph J. (1962) The Serpentine-Group Minerals. Geological Survey Prof. Paper 384-A.

Fisher, Linda J. (1992) Asbestos; Manufacture, Importation, Processing and Distribution Prohibitions; Effect of Court Decision; Continuing Restrictions on Certain Asbestos-Containing Products. *EPA 57 FR 11364* U S Environmental Protection Agency. Washington, DC, USA.

Hey, M. H. and Bannister, F. A. (1948) A note on the thermal decomposition of chrysotile. *Min. Mag*. **28**, 333-337.

Hodgson, A. A. (1979) Chemistry and physics of asbestos. In *Asbestos Vol I: Properties, Applications, and Hazards* (ed. Michaels and Chissick). John Wiley & Sons, Inc., New York.

Klugg, Harold P. and Alexander, Leroy E. (1974) *X-ray Diffraction Procedures.* John Wiley & Sons, New York.

Langer, Arthur M. (2003) Reduction of the biological potential of chrysotile asbestos arising from conditions for service on brake pads. *Regulatory Toxicology and Pharmacology*. **38**, 71-77.

Lasaga A. C. (1998) *Kinetic Theory in the Earth Sciences*. Princeton University Press.

MacKenzie, K. J. D. and Meinhold, R. H. (1994) Thermal reactions of chrysotile revisited: A 29Si and 25Mg MAS NMR Study. Am. Min. 79, 43-50.

McCrone, Walter C. (1974) Detection and Identification of Asbestos by Microscopical Dispersion Staining. *Environ. Health Perspect*. **9**, 57-61.

Martin, C. J. (1977) The thermal transformation of chrysotile. Min. Mag. 41, 453-459.

Martinez, Edward. (1966) Chrysotile Asbestos: Relationship of the Surface and Thermal Properties to the Crystal Structure. *Can. Mining Metallur. Bull*. **69**, 414-420.

Materials Data, "Jade 5 XRD Pattern Processing", 1991.

Myer, George H. (1990) Mineralogical and Geological Aspects of Asbestos. In *Asbestos: The Hazardous Fiber* (ed. Melvin A. Benarde). CRC Press, Inc., Boca Raton, FL.

Nagy,K. L. and Lasaga, A. C. (1992) Dissolution and precipitation kinetics of gibbsite at 800˚C and pH 3: The dependence on solution saturation state. *Geochim. Cosmochim. Acta*. **56**, 3093-3111.

Nesse, William, D. (1991) *Introduction to Optical Mineralogy, 2nd Edition*. Oxford University Press, New York.

O'Hanley, David S. (1987) The origin of the chrysotile asbestos veins in southeastern Quebec. *Can. J. Earth*. Sci. 24 (1), 1.

O'Hanley, David S. (1996) *Serpentinites: Records of Tectonic and Petrological History*. Oxford University Press, New York.

Ross, Malcolm. (1984) A Survey of Asbestos-Related Disease in Trades and Mining Occupations and in Factory and Mining Communities as a Means of Predicting Health Risks of Nonoccupational Exposure to Fibrous Materials. *ASTM Special Technical Publication.* **834**, 51-104.

Ross, R. A. and Vishwanathan, V. (1981) Dehydration Reactions of Chrysotile Asbestos Below 500˚C. *Surface Tech.* **14**, 233-240.

Tiscali Reference Center (webpage) Accessed March 2005
URL : http://www.tiscali.co.uk/reference/encyclopaedia/hutchinson/m0013099.html.

Virta, Robert L. (2001) Some Facts About Asbestos. USGS Fact Sheet FS-012-01.

Virta, Robert L. (2002) Asbestos. In *U.S. Geological Survey Minerals Yearbook 2002*. USGS, 8.1-8.3.

Whittaker, E. J. W., and Zussman, J. (1956) The characterization of serpentine minerals by X-diffraction. *Miner. Mag*. **31**, 107-126.

Wicks, F. J. (2000) Status of the reference X-ray powder-diffraction patterns for the serpentine minerals in the PDF database-1997. *Powder Diffraction*. **15** (1), 42-50.

Wicks, F. J., and Whittaker, E. J. W. (1975) A reprassial of the structure of serpentine minerals. *Can . Mineral.* **13**, 227-243.

Zussman, Jack (1979) In *Asbestos Vol I: Properties, Applications, and Hazards* (ed. Michaels and Chissick). John Wiley & Sons, Inc., New York.